WATER CAN INCREASE ZEOLITE CATALYST REACTIVITY

By

KUIZHI CHEN

Bachelor of Science in Chemistry
Lanzhou University
Lanzhou, China
2011

Submitted to the Faculty of the
Graduate College of the
Oklahoma State University
in partial fulfillment of
the requirements for
the Degree of
DOCTOR OF PHILOSOPHY
May, 2017

WATER CAN INCREASE ZEOLITE CATALYST

REACTIVITY

Dissertation Approved:

Dr. Jeffery L. White

Dissertation Adviser

Dr. Frank D. Blum

Dr. Nicholas F. Materer

Dr. Allen W. Apblett

Dr. Clint P. Aichele

ACKNOWLEDGEMENTS

First and foremost, I would like to gratefully acknowledge the guidance, support, and encouragement of my doctoral advisor, Dr. Jeffery White. He is the mentor who has and will continually influence the rest of my life. From him I have gained not only the technical knowledge in NMR and catalysis, but also great philosophies of life. After a dinner with him in San Francisco at an ACS conference, I was enlightened that gaining the capability of independent and original thinking is more important and actually more difficult than gaining knowledge itself. The way he influences me is not limited to school. At another dinner at his house, I learned that enjoying the journey of life is as important as pursuing the destination. And further, Dr. White most resembles a friend unintentionally passing on years of life experience and key values to me. I also want to thank him for standing behind me during my "tough time".

My second acknowledgement goes to Dr. Daniel Resasco, from the University of Oklahoma, for providing me with the opportunity to join the DOE funded CIRE (Center for Interfacial Reaction Engineering) project. Besides financial support, the long-term CIRE project has given me invaluable opportunities of working with people from different scientific disciplines. As well, he has set an example for me as a great group leader and incisive scientist.

I would also like to acknowledge my lab mates with whom I worked. Thank you to Nitin, Gaumani, Tapash, and Mathis for being great senior group members, patiently training me on NMR skills and lab routines. Thanks to Jarred, Maryam, and Nathan for being great lab mates.

Special thanks to Dr. John Gelder, a great and respected educator, for showing me the professionalism and enthusiasm in teaching and for his guidance and patience with me during my time as a teaching assistant in the early years of my graduate school. I have always enjoyed working with him and will never forget the delicious pizzas while grading. Also, I acknowledge Dr. Frank Blum for the considerate long conversations through my PhD education, especially those after my proposal and thesis defenses.

The transition from a city of 8 million people in China, to a town of 60,000 people in Midwest America could have caused me many troubles. However, the people in Stillwater have shown me the greatest hospitality. They have helped me not only to overcome the culture shock, but also to enjoy the life here. I would like to thank Kip, Janie, and their family for the dinner invitations to their Midwest ranch each Thanksgiving. Talking to Murr, Janie's grandmother, will always be one of my favorite memories from our Thanksgiving dinners. Many thanks to the Han family and the Walton family for bringing me into their lives, being friends with me, and "demonstrating" that simple life and happiness does not conflict at all. Days spent with Han's three kiddos were always enjoyable. Probably, because doing research and playing with kids have something in common: they are both frank. Thanks to the Li

family for sharing their time with me on those memorable Christmas trips.

Finally, I would also like to express my sincere gratitude to my family for their strong support in China, especially my dad, Xuebin Chen. My dad is one among the conventional Chinese parents, who are always too shy to express their feelings to their kids. His “shyness” used to confuse me about his love for me when I was young. However, the journey at OSU has taught me to realize how much he cared about me. I thank you and love you, Dad.

Name: KUIZHI CHEN

Date of Degree: MAY, 2017

Title of Study: WATER CAN INCREASE ZEOLITE CATALYST REACTIVITY

Major Field: CHEMISTRY

Abstract: Historically, water is considered to reduce activity in zeolite-based hydrocarbon catalysis. Currently, there exists widespread interest in understanding synergistic impacts of water in catalytic transformation of non-traditional hydrocarbon feedstocks by zeolites, e.g. biomass feedstocks, since significant amounts of water are liberated in initial reaction stages. Questions regarding water's active or passive role in solid acid catalysis have prompted our work on studying fundamentals of water-zeolite interactions by in-situ magnetic resonance methods. We have developed multiple methods of introducing water into zeolite from trace amounts to access amounts. The small loading results, below 0.5 water molecules per acid site, have shown interesting onsite interaction information at molecular level, for example, suggesting the acid site proton can be deprotonated by a single water molecule. In addition, the introduction of water to hydrophobic organosilane modified zeolites shows liquid water can be blocked outside the crystallites, implying potential application of the hydrophobically modified zeolite. For water's positive impact on hydrocarbon reactions, we have experimentally shown that trace amounts of water enhance isobutane reactivity in HZSM-5 by up to an order of magnitude (*ACS Catalysis* **2014**, *4*, 3039). Subsequently, active sites were characterized in the presence of water for hydrophilic and hydrophobically-modified zeolites (*ACS Catalysis* **2015**, *5*, 7480). From that work, we determined that only vapor-phase water could access acid sites in organosilane modified catalysts, while liquid-phase water was excluded from the catalyst interior volume, leading to increased catalyst lifetimes in water-rich environments (*JACS* **2015**, *137*, 11810). Moving forward, we recognize that aromatic reaction centers are common to many important hydrocarbon conversions in zeolites. Specifically, alkylation-dealkylation steps have been shown as key steps in methonal-to-hydrocarbon (MTH) conversions. Aromatic alkylation-dealkylation reactions are investigated as test reactions to probe whether water can play an active role in lowering activation energies for the critical side-chain alkylation and dealkylation steps.

TABLE OF CONTENTS

LIST OF TABLES

Table Page

LIST OF FIGURES

Figure Page

CHAPTER I

INTRODUCTION

1.1 Introduction

Solid-acid catalysts are widely used in industrial hydrocarbon conversions. Zeolites, because of their high internal surface area, well-defined pore structure, and tunable acid density, are one of the most valuable catalysts in use. The majority of zeolite-based hydrocarbon conversions are in hydrophobic environments, e.g. FCC (fluid catalytic cracking), MTH (methanol to hydrocarbon) conversion. In MTH conversion, even though the starting reagent, methanol, is hydrophilic, the intermediates, i.e. the hydrocarbon pool molecules[1], and the products are all hydrophobic. In the past, water was always treated as a deleterious factor for zeolite catalyzed reactions, because of its much higher adsorption energy than hydrophobic molecules at the acid sites. In addition, the appearance of condensed water appears in zeolites at high temperature, at which most hydrocarbon conversions take place, causes dealumination and thus catalyst deactivation. Interestingly, despite the major deleterious role of water, positive roles of water were reported in the 1990s, however, via a negative machenism.[2-3] The reports indicated that water can suppress the secondary reaction in MTH conversion, leading to a selectively enhancement of primary products. So far, no report has shown that water can actively participate in zeolite-based hydrocarbon reactions. However, our group recently found that water is able to enhance the

reactivity of H/D exchange between isobutane-d_{10} and HZSM-5 acid site protons.[4] Only a sub-stoichiometric amount of water can increase the catalyst activity up to one order of magnitude.

Recently, it has been reported that only a small amount of water can improve the performance of some heterogeneous catalysts. Hibbitts and coworkers showed that water-mediated hydrogen transfer increases CO activity in Ru-involved Fischer-Tropsch catalysis.[5] Barron and coworkers reported small amounts of water have 'Goldilocks effects' on homogeneous acid and base catalysis.[6] In 2012, Motokura and coworkers demonstrated that addition of water in the range of 1-5 wt% relative to the mass of the proton-exchanged montmorillonite catalyst increased reaction rates between bulky alkenes by over an order of magnitude relative to the catalyst with no water.[7]

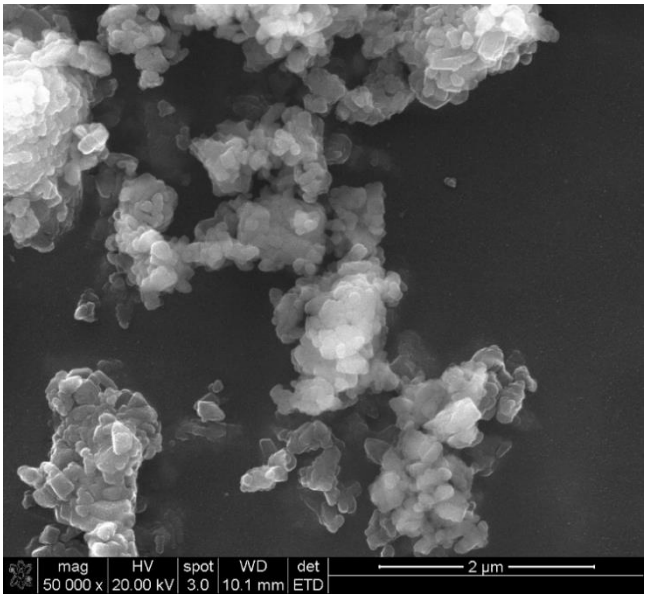

Figure 1.1. ZSM-5 crystallites shown by SEM method.

1.2 Zeolites

Zeolites are crystalline aluminosilicates that contain well-defined microscopic pore systems, with pore diameters measuring from 0.3-1.2 nm. For comparison, mesopores generally measure from 2-50 nm. Discovered in nature, zeolites were known as 'boiling stones' due to the fact that their micropores generate large amounts of steam from water upon heating. Zeolites have also been known as 'molecular sieves' because of their uniform pore dimensions. Even though the first zeolite was discovered in 1756, it was not until the early 1950s that they were synthesized in large quantities and commercialized; to now, over 200 types of zeolites have been registered.[8-9] However, because of the limitation of thermal and mechanical stabilities, as well as high synthesis costs, many zeolites are not available industrially. Actually, there are only about 10 types of zeolites used in industrial processes, e.g. Y zeolite, ZSM-5, mordenite, MC-22, beta zeolite, SAPO-34.[10] Zeolites for catalytic uses are typically synthesized in small crystallite sizes, i.e. micro- and sub-micrometers, to reduce the diffusion path lengths of reactants and products.[11-12] For the same purpose, mesopores, considered as 'molecular highways', are also generated artificially via post-synthetic modifications to enhance mass transport behavior.[13] Among those popular zeolites, ZSM-5 is the catalyst used in this dissertation, therefore, will be used as an example for introductory purposes. Figure 1.1 depicts a Scanning Electron Microscope (SEM) picture of ZSM-5 zeolite purchased from Zeolyst, showing a general crystallite size of 0.5 μm. A TEM picture of a ZSM-5 surface is shown in Figure 1.2a[14] to illustrate the highly organized pore structures. A computer-simulated framework (adapted from the International Zeolite Association website) is displayed in Figure 1.2b, showing that the pores in Figure 1.2a are actually the openings of channels. Besides the pore structures, there usually exist Brønsted acid sites on the internal walls of the pores. Generally, the special properties of zeolite originate from the acid sites and special confinement of the framework structures.

a. 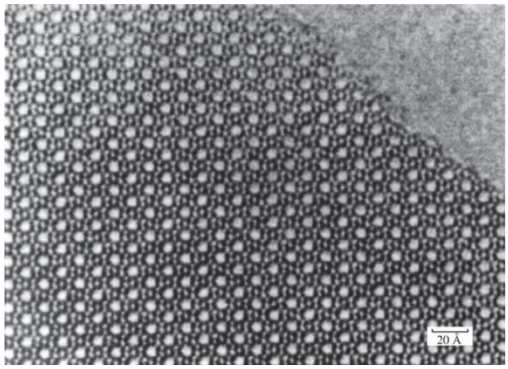

b. 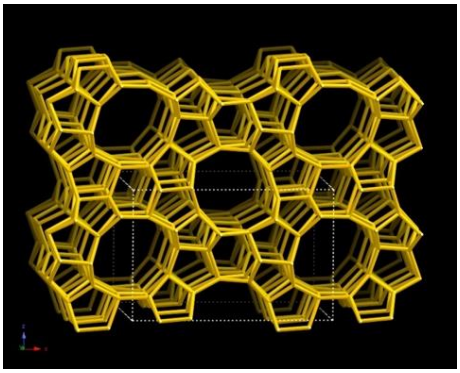

Figure 1.2. a) TEM picture showing ZSM-5 pore structure[14] **b)** computer-generated framework of the same orientation.

1.2.1 Acid sites

The Brønsted acid site is derived from the replacement of Si atoms with Al atoms in a silica-like structure, as shown in Figure 1.3. Each replacement generates a negative charge in the framework at the Al site, and the introduction of a cation, e.g. H^+, NH_4^+, can preserve the electroneutrality acts as the charge balancing cation. When it proton, the zeolite performs as a solid acid catalyst. However, the acidity of the zeolite acid proton is weak, with a ca. 1200 kJ/mol deprotonation energy estimated by the DFT method.[15-16] Lewis acid sites can also be found in zeolites, appearing where framework Al-O bonds cleave, as demonstrated in Figure 1.4.

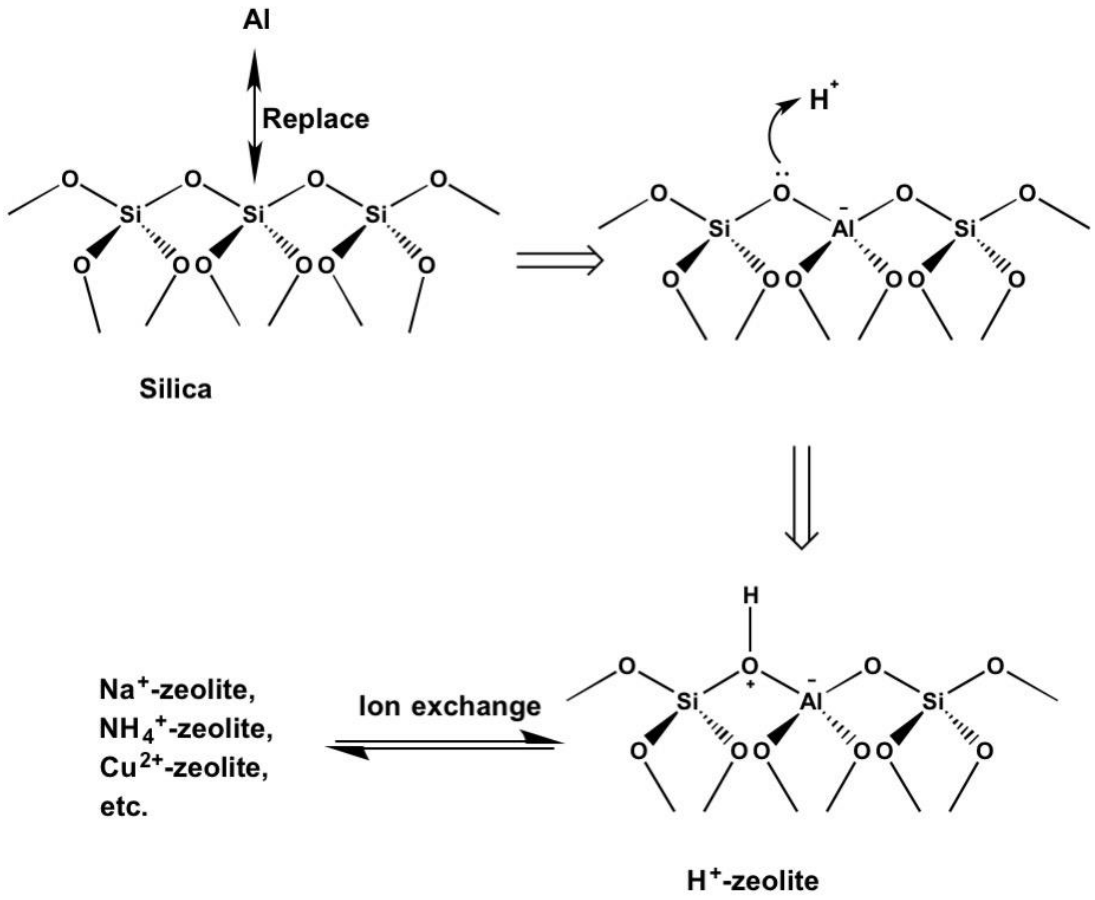

Figure 1.3. Illustration of origination of a Bronsted acid site.

The acid density is usually characterized by the Si/Al ratio of a zeolite. For example, a series of zeolite catalysts will be mentioned in Chapter II, which are all ZSM-5 catalyst but at different Si/Al ratios. Acid densities decrease at increased Si/Al ratios, due to the fact that each Al site in the framework only brings in one acid site, i.e. number (Al) = number (H^+). Therefore, the increasing of Si/Al ratios usually means decreasing of the number of Al or acid sites. However, in most cases, the Si/Al ratios are reported using as-synthesized values, and actual acid densities are usually lower, because part of the Al atoms are extraframework species, such as $Al(OH)_3$. Typically, there are 3 ways to control the Si/Al ratios: *1) To control the ratios of starting materials*, specifically the amounts of Al and Si sources used; *2) To dealuminate as-synthesized*

zeolites by steaming, where some of the Al sites are turned from framework into extraframework species by hot water vapor; *3) To use chemical treatment, such as tetrachlorosilane*[17], which can substitute framework Al with Si *in-situ* without damaging the framework.

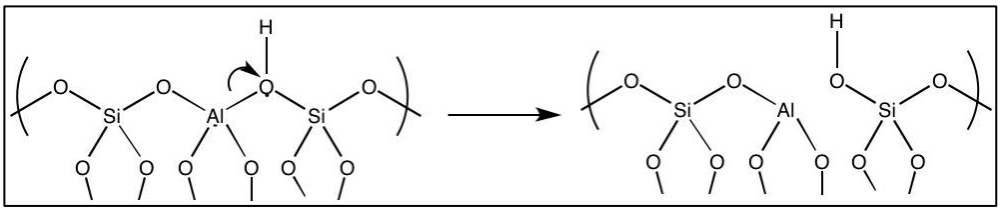

Figure 1.4. Illustration of the formation of a Lewis acid site.

1.2.2 Framework

Acid sites reside in unique intracrystalline channels or interconnected voids, depicted in Figure 1.5.[18] Usually, each framework type is assigned with a three-letter code, e.g. MFI, FAU, TON, etc.[19] MFI type zeolites contain straight and sinusoidal channels, FAU type contain cages and channels, TON zeolites contain 1-dimentional channels, etc. For example, ZSM-5 and Y zeolites belong to MFI and FAU framework topologies, respectively. Typically the pore sizes are categorized into four regime: (i) *small,* zeolites with eight-member-ring pores, free diameters of 0.30-0.45 nm (e.g., zeolite A), (ii) *medium,* zeolites with 10-member-ring pores, 0.45-0.60 nm in free diameter (ZSM-5), (iii) *large,* zeolites with 12-member-ring pores of 0.6-0.8 nm (e.g., zeolites X, Y) and (iv) *extra-large,* zeolites with 14-member-ring pores (e.g., UTD-1).[20] A thorough zeolite database, which includes topologies, characterization data, and synthetic methods of all registered zeolites, can be found at the International Zeolite Association (IZA) webpage, http://www.iza-online.org/. Diffusion simulated pore topologies can be found at ZEOMICS, http://helios.princeton.edu/zeomics/.

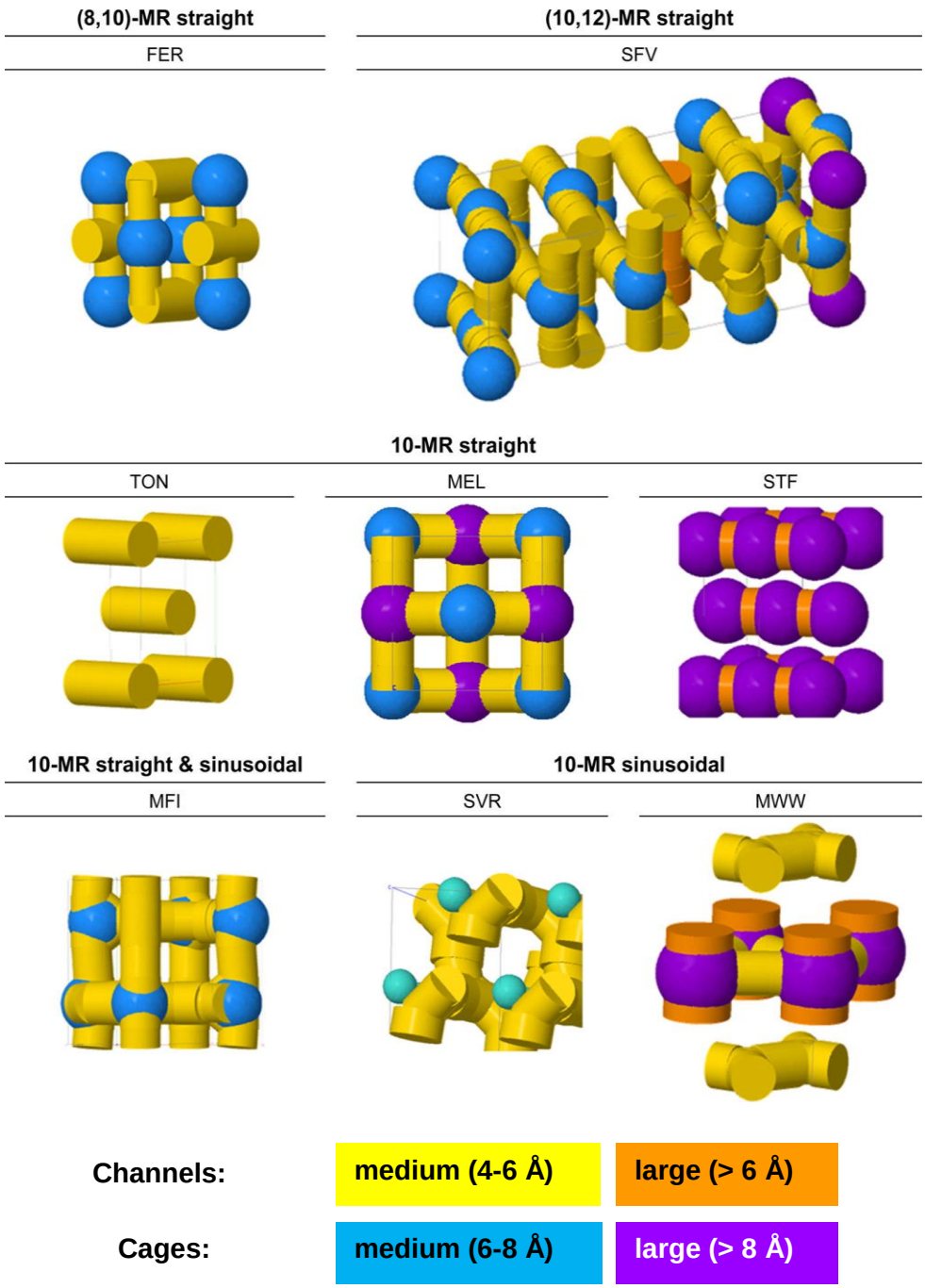

Figure 1.5. Diffusion simulations of different type of framework. Adapted from reference 18.

1.2.3 Properties and characterization

Acidity and well-defined porosity make zeolites exceptional catalysts with respect to both activity and selectivity. The framework confinements are able to provide shape selectivity and even partial confinement that could possibly reduce the transition state energy of some intermediates.[21] Mechanistic understanding of zeolite catalysis is incomplete, even though they are used industrially. The acid strength, acid density and the pore confinement are the conventional properties considered for zeolite performances. Recently the Iglesia group has reported fundamental studies of acid strength and confinement influences in hydrocarbon reactions.[15, 22-25] Also, it has been noticed that the location of the acid site inside zeolites may influence the catalyst performances. For example, Janda et al. have shown acid sites in channels and channel intersections (yellow and blue in Figure 1.5) have different activity due to the different confined environments.[18, 26-27]

The Brønsted acid site, while studied for decades, does not have its properties fully understood. Their acid density, strength and even their location have been and are still being investigated. Compared to Brønsted sites, Lewis type of acid sites are believed to have less impact on catalysis, because of their small amounts, i.e. 10% of framework Al^{27}. Silanol groups, and extraframework Al (EFAL) are other species existing in zeolites but usually nonreactive in catalysis.[28] Regular characterization methods for zeolites include ^{1}H / ^{27}Al / ^{29}Si solid-state NMR, BET, X-ray diffraction, Infrared spectroscopy, Raman spectroscopy, temperature programmed desorption (TPD), etc. Zeolite materials can be studied in both powder and single crystal forms. ZSM-5 and Y zeolites, the most used zeolites in this research, are illustrated below with their fundamental properties.

1.2.4 Two specific zeolites

ZSM-5

ZSM-5 is an artificial zeolite by Exxon Mobil, patented in 1972.[29] As mentioned above, ZSM-5 zeolite belongs to the MFI framework type, which consists of 3-dimensional structures including straight, sinusoidal 10-member ring channels and channel intersections, as shown in Figure 1.6. The size of the channel (yellow) is 5.1-5.6 Å and the channel intersection (blue) is about 8 Å. As reported in the IZA database, the maximum size of a 'sphere' that can diffuse along and be included in a MFI-type catalyst is 4.46-4.70 Å and 6.36 Å, respectively.

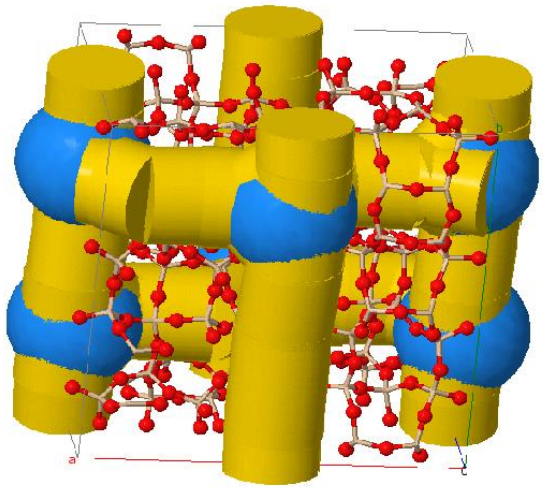

Figure 1.6. Framework of MFI, adapted from reference 26

There is only one rule that is generally valid for the arrangement of Al atoms in a zeolite, which is the Loewenstein rule, stating that the formation of an Al-O-Al sequence is forbidden because of its low stability. For the MFI type framework, the acid site density can be varied from about Si/Al = 11.6 to Si/Al = +∞, according to the Loewenstein rule.[30] ZSM-5 zeolites with

certain Si/Al ratios are noted as the following format in this dissertation: ZSM-5 (Si/Al = 15), ZSM-5 (Si/Al = 40), and ZSM-5 (Si/Al =140).

Y zeolite

Compared to ZSM-5, zeolite Y (FAU) is another 3-dimensional zeolite with large cavities, known as super cages (see Figure 1.7a, purple), with 11.24 Å diameter, interconnected by 12-member ring channels (orange), diameter of 7.35 Å. There is also another type of cage having a much smaller size, called the sodalite cage, shown in Figure 1.7b[10]. The HY zeolite is very important for industry, for example, it has been used as the main catalyst in fluid catalytic cracking (FCC) process, the main step of gasoline refinery.

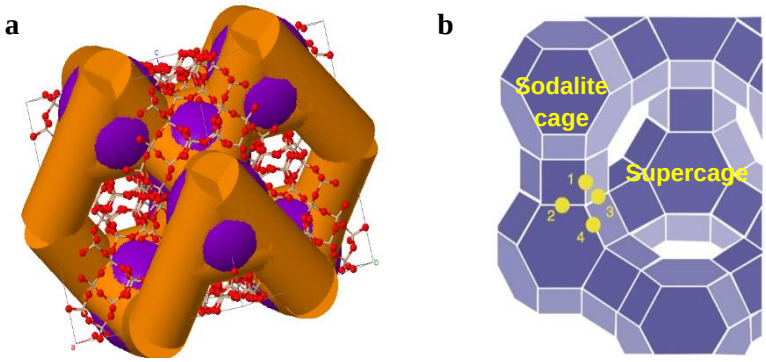

Figure 1.7. Showing of framework of FAU: **a)** connection between cages and channels, adapted from reference 26. **b)** the supercage and sodalite cage, adapted from reference 10.

1.2.5 Zeolite synthesis

Conventionally, organic structure-directing agents (SDA) are used as template in hydrothermal synthesis of zeolite. The size of a structure-directing agent determines a framework type. Larger-sized templates form larger pores and vice versa, e.g. tetramethylammonium (TMA) for **SOD** type of zeolite, containing pore opening at 2.53 Å, and tetrapropylammounium (TPA) for **MFI**,

containing pore size ranged at 5.1-5.6 Å, etc. With templates, zeolites can be synthesized via two routes, the hydroxide and flouro-routes. The former produces defect-rich and the latter produces defect-free zeolites.[31-32] Recently, the Al siting has drawn significant attentions. Numerous studies have shown that the Al location has impacts on catalysis mechanisms.[22, 27, 30, 33-34] In addition, Al sites are not evenly distributed in the framework.[22, 35-36] Furthermore, the Al site location can be synthesized via the control of Na^+ concentrations.[33, 37-39]

1.2.6 Quantitative conversion of Si/Al ratios to acid site densities

The acid density can be quantified by the number of acid sites per unit cell. In this dissertation, the amount of reagent molecules adsorbed in zeolite catalysts are noted by *eqv (equivalence)*. For instance, 1 eqv of adsorbed benzene means the molar ratio of acid site numbers and benzene molecules is 1:1. On average, there are 96 tetrahedral atoms (T-atom) in a unit cell of MFI, thus the Al density can be presented in formula: Al/u.c. = 96/(1+Si/Al). In zeolite Y, there are twice as many T-atoms in each unit cell, resulting in the formula: Al/u.c.=192/(1+Si/Al).

For example, with these formula, we find for ZSM-5 catalyst at Si/Al=15, there exists ca. 6 acid sites per unit cell. For convenience, the acid density of some common catalysts with varying Si/Al ratios are calculated and shown in Table 1.1.

		Si/Al ratio			
		15	**25**	**40**	**140**
Acid sites/u.c.	**ZSM-5**	6	3.7	2.3	0.7
	Y zeolite	12	7.4	4.6	1.4

Table 1.1. Si/Al ratios and their corresponding Al densities (per u.c.)

1.3 Introduction of NMR

1925-45 was the dawn before the explosion of NMR technique. The concept was established during this period. In 1939, Rabi et al. found a hydrogen stream could absorb measurable electromagnetic energy at a sharply defined frequency in a magnetic field, while under high vacuum.[40] Although, such studies were limited to small molecules under high vacuum. The method for bulk materials was not reported until 1946 by the Bloch group at Stanford[41-42] and Purcell group at Harvard[43], who observed radio frequency energy absorptions of a sample of water and a block of paraffin, separately. The 1952 Nobel Prize was awarded to them, and since then, NMR technology has undergone a great evolution. In its first few decades, the early NMR technique was called continuous wave (CW) spectroscopy. In this method, a NMR spectrum was obtained by sweeping the radio frequency in a fixed magnetic field, or vice versa, by varying the electromagnetic field using a fixed radio frequency. However, the continuous wave method is limited by its poor signal-to-noise ratio and long acquisition time and has now been replaced by a modern pulsed Fourier-transform NMR technique. During the 1960s, the development of FT-NMR truly revolutionized its applications, not only due to the sensitivity enhancement, but its fast acquisition time that allows one to study fast chemical processes and time-dependent NMR phenomena (i.e., relaxation).

1.3.1 Characteristics of a nucleus

Table 1.2 shows the basic characteristics of ^{1}H, ^{2}H, ^{27}Al, ^{29}Si and ^{13}C nuclei that are most commonly studied in zeolite-based catalysis. *Spin, natural abundance* and *gyromagnetic ratio* are natural characteristics of a nucleus. NMR spectroscopy originates from the fact that nuclei have spins, which is usually characterized by a quantum spin number, *I*. For example, ^{1}H and ^{29}Si have spin number of I = ½, called spin-half nuclei, while ^{2}H and ^{27}Al are called quadrupolar nuclei

because their spin number I > ½. Spin-half and quadrupolar nuclei differ greatly due to the strong quadrupolar coupling in the latter case. The quadrupolar couplings usually lead to strong line broadening and fast relaxations. The natural abundance is an important property that directly affects the signal-noise-ratio of a spectrum and the homo-nucleus dipolar interactions. Gryromagnetic ratio, γ, determines the Larmor frequency, ω, of a nucleus. Their relationships are shown in Equation 1.1.

Isotope	Spin	Natural abundance / %	Gyromagnetic ratio γ / 10^6 rad T^{-1} s^{-1}
^{1}H	1/2	99.985	267.522
^{2}H	1	0.015	41.066
^{27}Al	5/2	4.7	69.763
^{29}Si	1/2	100	-53.19
^{13}C	1/2	1.07	67.283

Table 1.2. Characteristics of common nuclei related in zeolite-based catalysis.

$$\omega_0 = -\gamma B_0 = 2\pi v_0 \qquad \text{Equation 1.1}$$

Since γ value is a naturally fixed, the Larmor frequency of a nucleus is determined by the external magnetic field, $\mathbf{B_0}$. Typically, in solution NMR regime, 'The higher the Larmor frequency, the higher the resolution' is a true statement, but not in solid state cases, due to the strong anisotropic dipolar interactions.

1.3.2 Single-90° pulse sequence

The energy levels and selection rules can explain most kinds of spectroscopy, but not for NMR. For instance, the most basic pulsed NMR experiment cannot be explained by energy level approach. The *vector model,* that has been around as long as NMR itself, is an extensively used tool to describe NMR theory, even though it can only be applied to a small number of situations. Here, single pulse NMR is demonstrated by using the simplest spin ½ nuclei, e.g. ^{1}H or ^{13}C.

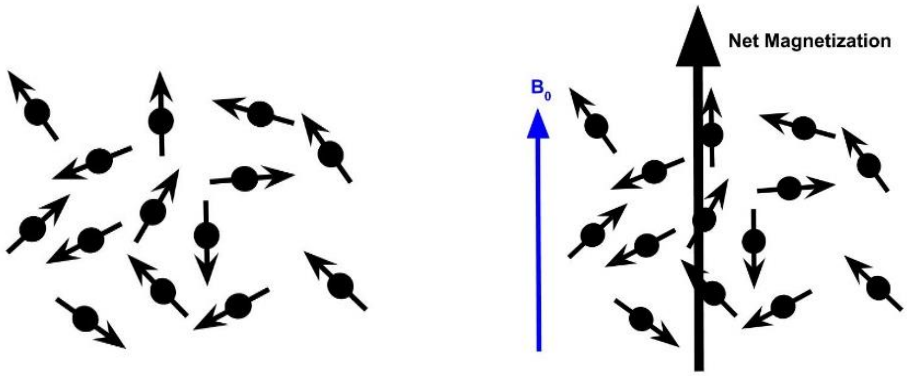

Figure 1.8. Showing of external magnetic field inducing net magnetization.

In an NMR experiment, we do not observe just one nucleus but a large quantity (10^{20}) of them, so the net magnetization should be concerned instead of single nuclear spins. In a spin ½ situation, each nucleus can be thought of a small bar magnet that randomly aligns to all directions, with the magnetic moment, μ, quantified by spin number *I* (Equation 1.2), leading to a

$$\mu = \gamma \hbar I \qquad \text{Equation 1.2}$$

net magnetization of zero. However, when an external magnetic field is applied, a non-zero net magnetization, called the *bulk magnetization,* quantified by Boltzman equation (not shown), rises because of Zeeman interactions. The magnetization can be presented by a vector, $\mathbf{M_0}$, called the *magnetization vector,* displayed in Figure 1.10. A vector model is a convenient tool to explain and explore, not all of, but the most fundamental NMR sequences.

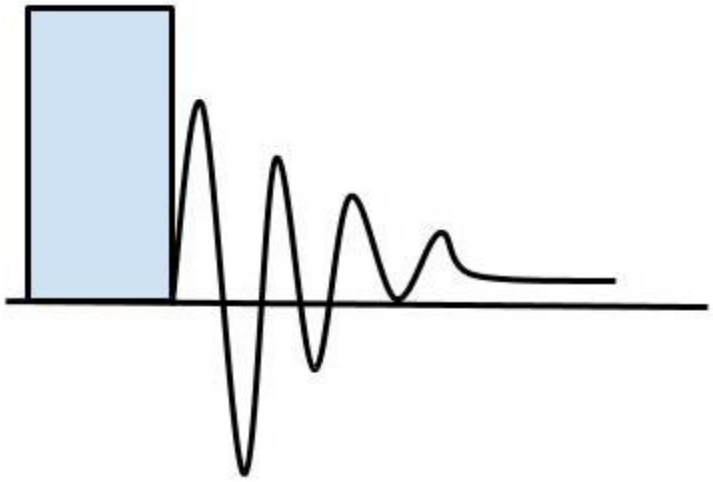

Figure 1.9. Drawing of single pulse diagram.

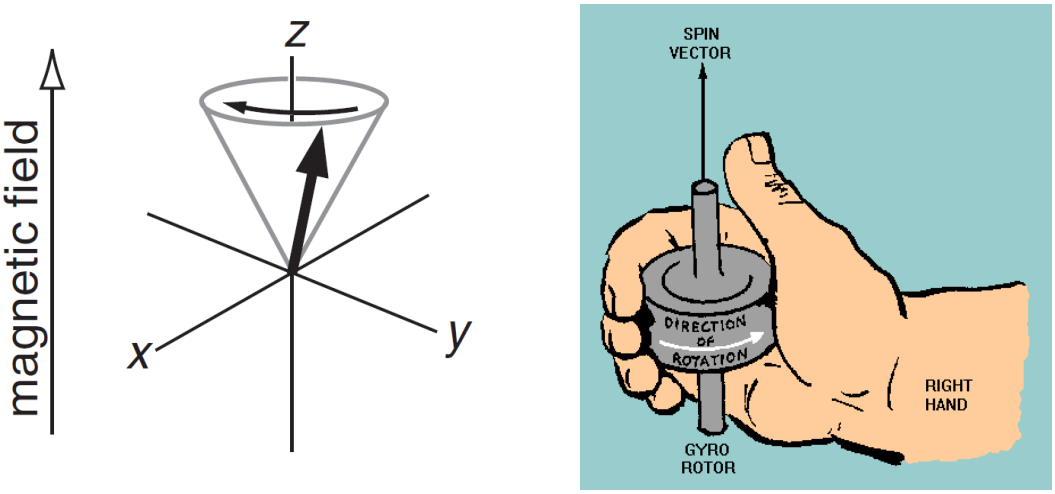

Figure 1.10. Drawing of **a)** Larmor precession, adapted from http://www-keeler.ch.cam.ac.uk/lectures/. **b)** Right-handed rule, adapted from http://www.tpub.com/neets/book15/63b.htm.

Briefly, a pulsed NMR experiment is monitored by sending one or a series sequences of radiofrequency pulses to a sample material at the Larmor frequency of target nucleus, followed by acquiring and processing the relaxation signal generated by the material, illustrated in Figure 1.9. Note that the same coil is used for transmitting and receiving radiofrequencies.

If $\mathbf{M_0}$ is tilted away from the equilibrium position, z axis, it will rotate around B_0 at the Larmor frequency, as displayed in Figure 1.10. The rotating is governed by the right-handed rule, shown in Figure 1.10b, and Equation 1.1. Figure 1.10a is an example of Larmor precession of a nucleus with positive gyromagnetic ratio value, such as ^{1}H and ^{13}C. It appears like 'left-handed' rule due to the negative sign in Equation 1.1. Once the magnetization vector is tilted away, it always wants to relax back to equilibrium position, and during the relaxation, a signal contains the nuclear information is released and will be detected by the coil. The $\mathbf{M_0}$ always rotates around B_0 at Larmor frequency (in mega Hz), which is hard to manipulate. However, a rotating frame

approach can simplify the situation, by imagining putting the observer rotating around $\mathbf{B_0}$ along with $\mathbf{M_0}$ at Larmor frequency. In the rotating frame, $\mathbf{M_0}$ and $\mathbf{B_0}$ are relatively static to each other.

1.3.2.1. Excitation

A pulse of radiofrequency at Larmor frequency shows up as a magnetic field in rotating frame, known as the applied magnetic field, $\mathbf{B_1}$, and could rotate $\mathbf{M_0}$ off $\mathbf{B_0}$, with the rotating direction and flip angle determined by right-handed rule and pulse width, respectively. The pulse lasting just long enough to rotate $\mathbf{M_0}$ to +y axis is called a 90˚ pulse, see Figure 1.11. The experiments in this dissertation usually have 90˚ pulse widths as 3 ~ 5 microseconds. By applying longer pulses, 180˚, 270˚, 360˚ flip angles can be approached, which are similar to rotating $\mathbf{M_0}$ to –z, -y, and back to +z, individually. Overall, the pulses with varying pulse widths have the ability to tilt $\mathbf{M_0}$ to any angle off z-axis.

1.3.2.2. Relaxation

$\mathbf{B_0}$ is along the equilibrium direction, where $\mathbf{M_0}$ always tend to rotate back once tilted. As illustrated in Figure 1.11, $\mathbf{M_0}$ is tilted to x-y plane by a 90° pulse. However, after the pulse it will naturally relax back to z-axis, during which time, the free induction decay (FID) signal is generated and could be acquired and processed to a real spectrum via Fourier transform technique. The relaxation time, measuring the relaxing time from x-y plane to z-axis, denoted as T_1, ranges from milliseconds to hundreds of seconds. T_1 is also known as spin-lattice relaxation, and its value is dependent upon multiple factors, i.e. the nucleus type, the state of the material (solid or liquid), temperature, etc. For example, the T_1 value of proton in a dry HZSM-5 catalyst is much longer than in its wet conditions. There is also another relaxation mechanism called spin-spin relaxation, known as T_2 relaxation.

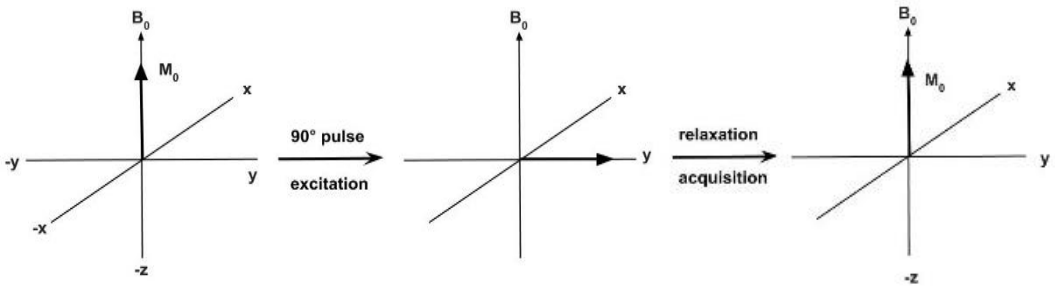

Figure 1.11. The 90°-pulse sequence

1.3.2.3. Acquisition and processing

A free induction decay (FID) signal, as mentioned above, is obtained during the relaxation. The FID signal is a mixture of all nuclear frequencies and must be converted to a frequency-domain spectrum for further analysis. The conversion is made via a mathematical method known as Fourier transformation, shown in Figure 1.12. (Adapted from http://mriquestions.com/fourier-transform-ft.html) The relaxation time is called spin-lattice relaxation time, denoted as T1.

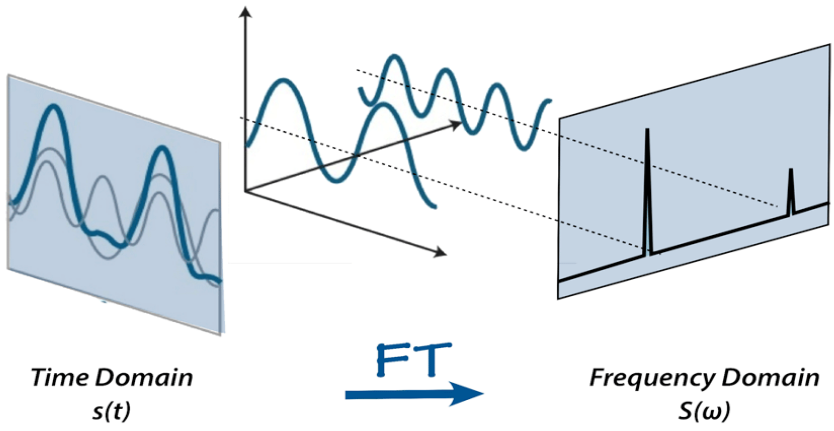

Figure 1.12. A time-domain function (the FID, on left), which contains two individual frequencies, is converted into a frequency-domain function (the spectrum, on right). Adapted from http://mriquestions.com/fourier-transform-ft.html

1.3.3 Solid-state Magic Angle Spinning (MAS) NMR

Solution NMR spectra consist of sharp peaks because the anisotropic interactions are canceled out by rapid random tumbling. By contrast, solid-state NMR spectra are generally broad due to the strong orientation-dependent interactions (mostly contributed from dipolar interactions). Magic-angle spinning (MAS) is a great method to minimize the large anisotropic NMR interactions between nuclei. In MAS, artificial spinning is introduced by place the axis of the sample rotor (Figure 1.13) at magic angle (54.7^0) against $\mathbf{B_0}$, to mimic fast molecular motions in solution conditions, depicted in Figure 1.13. Several Bruker-type MAS rotors are shown in Figure 1.13. Typically, the dipolar interactions are in the range of 1-50 kHz, which for instance, covers up to 170 ppm in a 300 MHz proton spectrum. Standard NMR probes spin from 7 to 35 kHz. The presence of broad NMR line shapes used to be considered a hindrance, but now they actually provide tremendous information of chemistry, structure and dynamics in solid-state materials.

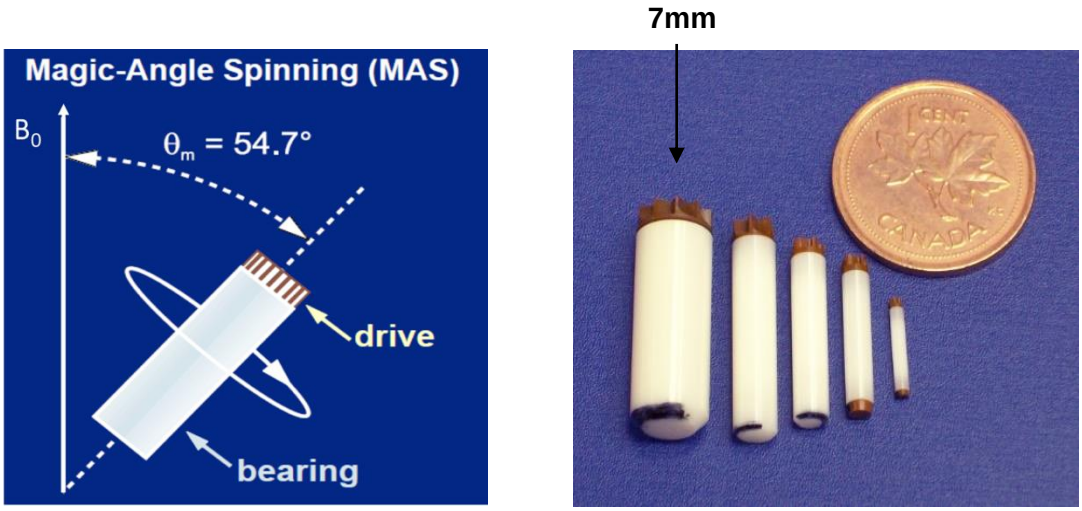

Figure 1.13. Magic Angle spinning **(left)**, adapted from http://schmieder.fmp-berlin.info/teaching/selenko_seminars/solids_rossum5.pdf, and Bruker-type rotors **(right)**

1.3.4 Variable temperature NMR technique

A solid-state NMR can be modified to approach variable temperature (VT) demands. The combination of variable temperature and in-situ solid-state NMR has provided great approaches for heterogeneous catalysis studies. This brings the convenience of investigating the dynamics, kinetics, transition energies, activities, mechanisms, chemical exchanges, etc. Importantly, VT in-situ NMR has provided a facile way to study the initial stages of catalytic reactions, for instance, the early products and mechanisms zeolite-based methanol to hydrocarbon conversion, which is always an interesting and challenging area.

There are multiple types of techniques that can provide variable temperature needs for in-situ NMR. The most common one is approached by flowing hot/cold gas onto the rotor inside the stator, illustrated in Figure 1.14[44]. The heating gas can be dry air at lower temperature (usually below 150 ℃), but has to be dry N_2 above 150 ℃ to protect the electronics inside the probe from being oxidized. Because the hot gas flow is blown on the center of the rotor, there exists a temperature gradient from the center to each end. Also a thermocouple measuring the temperature of the gas in the stator is placed outside the rotor, so there is a deviation of the temperature measurements. One can run control VT experiments to have a sense of the deviation. For example, hexamethylbenzene (HMB), which has melting point at 165 ℃, is usually used as a standard for temperature correction. A broad solid-like spectrum is dramatically changed to a sharp liquid-like spectrum when the temperature reaches 165 ℃. By comparing to the temperature read by the thermocouple, a deviation can be estimated. The VT method in this dissertation (Chapter IV) is adapted on a Chemmagnetic NMR, which provides a smooth control of temperature from room 25 ℃ to 250 ℃.

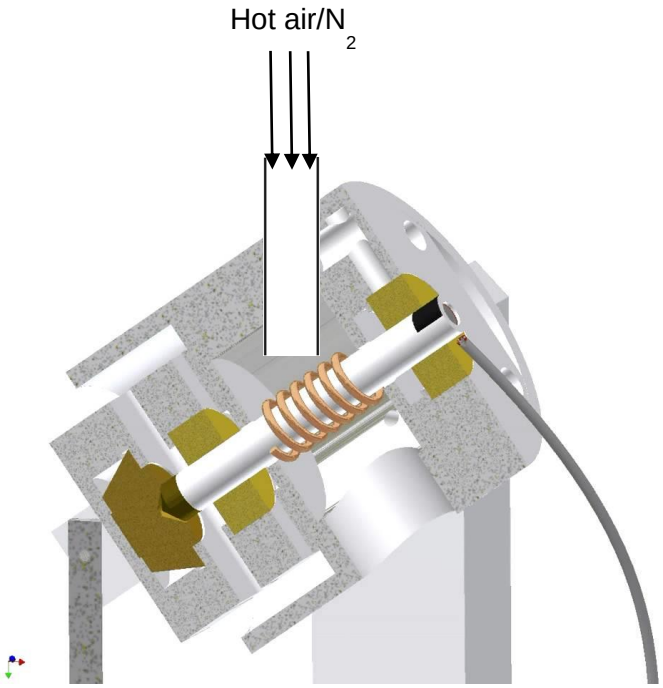

Figure 1.14. Showing of variable-temperature setup in a MAS stator. Hot dry air or nitrogen gas is flowed onto the center of the rotor for heating or cooling, reproduced from reference 44.

1.4 Chemical exchange

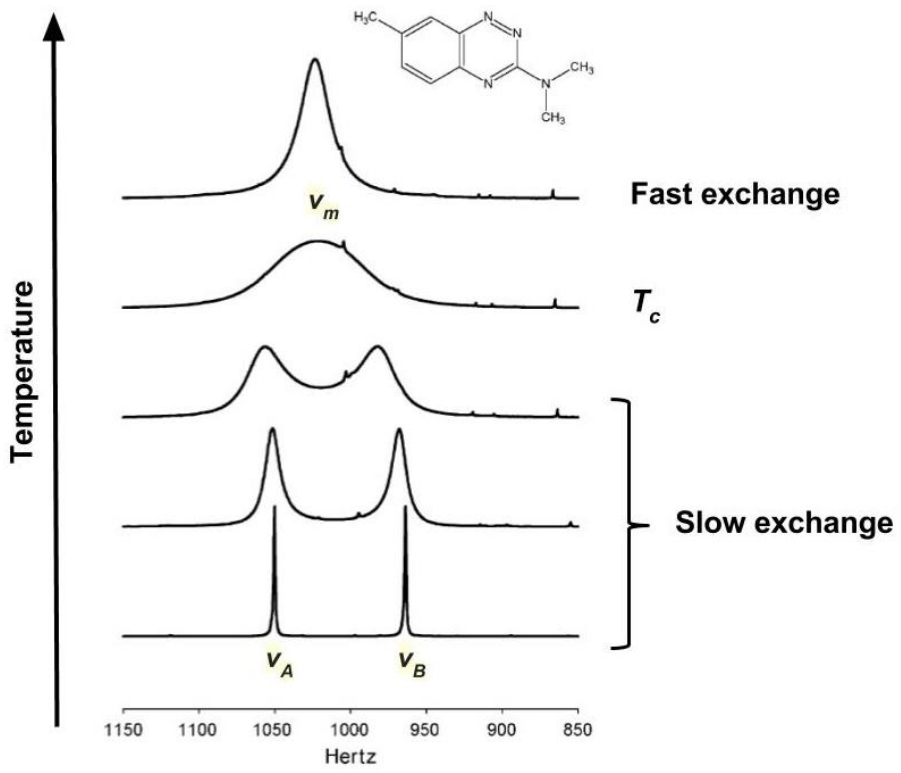

Figure 1.15. Schematic depiction of chemical exchange characterized by NMR spectroscopy, reproduced from reference 45.

The NMR spectroscopic methods are powerful for resolving chemical exchanges. Figure 1.15 illustrates variable temperature NMR spectra of a two-site chemical exchange:

$$A \rightleftharpoons B$$

At low temperatures, noted as "slow exchange" in Figure 1.15[45], where the exchanging rate/frequency k_{AB} is much slower than the difference of the resonant frequencies between A and B, i.e. $\Delta\nu$ $(= \nu_A - \nu_B)$, the peaks are well resolved. As the temperature increases, shown in the middle spectrum labeled as T_c, where k_{AB} reaches the time scale of $\Delta\nu$, the chemical exchange is in coalescence with the resonance difference, the two resonances merge to an averaged

resonance. The averaged peak will get narrower by further increase of the temperature, reaching the condition known as the fast exchange regime.

With fast exchange happening between the two sites A and B, the single centered average frequency can be found at,

$$\upsilon = f_A \upsilon_A + f_B \upsilon_B \qquad \text{Equation 1.3}$$

f_A and f_B stand for the weight population fraction of site A and B, respectively.

The apparent T_1 and T_2 of the centered peak related to the original sites A and B as,

$$\frac{1}{T_1} = \frac{1}{T_{1A}} + \frac{1}{T_{1B}} \qquad \text{Equation 1.4}$$

$$\frac{1}{T_2} = \frac{1}{T_{2A}} + \frac{1}{T_{2B}} \qquad \text{Equation 1.5}$$

The exchange rate at coalescence temperature is,

$$k_{T_c} = \frac{\pi}{\sqrt{2}} |\upsilon_A - \upsilon_B| \qquad \text{Equation 1.6}$$

The chemical exchange mechanism has been well studied and is powerful to reveal the water-zeolite interaction in Chapter II.

1.4. References

1. Ilias, S.; Bhan, A., Mechanism of the Catalytic Conversion of Methanol to Hydrocarbons. *ACS Catalysis* **2013,** *3* (1), 18-31.
2. Wu, X.; Anthony, R. G., Effect of Feed Composition on Methanol Conversion to Light Olefins over SAPO-34. *Applied Catalysis A: General* **2001,** *218* (1–2), 241-250.

3. van Niekerk, M. J.; Fletcher, J. C. Q.; O'Connor, C. T., Effect of Catalyst Modification on the Conversion of Methanol to Light Olefins over SAPO-34. *Applied Catalysis A: General* **1996,** *138* (1), 135-145.

4. Chen, K.; Damron, J.; Pearson, C.; Resasco, D.; Zhang, L.; White, J. L., Zeolite Catalysis: Water Can Dramatically Increase or Suppress Alkane C–H Bond Activation. *ACS Catalysis* **2014,** *4* (9), 3039-3044.

5. Hibbitts, D. D.; Loveless, B. T.; Neurock, M.; Iglesia, E., Mechanistic Role of Water on the Rate and Selectivity of Fischer–Tropsch Synthesis on Ruthenium Catalysts. *Angewandte Chemie* **2013,** *125* (47), 12499-12504.

6. Barron, B. J.; Wong, W.-T.; Chiu, P.; Hii, K. K., "Goldilocks Effect" of Water in Lewis-Brønsted Acid and Base Catalysis. *ACS Catalysis* **2016**, 4189-4194.

7. Motokura, K.; Matsunaga, S.; Noda, H.; Miyaji, A.; Baba, T., Water-Accelerated Allylsilylation of Alkenes Using a Proton-Exchanged Montmorillonite Catalyst. *ACS Catalysis* **2012,** *2* (9), 1942-1946.

8. Sherman, J. D., Synthetic Zeolites and other Microporous Oxide Molecular Sieves. *Proceedings of the National Academy of Sciences* **1999,** *96* (7), 3471-3478.

9. Jiří Čejka, H. v. B. A. C.; Ferdi, S., Studies in Surface Science and Catalysis. Elsevier: 2007; Vol. Volume 168.

10. Niwa, M.; Katada, N.; Okumura, K., Characterization and Design of Zeolite Catalysts: Solid Acidity, Shape Selectivity and Loading Properties. *Springer Berlin Heidelberg*: **2010**.

11. Wang, H.; Pinnavaia, T. J., MFI Zeolite with Small and Uniform Intracrystal Mesopores. *Angewandte Chemie International Edition* **2006,** *45* (45), 7603-7606.

12. Valiullin, R.; Kärger, J.; Cho, K.; Choi, M.; Ryoo, R., Dynamics of Water Diffusion in Mesoporous Zeolites. *Microporous and Mesoporous Materials* **2011,** *142* (1), 236-244.

13. Garcia-Martinez, J.; Xiao, C.; Cychosz, K. A.; Li, K.; Wan, W.; Zou, X.; Thommes, M., Evidence of Intracrystalline Mesostructured Porosity in Zeolites by Advanced Gas Sorption, Electron Tomography and Rotation Electron Diffraction. *ChemCatChem* **2014,** *6* (11), 3110-3115.

14. Thomas, J. M., The Societal Significance of Catalysis and the Growing Practical Importance of Single-Site Heterogeneous Catalysts. *Proceedings of the Royal Society A: Mathematical, Physical and Engineering Science* **2012,** *468* (2143), 1884-1903.

15. Jones, A. J.; Iglesia, E., The Strength of Brønsted Acid Sites in Microporous Aluminosilicates. *ACS Catalysis* **2015,** *5* (10), 5741-5755.

16. Brändle, M.; Sauer, J., Acidity Differences between Inorganic Solids Induced by Their Framework Structure. A Combined Quantum Mechanics/Molecular Mechanics ab Initio Study on Zeolites. *Journal of the American Chemical Society* **1998,** *120* (7), 1556-1570.

17. Zhang, L.; Chen, K.; Chen, B.; White, J. L.; Resasco, D. E., Factors that Determine Zeolite Stability in Hot Liquid Water. *Journal of the American Chemical Society* **2015,** *137* (36), 11810-11819.

18. Janda, A.; Vlaisavljevich, B.; Lin, L.-C.; Smit, B.; Bell, A. T., Effects of Zeolite Structural Confinement on Adsorption Thermodynamics and Reaction Kinetics for Monomolecular Cracking and Dehydrogenation of n-Butane. *Journal of the American Chemical Society* **2016,** *138* (14), 4739-4756.

19. Baerlocher, C.; McCusker, L. B.; Olson, D. H., In Atlas of Zeolite Framework Types, *Sixth ed.; Elsevier Science B.V.:* **2007**.

20. Flanigen, E. M.; Broach, R. W.; Wilson, S. T., Introduction In Zeolites in Industrial Separation and Catalysis, *Wiley-VCH Verlag GmbH & Co. KGaA:* **2010**; pp 1-26.

21. Gounder, R. P. Consequences of Confinement in Zeolite Acid Catalysis. Ph.D., University of California, Berkeley, Ann Arbor, **2011**.

22. Jones, A. J.; Carr, R. T.; Zones, S. I.; Iglesia, E., Acid Strength and Solvation in Catalysis by MFI Zeolites and Effects of the Identity, Concentration and Location of Framework Heteroatoms. *Journal of Catalysis* **2014,** *312* (0), 58-68.

23. Gounder, R.; Iglesia, E., The Catalytic Diversity of Zeolites: Confinement and Solvation Effects within Voids of Molecular Dimensions. *Chemical Communications* **2013,** *49* (34), 3491-3509.

24. Gounder, R.; Jones, A. J.; Carr, R. T.; Iglesia, E., Solvation and Acid Strength Effects on Catalysis by Faujasite Zeolites. *Journal of Catalysis* **2012,** *286*, 214-223.

25. Gounder, R.; Iglesia, E., Effects of Partial Confinement on the Specificity of Monomolecular Alkane Reactions for Acid Sites in Side Pockets of Mordenite. *Angewandte Chemie International Edition* **2010,** *49* (4), 808-811.

26. Janda, A.; Vlaisavljevich, B.; Lin, L.-C.; Mallikarjun Sharada, S.; Smit, B.; Head-Gordon, M.; Bell, A. T., Adsorption Thermodynamics and Intrinsic Activation Parameters for Monomolecular Cracking of n-Alkanes on Brønsted Acid Sites in Zeolites. *The Journal of Physical Chemistry C* **2015,** *119* (19), 10427-10438.

27. Janda, A.; Bell, A. T., Effects of Si/Al Ratio on the Distribution of Framework Al and on the Rates of Alkane Monomolecular Cracking and Dehydrogenation in H-MFI. *Journal of the American Chemical Society* **2013,** *135* (51), 19193-19207.

28. Schallmoser, S.; Ikuno, T.; Wagenhofer, M. F.; Kolvenbach, R.; Haller, G. L.; Sanchez-Sanchez, M.; Lercher, J. A., Impact of the local environment of Brønsted acid sites in ZSM-5 on the catalytic activity in n-pentane cracking. *Journal of Catalysis* **2014,** *316*, 93-102.

29. Argauer, R. J.; Landolt, G. R., U.S. Patent US3702886 A (1972), Crystalline Zeolite ZSM-5 and Method of Preparing the Same.

30. Dědeček, J.; Sobalík, Z.; Wichterlová, B., Siting and Distribution of Framework Aluminium Atoms in Silicon-Rich Zeolites and Impact on Catalysis. *Catalysis Reviews* **2012,** *54* (2), 135-223.

31. Eroshenko, V.; Regis, R.-C.; Soulard, M.; Patarin, J., Energetics: A New Field of Applications for Hydrophobic Zeolites. *Journal of the American Chemical Society* **2001,** *123* (33), 8129-8130.

32. Trzpit, M.; Soulard, M.; Patarin, J.; Desbiens, N.; Cailliez, F.; Boutin, A.; Demachy, I.; Fuchs, A. H., The Effect of Local Defects on Water Adsorption in Silicalite-1 Zeolite: A Joint Experimental and Molecular Simulation Study. *Langmuir* **2007,** *23* (20), 10131-10139.

33. Pashkova, V.; Sklenak, S.; Klein, P.; Urbanova, M.; Dědeček, J., Location of Framework Al Atoms in the Channels of ZSM-5: Effect of the (Hydrothermal) Synthesis. *Chemistry – A European Journal* **2016,** *22* (12), 3937-3941.

34. Liang, T.; Chen, J.; Qin, Z.; Li, J.; Wang, P.; Wang, S.; Wang, G.; Dong, M.; Fan, W.; Wang, J., Conversion of Methanol to Olefins over H-ZSM-5 Zeolite: Reaction Pathway Is Related to the Framework Aluminum Siting. *ACS Catalysis* **2016,** *6* (11), 7311-7325.

35. Perea, D. E.; Arslan, I.; Liu, J.; Ristanovic, Z.; Kovarik, L.; Arey, B. W.; Lercher, J. A.; Bare, S. R.; Weckhuysen, B. M., Determining the Location and Nearest Neighbours of Aluminium in Zeolites with Atom Probe Tomography. *Nat Commun* **2015,** *6*.

36. Vjunov, A.; Fulton, J. L.; Huthwelker, T.; Pin, S.; Mei, D.; Schenter, G. K.; Govind, N.; Camaioni, D. M.; Hu, J. Z.; Lercher, J. A., Quantitatively Probing the Al Distribution in Zeolites. *Journal of the American Chemical Society* **2014,** *136* (23), 8296-8306.

37. Di Iorio, J. R.; Gounder, R., Controlling the Isolation and Pairing of Aluminum in Chabazite Zeolites Using Mixtures of Organic and Inorganic Structure-Directing Agents. *Chemistry of Materials* **2016,** *28* (7), 2236-2247.

38. Yokoi, T.; Mochizuki, H.; Namba, S.; Kondo, J. N.; Tatsumi, T., Control of the Al Distribution in the Framework of ZSM-5 Zeolite and Its Evaluation by Solid-State NMR Technique and Catalytic Properties. *The Journal of Physical Chemistry C* **2015,** *119* (27), 15303-15315.

39. Dedecek, J.; Balgová, V.; Pashkova, V.; Klein, P.; Wichterlová, B., Synthesis of ZSM-5 Zeolites with Defined Distribution of Al Atoms in the Framework and Multinuclear MAS NMR Analysis of the Control of Al Distribution. *Chemistry of Materials* **2012,** *24* (16), 3231-3239.

40. Becker, E. D., A Brief History of Nuclear Magnetic Resonance. *Analytical Chemistry* **1993,** *65* (6), 295A-302A.

41. Bloch, F.; Hansen, W. W.; Packard, M., The Nuclear Induction Experiment. *Physical Review* **1946,** *70* (7-8), 474-485.

42. Bloch, F.; Hansen, W. W.; Packard, M., Nuclear Induction. *Physical Review* **1946,** *69* (3-4), 127-127.

43. Purcell, E. M.; Torrey, H. C.; Pound, R. V., Resonance Absorption by Nuclear Magnetic Moments in a Solid. *Physical Review* **1946,** *69* (1-2), 37-38.

44. Barnes, A. B.; Mak-Jurkauskas, M. L.; Matsuki, Y.; Bajaj, V. S.; van der Wel, P. C. A.; DeRocher, R.; Bryant, J.; Sirigiri, J. R.; Temkin, R. J.; Lugtenburg, J.; Herzfeld, J.; Griffin, R. G., Cryogenic Sample Exchange NMR Probe for Magic Angle Spinning Dynamic Nuclear Polarization. *Journal of Magnetic Resonance* **2009,** *198* (2), 261-270.

45. Bain, A. D., Chemical exchange in NMR. *Progress in Nuclear Magnetic Resonance Spectroscopy* **2003,** *43* (3–4), 63-103.

CHAPTER II

COMPREHENSIVE INSIGHTS INTO WATER INTERACTIONS IN ZEOLITE CATALYSTS

2.1. Introduction

Solid-acid catalysts are valuable in many existing industrial hydrocarbon conversion processes, the majority of which occur in the gas-phase, but are also promising for new applications in biomass utilization and environmental remediation.[1-3] Microporous zeolites with pore diameters in the sub-nanometer range are the most commonly employed solid-acid catalysts, although variations in hydrocarbon distributions from currently available petroleum sources have generated interest in mesoporous aluminosilicates possessing Brønsted acid sites.[4-6] In addition, new solid-acid catalyzed upgrading of renewable feedstocks in the liquid-phase demonstrates the catalytic diversity of zeolite structures.[7-8] Water can be incorporated in the reaction system in the feed or evolved as a side product inside the solid acid catalyst during reaction. For example, in biomass conversion processes, water is a major component of the feedstock[2, 9] and in reactions involving oxygenates (alcohols, aldehydes, acids) water may be produced stoichiometrically in-situ. Such reactions include methanol-to-hydrocarbon, aldol condensation, ketonization, and alkylation catalyzed by zeolites and other solid acids.[10-16] Multiple reports have discussed the difficulty in completely removing water from acidic zeolites.[17-18] Therefore, zeolite catalysis is an attractive route for their catalytic upgrading, but traditional vapor phase chemistries pose problems for

cellulosic and saccharide-based feedstocks. Due to the high internal surface area of microporous zeolites and their mesoporous analogues, and the hydrophilicity of Brønsted acid sites, water is likely to present at some level in many existing reactions,[19] including gas phase chemistry at elevated temperatures. Recently, Resasco and coworkers have shown that zeolite catalyzed reactions in water is a viable route for conversion of some biomass molecules, based on hydrophobic modifications of zeolite crystallites designed to prevent their dealumination in an aqueous solvent environment.[9, 20] The degree to which water positively or negatively influences reaction chemistries should depend upon the relative water loading present near the solid acid site in a zeolite under reaction conditions. In addition, the dynamics of water diffusion and the average distance between solid acid sites will also contribute to the impact of co-adsorbed water, i.e., water which is simultaneously proximate to the acid site in the presence of reagent and product molecules. Recent reports suggest that water provides an assisting role in stabilizing transition states and side-chain elimination reactions in methanol-to-hydrocarbon chemistry, where the origin of this water comes from acid-catalyzed methanol conversion to dimethyl ether.[21] This stoichiometric water represents one extreme in reaction conditions, in which water is produced from the reagent at the active site, which can be contrasted to the case where water is present as a solvent or as part of a biphasic solvent system.

The fundamental water-zeolite chemistry has been continuously studied for over three decades. In 2000, Olson et al. revealed a detailed isothermal study for zeolite and water interactions.[19] While to further obtain molecular level information, solid state NMR has been playing important roles. The application of NMR into basic water-zeolite study started from late 1980s. In 1996, Hunger and Freude thoroughly reviewed the previous achievements of water-zeolite studies via solid state NMR technologies and proposed plausible molecular mechanisms.[22] Later, neutron diffraction came into this series water zeolite research, and evidently showed that both H_2O and H_3O^+ are present in water loaded HSAPO-34 zeolite, led by Smith et al.[23] It is well

accepted that water clusters are more basic than a single water molecule, which means, the former is easier to deprotonate the Brønsted proton than latter.[24-27] Whereas it was not clear how much water is necessary to deprotonate the Brønsted acid site. Haw claimed one water molecule is not able to deprotonate an acid site, based on ^{27}Al MAS NMR results.[27] On the contrary, our results, with better control of water loadings and ^{1}H MAS NMR, which is more sensitive to water-zeolite interactions than ^{27}Al NMR, suggest the acid proton could possibly be deprotonated by only one water molecule, at least for the case of Si/Al = 15 HZSM-5 catalyst. There have been long-time debates about whether water can mediate the proton transfer,[28-29] a recent Neutron diffraction experiment has revealed that water can mediate the proton transfer, even in undetectable amounts.[30] Starting with Sauer,[25, 31] the computational method has become an significant tool to reach molecular level interactions. Despite the variety of technologies, solid state NMR is still one of the most powerful methods in this series of research. For example, a calcined HZSM-5 spectrum always has a shoulder on the downfield of acid peak at 5-7 ppm region. This broad signal was believed to be residual ammonium after calcination or secondary acid sites[32] for almost two decades, whereas it is experimentally proven to be residual water by Grey group, in 2009, via basic single pulsed NMR method.[17]

In this chapter, solid state MAS and diffusion NMR techniques are used to examine the behavior of water in acidic HZSM-5 zeolites with different Si/Al ratio as function of water loading, ranging from about 0.3 water molecule per unit cell (0.05 eqv) up to ca. 500 water molecules per unit cell (excess amounts). The experiments were designed to (1) directly probe the interaction of water with the interior surface of acidic zeolites, including the acid site itself, (2) measure the diffusion coefficient of water inside zeolites as a function of water loading and acid site density, and (3) investigate whether specific chemical modifications designed to increase catalyst stability in water alters the molecular-level behavior of water within the catalyst particles. In this research, we sort the water loading-dependent interactions into three stage: 0 ~ 0.05 eqv,

0.05 ~ 3 eqv and 3 ~ +∞. The interaction types and possible proton species in each stage are discussed thoroughly. A new model, the "coverage sphere", which is consistent with most of the NMR observations, is proposed. The pulsed field gradient NMR measurements and adsorption experiments on hydrophobically-modified catalysts have both shown consistent information to the regular ^{1}H NMR results.

2.2. Experimental

2.2.1. Zeolite activation. Zeolite ZSM-5 samples with different aluminum content (Si/Al=15 CBV 3024E and Si/Al= 40 CBV 8014) were obtained from Zeolyst in the ammonium-exchanged form**.** As reported by the vendor, the average crystallite size of all these samples was 1μm, the BET surface areas vary from 379-386 m^2/g independent of Si/Al ratios.[18] SEM experiments indicated that the average particle size was closer to 0.6-0.7 μm. Calcined and dehydrated zeolite samples were prepared from the ammonium form in a glass reactor body via a stepwise vacuum procedure. The temperature controller was a 6-zone ramp/soak controller, model CN616 purchased from Omega Engineering, Inc. The ZSM-5 samples were heated via the following procedure: heat from room temperature to 110 °C at 1 °C/min, hold at 110 °C for 1 hour, heat to 500 °C at 2 °C/min, hold at 500 °C for 8 hours, and then power off. High vacuum conditions with pressures of 2×10^{-5} torr during the activation were achieved with an Edwards EO4K diffusion pump. Dry catalyst samples were sealed and immediately placed in a dry argon glove box following activation in order to facilitate transfer to zirconia MAS rotors for the in-situ experiments. Complete calcination and dehydration of samples was verified by ^{1}H MAS NMR. Figure 2.1 displays the ^{1}H NMR spectra before and after activation: in spectrum a), the peaks at 7.2 ppm and 4.0 ppm respond to protons in ammonium ions and adsorbed water, respectively; in spectrum b) 4.2 ppm and 2.0 ppm respond to protons at acid sites and silanol groups, respectively.

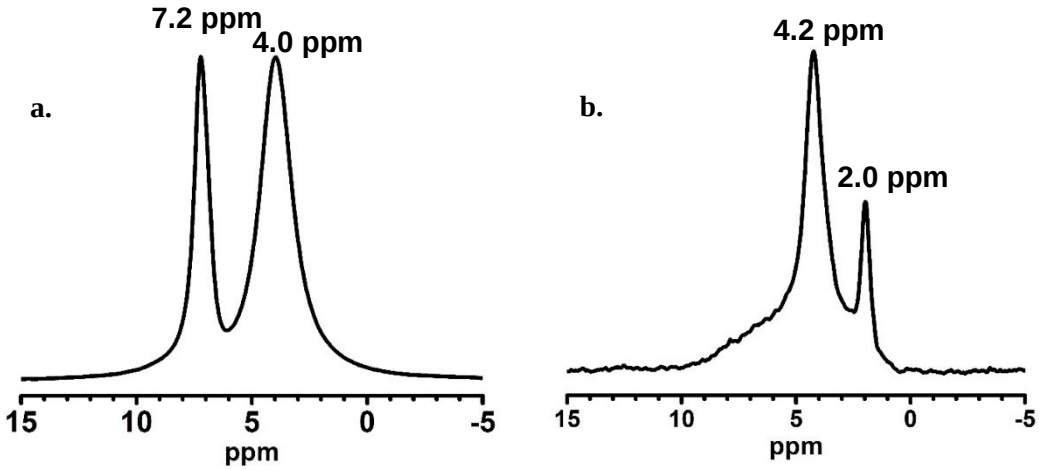

Figure 2.1. ^{1}H NMR spectra of: a) NH_4^+-ZSM-5 and b) H^+-ZSM-5 catalysts.

2.2.2. Preparation of hydrophobic zeolites. Following a previous hydrophobic functionalization procedure,[18] the organosilanes ethyltrichlorosilane (ETS) and octadecyltrichlorosilane (OTS)

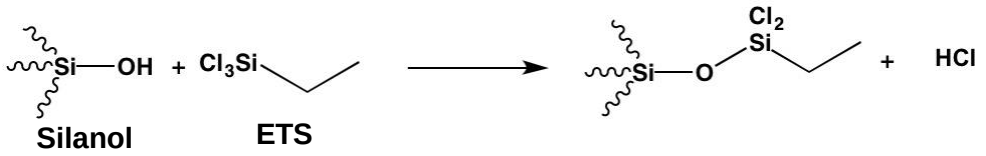

Figure 2.2. Hydrophobic functionalization of silanol groups, using ETS as an example.

were used as reagents to increase the hydrophobicity of the zeolite crystallites, illustrated in Figure 2.2. In this procedure, 1 g of NH_4^+-ZSM5 (15) was dispersed in 20 ml of toluene by sonication with a Horn sonicator (Fisher Scientific 600 W, 20 kHz) at 25% amplitude. Then, the zeolite suspension was added to a 50 mL solution of ETS (0.5 mmol/g zeolite) in toluene (ETS and toluene provided by Sigma Aldrich). The final suspension was stirred for 24 h at 500 rpm at room temperature. The zeolite was then collected by filtration with a nylon filter (0.22 μm pore size). After washing several times with ethanol, the functionalized zeolite was dried at 100 °C

overnight. OTS-NH_4^+-ZSM5 (15) was obtained the same way. Activation procedures for dehydration were identical to that of the normal H^+-ZSM-5 catalysts. Figure 2.3 compares ^1H NMR spectra of calcined regular HZSM-5 (left) and ETS modified ZSM-5 (right). The ethyl groups on ETS show a strong signal at 1 ppm while the acid site peak is still resolved, indicating the successful modification and that no involvement of acid sites in the reaction.

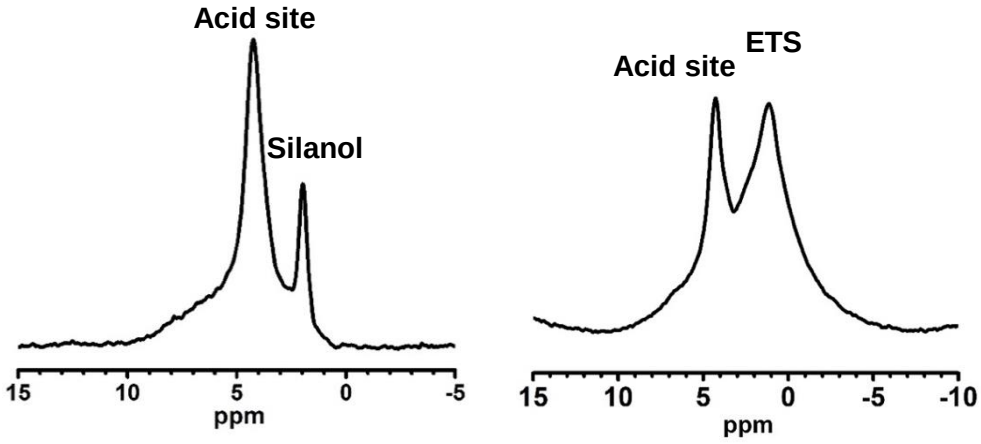

Figure 2.3. Representative ^1H MAS NMR spectra for calcined and dehydrated **(left)** HZSM-5 and **(right)** ETS-HZSM-5.

2.2.3. Water adsorption.

Water was introduced to zeolite samples from both vapor phase and liquid phase. For convenience, all water loading values are reported as the number of water molecules per unit cell. Vapor-phase adsorptions are expected for water adsorptions less than 32 molecules per unit cell, and liquid-phase adsorptions for >32/u.c. To adsorb water from vapor phase fast and qualitatively, in-situ adsorption was applied by opening the NMR rotor cap to allow catalyst exposure to the ambient environment. To quantitatively adsorb vapor-phase water, two methods are optimum: vacuum line adsorption and gravimetric adsorption. Notice that initial loosely packed catalysts in NMR rotor are always centrifuged to a thin and tight layer, ca. 1 mm, against the interior rotor wall by MAS, shown in Figure 2.4. Practically, adsorption applied before and

after spinning can cause different adsorption rate, faster in the latter case, but does not affect the equilibrium.

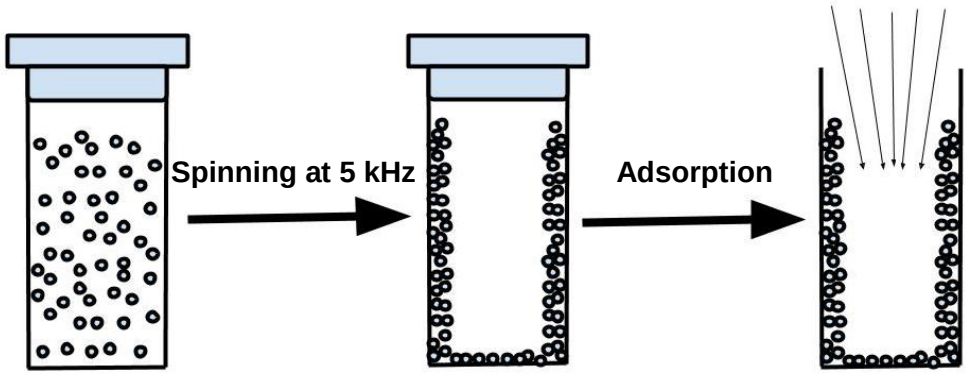

Figure 2.4. Schematic diagram showing ambient water-vapor adsorption in a rotor after Magic Angle Spinning.

Gravimetric methods are conducted by adsorbing water vapor from ambient environment. Dry zeolite samples were first sealed inside the glove box in NMR rotors or plastic weigh boats and then taken out to the ambient environment for adsorption. The amount of water loaded from the vapor phase was controlled by the various exposure times to ambient environment, with weight changes measured by a microbalance. Via this method, real time measurements of water adsorptions can be obtained, as shown in Figure 2.5.

Vacuum line adsorption methods are good for any amount of water below 32 water molecules per unit cell. This method has better control of water amounts, however, it takes much longer preparation time and only works for less than 60 mg catalyst each time. The vacuum line method is good for extreme small amounts of water, for instance, below 0.5 eqv. A vacuum adsorption was set up with a vacuum line equipped with a CAVERN type apparatus. Typically, a fixed quantity of catalyst was placed in a 7 mm zirconia MAS NMR rotor in the CAVERN, evacuated and sealed, and the adsorbate vapor introduced in the vacuum line to an initial

pressure. A desired pressure drop is used to control the adsorption quantity after exposure to the catalyst. The initial pressure and pressure drop vary with the vacuum line/CAVERN body volumes, the adsorbate molecules, the catalyst quantities and their Si/Al ratios. For example, to adsorb 1 eqv H_2O onto HZSM-5 with Si/Al = 15, 40 mg of catalyst was loosely packed into the rotor. Subsequently, 10 torr of initial pressure and 3.2 torr of pressure drop were used to determine when 1 eqv of benzene was adsorbed. Brønsted acid site densities are calculated from Si/Al ratios (e.g. acid density = 1.04 mmol/g for Si/Al = 15), even though literature has shown that the acid site content is less than that predicted from Al content.[33]

To adsorb higher loading of water, direct injections of liquid water are needed. Typically, controlled volumes of liquid water were injected to known amount of dry zeolite by a GC microsyringe. For convenience, all water loading values are converted and reported as number of water molecules per unit cell or water molecules per acid site, e.g. 1 μL water adsorbed on 50 mg HZSM-5 (15) results in 5~6 molecule/u.c. For convenience, the relationship of the loading units for HZSM-5 (15) is: 6 molecules/u.c. = 1 molecule/acid site = 1 eqv, with detailed calculation shown in Table 1.1.

2.2.4. NMR measurements. ^{1}H MAS NMR data were collected on a Bruker DSX-300 MHz spectrometer, with spinning rate of 5 kHz, using a single 3.8 μs π/2 excitation pulse. Recycle delays were 10 seconds for dry zeolites, and 1 second for all water-exposed samples. While faster MAS speeds are accessible in our laboratory, it is well known that increased MAS rates do not provide decreased linewidths over that obtained at 5 kHz, as protons are dilute spins in these zeolites.[34] It is important to note that background subtractions are generally required for analysis of ^{1}H MAS NMR spectra, because the proton density in zeolites are small, resulting in weak signals at the scale of the probe background signal.

Diffusion measurements were taken with a Bruker Ascend 400 MHz spectrometer with maximum gradients of 30 T/m. The stimulated echo pulse sequence with a longitudinal eddy

current delay of 5 ms was used to measure the attenuation.[35] The diffusion coefficient, D, was calculated from the following equation:

$$\ln\left(\frac{I_g}{I_{g=0}}\right) = -D(\gamma\delta g)^2\left(\Delta - \frac{\delta}{3}\right)$$

The intensity of a signal when a given gradient was used is represented by *I*, and gyromagnetic ratio for ^{1}H is represented by γ. The gradient strength, g, was varied from 0 T/m to 15 T/m. The gradient duration, δ, and the diffusion time, Δ, were held constant at 0.2 ms and 10 ms, respectively. For data sets that exhibited two diffusion coefficients, the equation was modified to account for the signal from each fraction, and the sum of the fractions, *f*, was set to 1.

$$\ln\left(\frac{I_g}{I_{g=0}}\right) = f_1\left[-D_1(\gamma\delta g)^2\left(\Delta - \frac{\delta}{3}\right)\right] + f_2\left[-D_2(\gamma\delta g)^2\left(\Delta - \frac{\delta}{3}\right)\right]$$

2.2.5. TGA. Thermal gravimetric analysis (TGA) data were collected by Hi-Res TGA 2950 Thermogravimetric Analyzer from TA Instrument. Inc. Samples were heated from room temperature to 900 °C, with a heating ramp of 20 °C / min. Dry air was used as the carrier gas.

2.3. Results and discussion

2.3.1. Gravimetric measurement

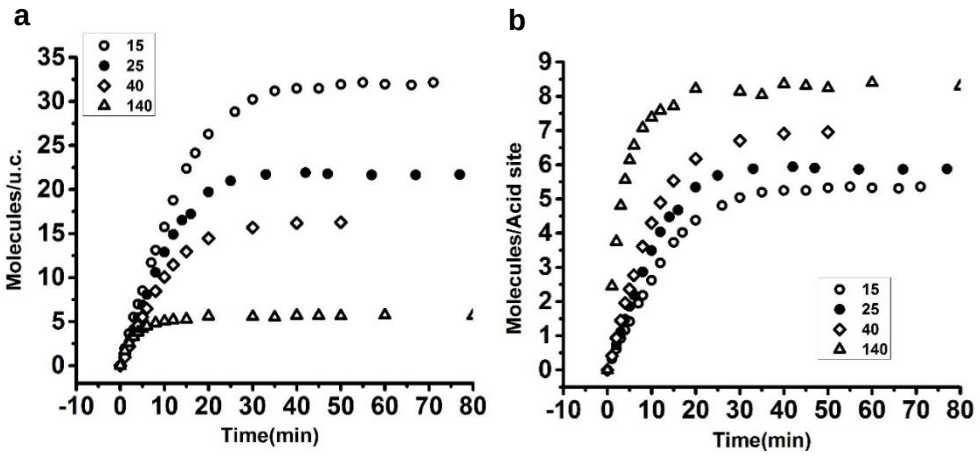

Figure 2.5. Gravimetrically determined water uptake rates and maximum loadings for dehydrated acidic HZSM-5 catalysts exposed to ambient moisture, plotted as a function of (a) number of water molecules per unit cell, and (b) number of water molecules per acid site. Different Si/Al ratios are identified in each legend. The catalyst particle bed thickness was 1-2 mm on average.

Ambient moisture is a convenient water vapor resource; its low water vapor partial pressure allows facile control of the water loading just by varying the exposure time. To adsorb water, HZSM-5 zeolites obtained from calcination and dehydration as described in section 2.2.1, were exposed to ambient humidity and pressure. Figure 2.5 displays water uptake curves for HZSM-5 catalysts with Si/Al ratio ranging from 15 to 140. It is apparent from Figure 2.5a that the adsorption rate, as well as the maximum water uptake, is higher with an increasing acid density (lower Si to Al ratio). Even though the catalyst bed thickness and the ambient humidity were not controlled exactly from run to run, the maximum uptake should reflect the unique water loading dependence on each catalyst. Note that for ZSM-5 (15), the water uptake cannot reach more than ca. 32 molecules per unit cell, or 5-6 molecules per acid site. Olson et al. has reported the

formation of 4-molecule water clusters on acid sites by low pressure isothermal adsorption analysis.[19] Note the capacity varies due to differences of the amounts of extra-framework aluminum sites and silanol groups etc., in different catalysts. In our observation, for more than 5-6 molecules per acid site adsorptions, liquid water must be directly introduced. Data of Figure 2.5b were converted from the same data as in Figure 2.5a, considering that 1 eqv. H_2O = 6 H_2O molecules/u.c. The apparent water cluster size, illustrated in Figure 2.5b, increases with the increase of Si/Al ratio, likely due to the contribution of other sites, i.e. extra-framework Al sites and silanol groups, and becomes relatively higher as the acid site density decreases. In other words, if similar experiments were conducted using defect-free ZSM-5 catalysts at the same Si/Al ratios, the water cluster size should converge, for example, to 4 water molecule per acid site, in Figure 2.5b.

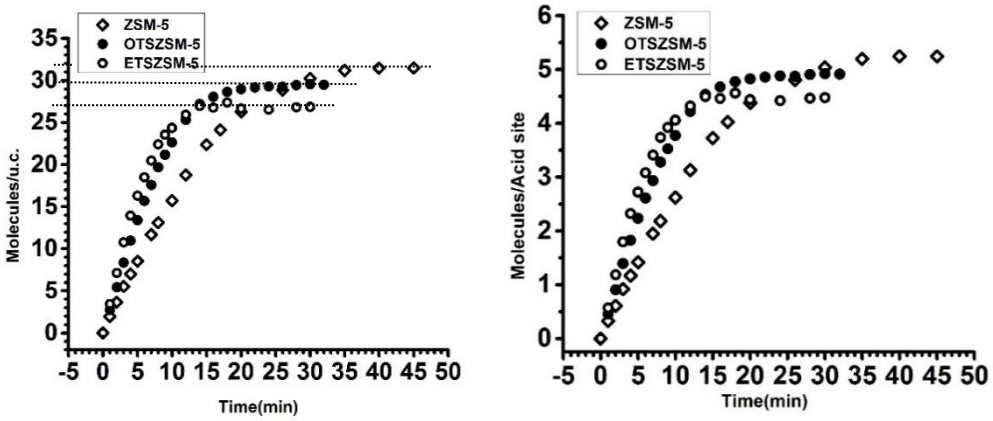

Figure 2.6. Gravimetrically determined water uptake and maximum loadings for an acidic HZSM-5 catalyst (Si/Al = 15) and its hydrophobically-modified analogues treated with ethyl-trichlorosilane (ETS) or octyltrichlorosilane (OTS). Water uptake following exposure to ambient moisture is plotted as a function of **(left)** number of water molecules per unit cell, and **(right)** number of water molecules per acid site.

Hydrophobically modified HZSM-5, prepared using either ethyltricholorosilane (ETS) or octyltricholosilane (OTS), were examined by the same adsorption method as described in Figure 2.5. In the synthesis, each organosilane reagent was in excess, thus each silanol group on the external surface is expected to be functionalized, forming a silyl ether group, depicted in Figure 2.2. The TGA data, obtained by using the heating program from room temperature to 900 °C at a heating ramp of 20 °C/min, illustrate that ETS groups take up ca. 3% of weight in the functionalized ZSM-5 catalyst, shown in Figure 2.7. Figure 2.6 illustrates the comparisons between the adsoption trend of regular HZSM-5, ETS- and OTS-functionalized analagous. Apparently, the modified catalysts (open and closed circles) show less capacity than the regular catalyst (diamond). However, the ETS-modified analogue shows less capacity than the OTS-modified catalyst, maybe due to the possibility that ETS molecules are small enough to enter into the zeolite pores to react with the internal silanol groups, and thus leads to a capacity of ca. 4 molecule/acid site, which is very similar to what Olson obtained in the low pressure isothermal condition. ^{1}H MAS NMR was then used as a spectroscopic tool to explore the molecular-level information of water interactions with these catalyst. In the following sections, the NMR spectrum results will be shown in the trend, where water is added from extremely small amounts to excess amounts. Water was adsorbed via both vapor and liquid phases, into both hydrophillic and hydrophobic zeolites with various Si/Al ratios.

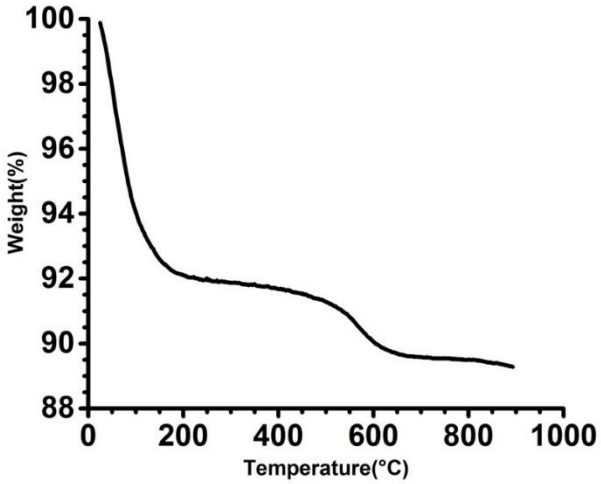

Figure 2.7. Thermal gravimetric analysis (TGA) curves for ETS-HZSM-5, with the experiment done in air. The 8% mass loss at 100-150 °C is from water, and the ca. 3% mass loss near 500 ^{0} C is from decomposition of the surface ETS groups.

2.3.2. Water interactions in zeolite investigated by ^{1}H MAS NMR

In this section, the solid-state NMR method was applied to investigate the interactions of water in zeolites as a function of water loading. To our knowledge, water loadings below 1 eqv have been generally overlooked in literature. However, even such small amounts of water can affect the catalyst activity dramatically, as shown in the following chapters. In this research, quantitative analysis of water in zeolites has been achieved to as low as 0.05 eqv, while even lower loadings have been achieved by semi-qualitative adsorption methods, see Figure 2.15. According to our NMR interpretation, the water-zeolite interaction as an increasing function of water loading described by three stages for convenience, 0 ~ 0.5 eqv, 0.5 ~ 3 eqv, and 3 ~ +∞, or Stage I, II and III, respectively. To clarify, 0.5 and 3 eqv are just suggested values from the NMR results. - The water peak at 5-7 ppm identified by Grey's group, which was controversial for two decades,

should belong to Stage I. To our understanding, Stage I provides more molecular level information of water interactions, which could also provide better understanding for other adsorbate interactions with zeolites, such as methanol and hydrocarbon molecules. Stage II is a transition region of Stage I and III. The following results and discussion will be presented in the sequence of increased water loadings.

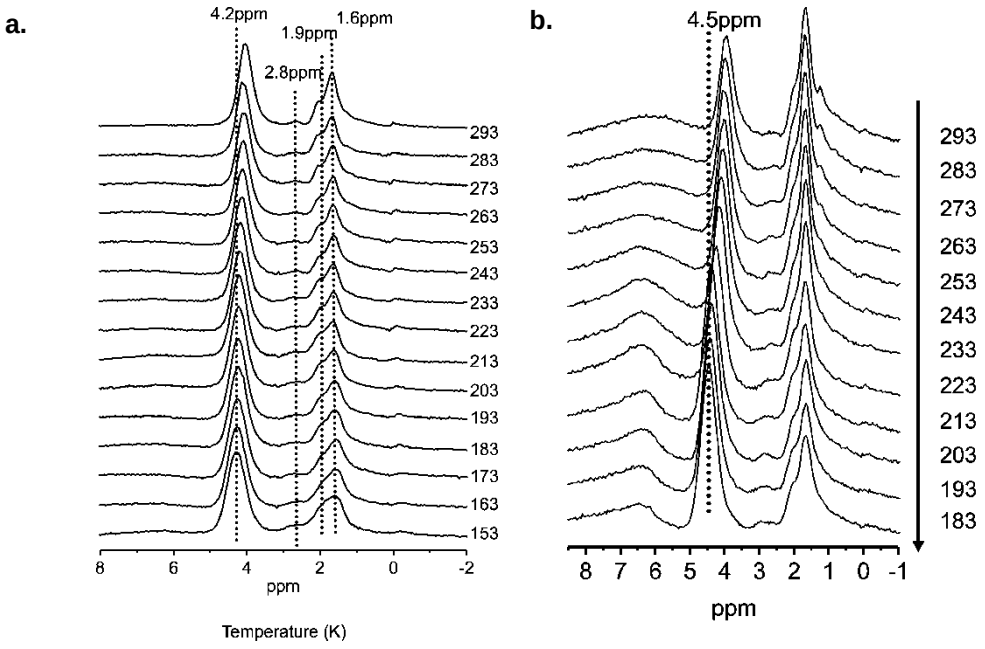

Figure 2.8. Variable NMR spectra of HZSM-5 (15) **(a)** without, and **(b)** with residual water shoulder, adapted from reference 17. Notice at 293K, the acid/silanol peak intensity ratio is apparently higher in **(a)** than **(b)**.

2.3.2.1. Stage I: 0 ~ 0.5 eqv, before the general formation of water clusters

While the gravimetric adsorption experiments revealed the adsorption behavior of water vapor into dry catalyst, more molecular-level information could be obtained via ^{1}H MAS NMR. Theoretically, only three different types of protons should appear in a proton NMR spectrum of H-zeolite, which are, the silanol group at 2 ppm, the aluminum hydroxide (extra-framework Al)

at 3 ppm, and the acid site at 4.2 ppm. Historically, there had usually been a downfield shoulder, unexpected, by the acid peak after calcination treatments, in the range of 5-7, illustrated in Figure 2.1. The unique shoulder used to be incorrectly assigned to a second type of acid site[32], or residual ammonium after calcination[36-38], until Grey's group confirmed that it is a residual water peak[17]. Figure 2.8, adapted from Grey's paper, clearly illustrates that the peak at 5-7 ppm, as seen in Figure 2.8b, was totally removed in Figure 2.8a.

Figure 2.9 shows representative ^{1}H MAS NMR spectra of HZSM-5 catalysts with four different Si/Al ratios, each of which was exposed to ambient vapor-phase water in a 7 mm rotor, see Figure 1.13. The spectra for the dehydrated acidic catalysts are shown as the time zero controls, and as expected, the Brønsted acid site signal at 4.2 ppm is decreased as the Si/Al ratio increases, in the sequence from Figure 2.9a to Figure 2.9d. In the cases of Si/Al = 15, 25, and 40, with increasing the water vapor exposure, the 4.2 ppm acid site signal decreases, and a broad water peak began to merge to the downfield region, similar to the data shown in Figure 2.10 obtained by vacuum-line adsorption on ZSM-5 catalysts. However, the water peak continuously shifts downfield with further exposure, but then stops and starts to rise at 7.0 ppm, 7.6 ppm and 8.0 ppm, respectively. At Si/Al = 140, shown in Figure 2.10d, the acid sites are quickly titrated up by water due to its low density. Then the silanol group, as the second-strongest hydrophilic site in the zeolite pore system, took over to control the adsorption. Note there is no downfield shift of water in the Si/Al = 140 case. The time-dependent MAS NMR results shown in Figure 2.9 reveal that 1) water vapor interaction with Brønsted acid sites appears to be the dominant interaction, and 2) within the limits of uncertainty of reproducibly packing catalyst particles in the MAS NMR rotor, water adsorption occurs more quickly for the higher acid density catalyst, evidenced by comparing the increasing rate of water peak formation in Figure 2.9a, 2.9b and 2.9c.

Figure 2.10 illustrates the quantitative adsorption results at similar water loadings with those presented in Figure 2.9. ^{1}H MAS NMR spectra of different amounts of water, up to 0.4 eqv,

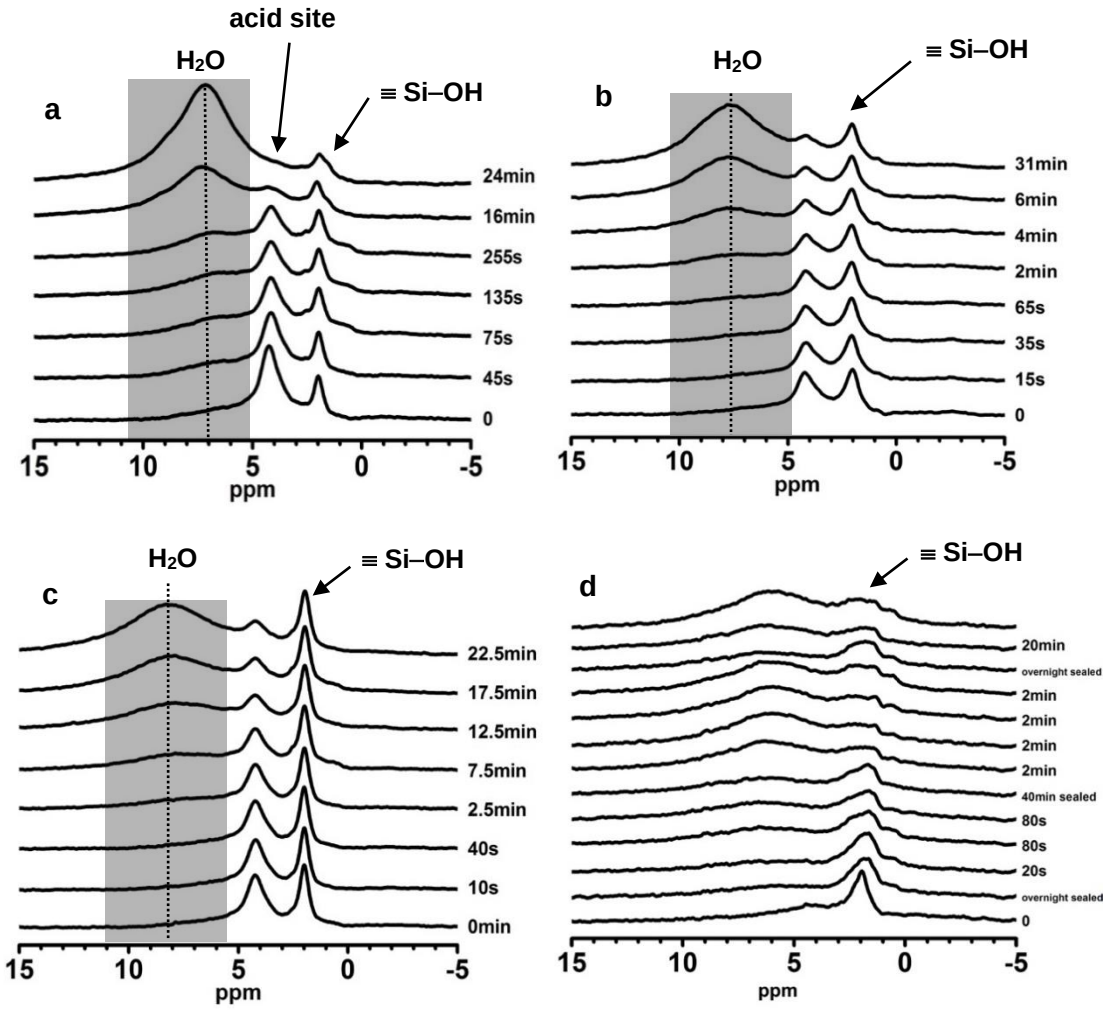

Figure 2.9. Representative ^{1}H MAS solid-state NMR spectra of HZSM-5 catalysts exposed to ambient moisture: **(a)** Si/Al = 15, **(b)** Si/Al = 25, **(c)** Si/Al = 40, and **(d)** Si/Al = 140. The total exposure time is shown on the right. The gray box highlights the water region of the spectra, and indicates the reduced water peak intensity at 22 minutes for the Si/Al=40 compared to the 16 or 24-minute point for the Si/Al=15 catalyst, and the dashed line indicates a 1 ppm difference (7.0 vs 8.0) in water chemical shift at that time for the two catalysts. Here, the exposure occurs when the catalyst is packed in the 7 mm MAS rotor, and cannot be quantitatively compared to the exposure times for the smaller bed depths used in Figures 2.5-2.6.

loaded in HZSM-5 catalysts at Si/Al = 15 and 40, were obtain for analysis. Each water adsorption was approached individually by the vacuum-line method described in Section 2.2. Evidence for strong interaction between water and the Brønsted acid site proton is observed at as low as 0.05 eqv, as the narrow and intense acid peak broadens due to the dynamic exchange between water protons and acid site protons, in both cases. As the water loading increased up to 0.4 eqv, the exchanged-average chemical shift moves downfield to 7 ppm. In this trace amount loading range, there is not enough water to cover all acid sites, and that pristine acid sites still exist, appearing as a hump at 3-4 ppm. By comparison, the 0.3-eqv spectrum in Figure 2.10a is similar to the 16-min spectrum in Figure 2.9a. Therefore, the spectra in Figure 2.9 are on the same scale of water loading as in Figure 2.10, but reveals more details from adsorptions lower than 0.05 eqv, i.e. 45-second to 225-second spectra. At dry conditions, shown by the bottom spectra of Figure 2.9a and 2.9c, Si/Al =15 catalyst has an expected larger acid/silanol peak intensity ratio than Si/Al = 40 catalyst. Figure 2.10b was the ^{1}H MAS NMR spectra obtained with the same method as in Figure 2.10a, but with HZSM-5 (40). In contrast, Figure 2.10a shows a more apparent trend of the downfield shift of the water peak, but Figure 2.10 shows a clearer trend of reduction of the acid peat at 4 ppm. A proposed reason will be explained by a water "coverage sphere" model shown later on. From both Figure 2.9 and Figure 2.10, two spectroscopic observations were noticed: First, the acid peak gradually moves downfield upon adsorption, with the shifting distance relative to the Si/Al ratio, i.e. 7 ppm for HZSM-5 (15), and 8 ppm for HZSM-5 (40); Second, the acid peak loses its intensity upon the adsorption of water, clearly observed in Figure 2.9a.

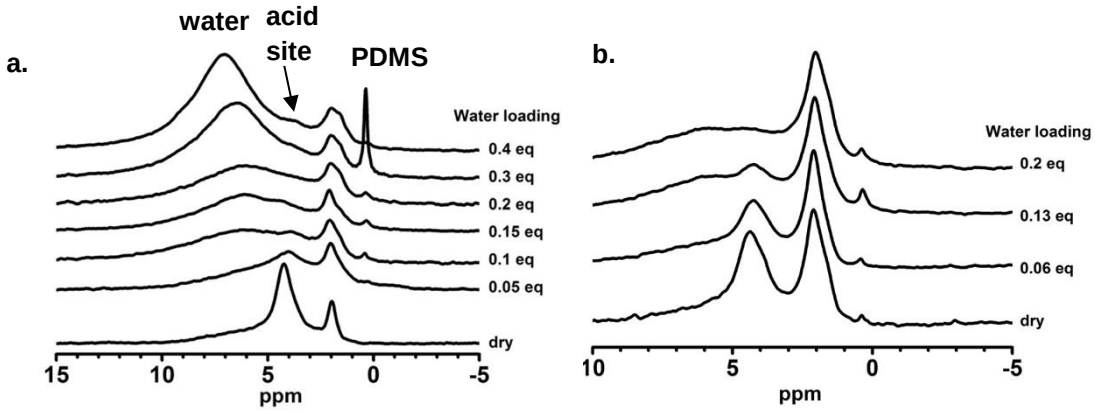

Figure 2.10. ^{1}H MAS NMR of solid HZSM-5 catalysts at Si/Al = 15 and 40, shown in **a)** and **b)**, respectively, as a function of controlled water loading, as noted, in number of equivalents relative to the acid site concentration. The Brønsted acid site peak, appearing at 4.2 ppm in the dry catalyst, undergoes exchange broadening and loss of resolution after addition of 0.1 eqv of water, in both cases. PDMS refers to an inert polydimethylsiloxane standard added for chemical shift and spin counting calibrations in some experiments. The emerging peak at 6-9 ppm with water addition arises from water at the acid site.

Undoubtedly, the downfield shift of the newly formed water peak is a consequence of fast chemical exchange between acid protons and adsorbed water molecules. Once a water molecule is adsorbed on an acid site, only two types of species can be formed, a) hydrogen bonded water by the acid proton, noted as $Z^{-}H^{+}\cdots H_2O$; or b) hydronium ion when a water molecule is protonated by an acid site, noted as $Z^{-}\cdots H_3O^{+}$. An ab initio calculation of water on acid site has been done by Sauer, showing that the proton transfer energy (10 kJ/mol) is much lower than the adsorption energy (50 kJ/mol), indicating the coexistence of both structures, illustrated in Figure 2.11.[25] Smith et al. (1996) and Alberto et al. (2010) both experimentally confirmed the coexistence of hydronium ions and hydrogen-bonded water via neutron diffraction approaches.[23, 30] The chemical shifts of $Z^{-}H^{+}\cdots H_2O$ and $Z^{-}\cdots H_3O^{+}$ are usually assigned to 4.8 ppm[39] and 13 ppm[36], according to the literature. Only four types of proton species can be found at this condition: $Z^{-}H^{+}\cdots H_2O$, $Z^{-}\cdots H_3O^{+}$, the Brønsted acid proton and free H_2O. Among the four

species, only $Z^{-}\cdots H_3O^{+}$ (13 ppm) contribute to the downfield shift. Free water at this condition is in a negligible population. Therefore, the Stage I downfield chemical shift must be due to existence of $Z^{-}\cdots H_3O^{+}$ which undergoes chemical exchanges with $Z^{-}H^{+}\cdots H_2O$ and Brønsted H^{+}. The 5-7 ppm downfield shifting peak has been reported in ZSM-5 catalysts, but was blurrily assigned to "disturbed bridging OH group".[40]

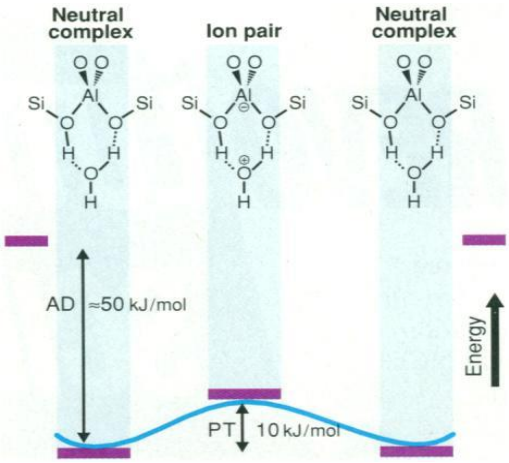

Figure 2.11. Ab initio calculations for adsorption (AD) and proton transfer (PT) energy. And they claimed a second water molecule stabilizes both neutral and ion paired structures. Adapted from reference 25.

At this small loading condition, where water clusters are rarely formed. Two types of exchanges can be addressed, noted as Exchange I and II, illustrated in Figure 2.12. "Exchange I" represents the two-site exchange between $Z^{-}\cdots H_3O^{+}$ and $Z^{-}H^{+}\cdots H_2O$, in close proximity to acid sites, with the exchanging rate k_1 determined by the 10 kJ/mol energy barrier calculated by Sauer. "Exchange II" is not a traditional two-site exchange. It represents the adsorption and desorption of water molecules on acid sites, with the hopping rate, k_2, determined by 50 kJ/mol energy

barrier calculated by Sauer. Note Sauer's calculated barriers are only a guidance for the discussion.

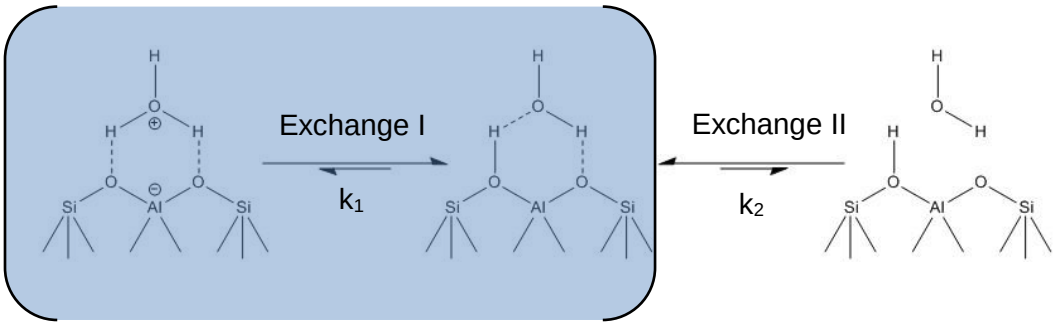

Figure 2.12. A scheme illustrating two types of exchanges. k_1 is on a much shorter time scale than k_2 so that the hydrogen bonded and physisorbed water sites can be treated a single exchange site for Exchange II process.

Now imagine an extreme condition, where only a few water molecules enter into a zeolite crystallite. Each water molecule will find an acid site at which to stay because of the large stabilization energy, 50 kJ/mol, benefiting from adsorption. At each adsorbed acid site, Exchange I takes place. However, room temperature is high enough to allow an adsorbed water molecule to desorb from an acid site. Haw's group (1994)[32] and Grey's group (2009)[17] had shown nice 2D proton NMR results showing cross peaks between the 4 ppm and the 6-7 ppm peak, which are the acid and adsorbed water peak at this extreme condition, even though the latter peak was not recognized as a water peak back in those days. From Haw's data, the cross peak appears even at 123 K, with a mixing time no smaller than 250 ms, indicating the exchanging rate k_2 is on a time scale of hundreds of milliseconds, knowing spin diffusion was not happening, because adsorbed water is segregated from other pristine acid protons more than a valid spin diffusion distance, i.e.

tens of nanometers. The prominent line broadening in Figure 2.10a at the 0.05-eqv spectrum suggests the fast water-hopping mechanism as well.

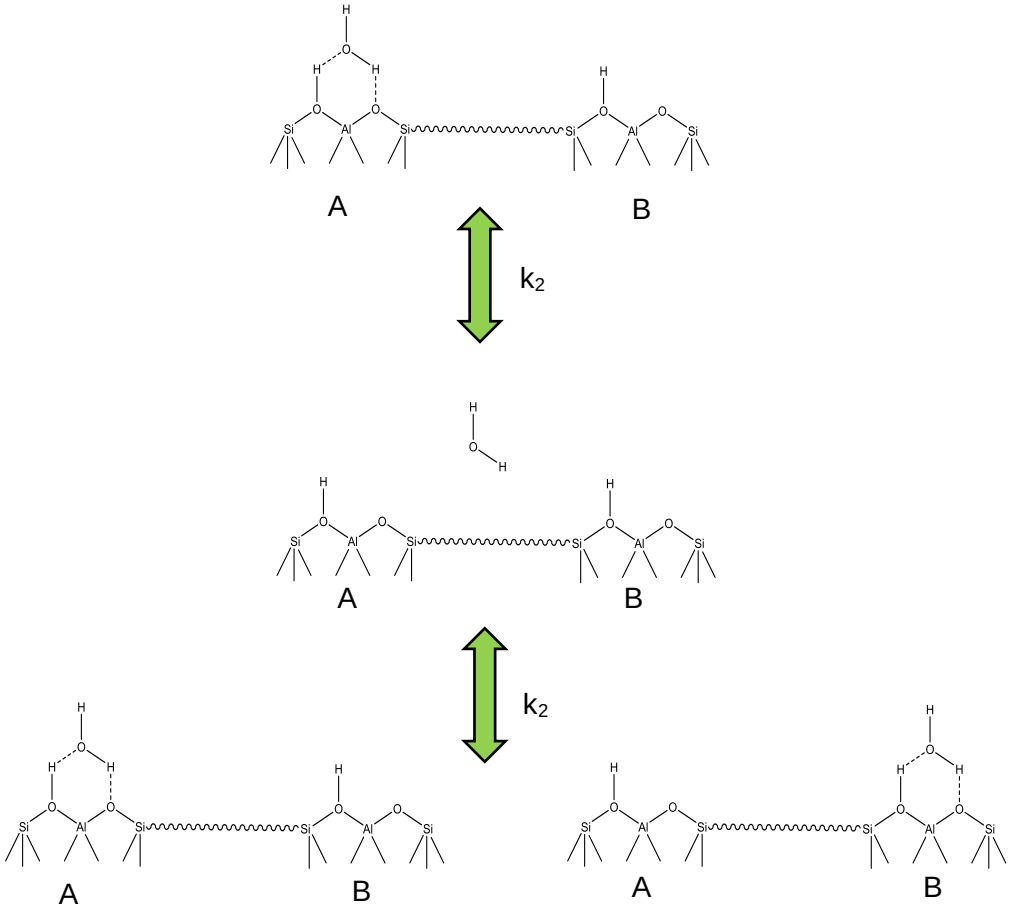

Figure 2.13. A scheme illustrating water hoppings, or Exchanging II.

A schematic drawing in Figure 2.13 illustrates the "non-traditional" Exchange II type scenario. Once an adsorbed water molecule overcomes the energy barrier to cleave from acid site A, it becomes a gaseous molecule that have equal probability to fall back on another close acid site, B. In other words, it is a one-way desorption but multiple-way re-adsorption. Note even

though only hydrogen bonded water is drawn as the adsorbed species, it always undergoes fast exchange, which is negligible on the time scale of k_2. The asymmetrical desorption and adsorption phenomenon results in a fact that one water molecule can cover multiple acid sites if the hopping rate is high enough, for example, at room temperature. There has been abundant evidence that indicates water molecule hops fast at room temperature. In addition to the line broadening occurring in Figure 2.10, the most other important evidence is the 2D proton NMR experiments. Haw's[32] and Grey's[17] group both had 2D proton NMR experiments on ZSM-5 at various temperatures, the former reached 123 K and the latter reached 183 K. Reported by Haw's group, the "exchange" time scale between water and acid sites was observed on a time scale of 250 ms, at 123 K. However, this time scale at room temperature is not clear from those data, thus, need to be measured in the future. As shown in Figure 2.13, we believe the 'exchange' is not a traditional two-site exchange, as for "Exchange I". It actually has four sites: The water bonded acid site (including hydrogen bonded and physisorbed water sites), the acid site and gaseous water. However, the gaseous water is in very low population, which can be readily approached by Boltzman distribution using 50 kJ/mol as the energy barrier, and thus not detectable by NMR. The hydronium ion and the hydrogen bonded water molecule undergoes much faster exchange, so that can be treated as one site. As a result, the exchange peak is actually a mixed signal of the water-bonded acid site and the Brønsted acid site. A "*coverage sphere*" model is proposed and depicted in Figure 2.14, demonstrating the number of acid sites a water molecule can occupy in the 300 MHz NMR time scale (a few milliseconds, discussed in the "Chemical Exchange" section). Note that this scheme is not specifically assigned to any type of zeolite or water loading, and does not include channel intersections, which are believed to play important roles on acid site locations. It is just a working model to illustrate the relative number of acid sites and water molecules for different condition. For example, in the schematic case in Figure 2.14a, the sphere covers ca. 2 acid sites on average. What is convenient about this model is, first, it compiles multiple factors, such as the water hopping-rate, the acid density and the water loading, into a

simple visual picture, and second, the size of the "coverage sphere" is only determined by the temperature.

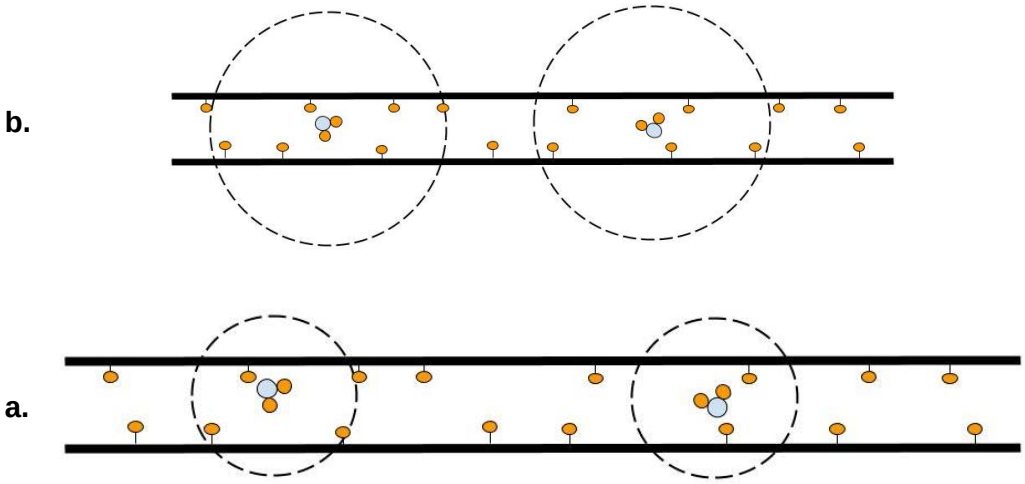

Figure 2.14. Schematic picture showing the cover-capability sphere of water molecules at **(a)** room temperature, **(b)** high temperature, leading to more coverage of acid sites due to the larger sphere.

Stage I_a adsorption Using this model, "Stage I" adsorption of water in zeolite can actually be characterized into two sub-stages, "Stage I_a" and "Stage I_b". Figure 2.14 specifically illustrate the extremely low water condition, "Stage I_a", where not only each water molecule, but also each coverage sphere is separated from one another. As a result, there are plenty of pristine acid site existing, showing as a residual acid peak in the spectrum. Figure 2.14a and 2.14b depict the cases of room temperature and elevated temperature, respectively. The most apparent observation of "Stage I_a" by proton NMR is the decrease of the acid peak. The acid peak decreases as a function of water loading, shown in both Figure 2.9 and Figure 2.10, due to water binding on acid sites. Clearly, the water titration is responsible for the acid peak intensity decreases. However, it is important to notice that the acid peak intensity diminishes faster than it supposed to be, upon the

adsorption of water. In Figure 2.10a, while increasing the water loading, there should be 80% and 60% acid peak intensity left on the 0.2 and 0.4 eqv spectra, respectively. Whereas, much less residual acid peak intensities were observed than their theoretical values, in each loading of both Si/Al ratio catalysts. Using the "coverage sphere model", we know one water molecule covers multiple acid sites on the NMR timescale, consequently, the acid sites are "consumed" faster than the number of water introduced. For example, if the sphere covers two acid sites on average, in the cases of 0.2 and 0.4 eqv adsorption, 60 % and 20 % acid peak intensities are expected on the spectrum instead of 80 % and 60 %. In Grey's ^{1}H NMR results in Figure 2.8, because the acid/silanol peak ratio is much higher in Figure 2.8a than Figure 2.8b, which is consistent with our control observation. Because of no overlap, the acid-occupation number of each water molecule is a constant. Therefore, according to the "Exchange II" model, the water peak should have a constant chemical shift, which can barely be seen in Figure 2.10a, when water loading is less than 0.2 eqv. An ambient exposure experiment with smaller exposure time increment reveals the constant water peak better, as seen in the water peak from 0-150 second in Figure 2.15.

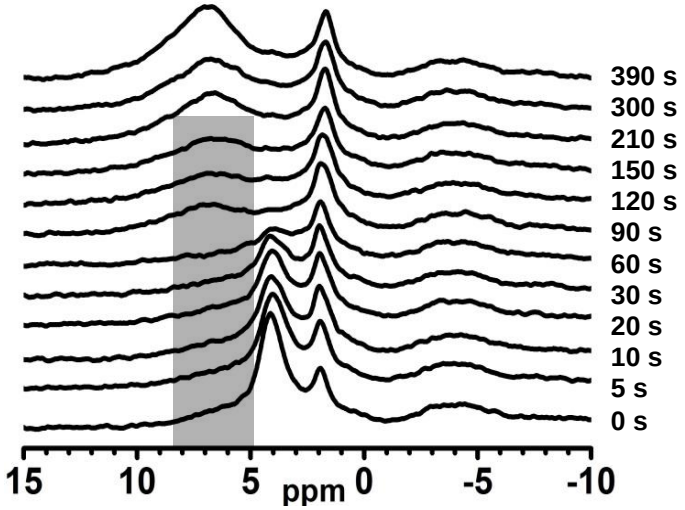

Figure 2.15. ^{1}H MAS NMR spectra of an HZSM-5 catalyst acquired at room temperature versus total time of exposure to ambient moisture (50-60 % relative humidity), starting from the dry catalyst. After each exposure step, the rotor was re-sealed with a grooved plug and cap and the next spectrum acquired.

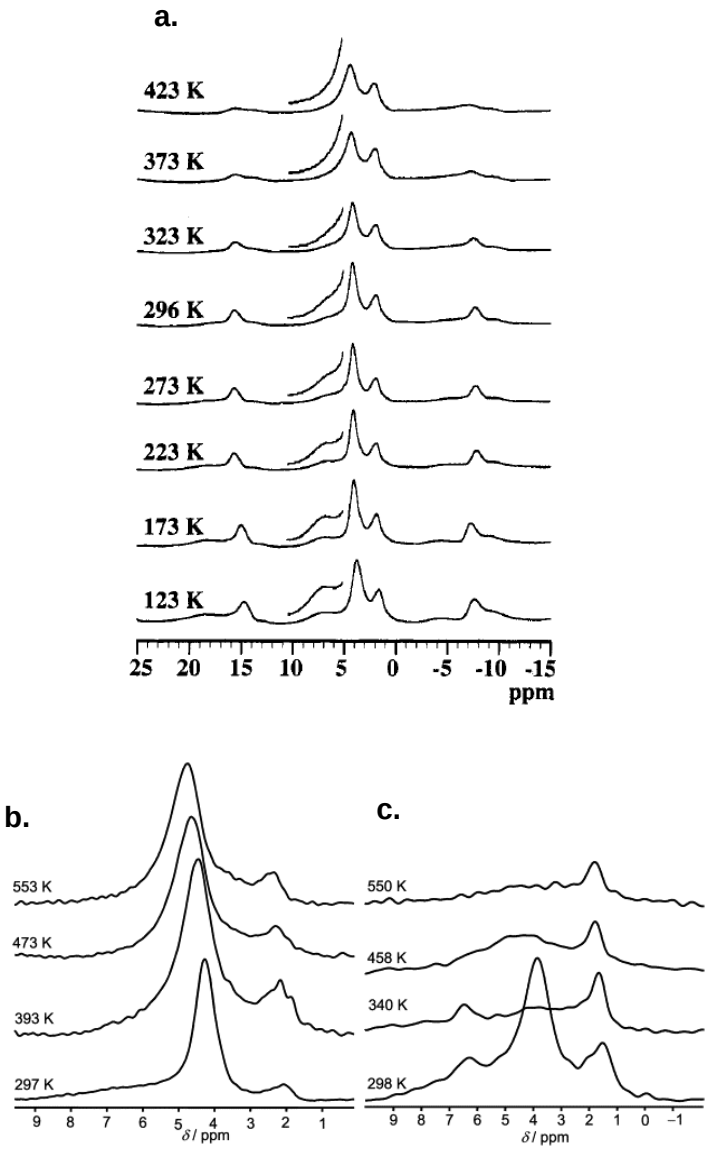

Figure 2.16. High temperature ^{1}H MAS NMR spectra adapted from **(a)** reference 32, **(b**) **and (c)** reference 18.

Two high temperature ^{1}H MAS NMR spectra are adapted from literature, shown in Figure 2.16. By eye, they are all on the Stage I_a level adsorption, because of the prominent acid

peaks at room temperatures. Figure 2.16c has more water loaded than Figure 2.16a, due to the more resolved water peak at 6.5 ppm. As the temperature increased, the acid peaks decrease dramatically in both cases, because the "coverage sphere" is enlarged, see Figure 2.15b, and thus, more pristine acid peaks are consumed by the same amount of water. When the catalyst is dry, see Figure 2.16b, temperature has no impact on the acid peak intensity.

Stage I_b adsorption. As the water loading increases, the "coverage spheres" start to overlap, depicted in Figure 2.17. Stage I_b has a reflection in ^1H NMR spectra as well, which is the downfield shift of the water peak towards 7 ppm, see the top a few spectra in both Figure 2.9a and 2.10a. It is because as the overlap starts to happen, some acid sites begin to be shared by two water molecules, which results in a decrease of the averaged "occupation number" of a water molecule. Losing the exchanging acid site population causes the averaged exchange peak to shift to the bonded-water side, i.e. 7 ppm. The prediction is consistent with the high temperature ^1H NMR spectra for 0.5-eqv D_2O adsorption, seen in the 300 K-340 K spectra in Figure 2.21. To our knowledge, this water dependent downfield shifting phenomenon of the water is illustrated for the first time.

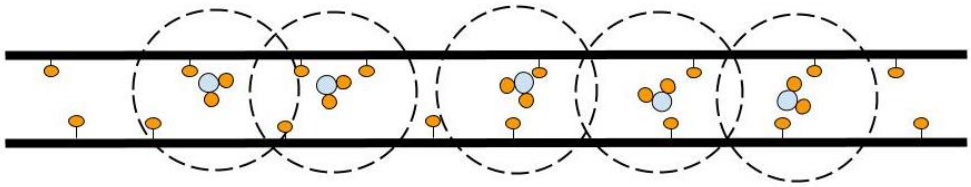

Figure 2.17. Schematic picture showing the "coverage spheres" of Stage I_b condition.

2.3.2.1. Chemical exchange discussion.

Exchange II. As mentioned earlier, "a few milliseconds" is the observable time scale for 300 MHz proton NMR. The value is obtained via conventional chemical exchange analysis, but with an assumption that the bonded-water on acid sites showing the NMR resonance at 7 ppm. There are two reasons 7 ppm is assigned to the bonded water species. First, Haw's group had obtained low temperature ^{1}H MAS NMR spectra for Stage I_a level water in HZSM-5 at 123 K, even though the water peak was incorrectly believed to be a second type of acid site, showing the water peak was resolved at 6.9 ppm. Second, at Stage I_b level adsorption, the water peak moves downfield but stopped at 7 ppm for ZSM-5 (15) catalyst. In other words, 7 ppm is where the bonded water starts to dominate over the acid site during the "Exchange II" process. Note this assignment is still an assumption, and there are flaws existing. For example, why does the bonded water have similar chemical shift at 123 K compared to 298 K? Apparently, more work need to be done to solve the problem. However, we can safely assign the bonded water chemical shift to the range of 6-8 ppm. Then its difference to an acid peak (4 ppm) is in the range of 2-4 ppm, corresponding to 600-900 Hz, or in the time scale range of of 0.8-2 ms, in the 300 MHz regime. Thus, "a few milliseconds" would be safe enough to address observable limit of the 300MHz NMR instrument. According to conventional chemical exchange theory, if the water molecules hop much faster than a few milliseconds, i.e. in a microsecond scale, an averaged water peak will be observed. On the contrary, when the hopping rate is much slower, i.e. 250 ms at 123 K reported by Haw's group, the peaks will be resolved. Interestingly, the coverage sphere can now be interpreted as "the number of the acid sites a water molecule can hop to during the a-few-millisecond NMR time scale". The ZSM-5 catalyst Haw group used in the low temperature experiment is at Si/Al = 19, which is comparable to ours Si/Al = 15.

Exchange I. $Z^-H^+\cdots H_2O$ (4.8 ppm) and $Z^-\cdots H_3O^+$ (13 ppm) are always under fast exchange regime, even at 123 K. Using Equation 1.3, and 7 ppm for the averaged exchange peak at 123K, surprisingly, 27 % $Z^-\cdots H_3O^+$ and 73 % $Z^-H^+\cdots H_2O$ are obtained. Consequently, applying the fractional values to Boltzman distribution calculation, via Equation 2.1, the energy barrier of 1 kJ/mol is obtained, which is quite different from Sauer's calculation, 10 kJ/mol.

$$\frac{p_I}{P_{II}} = e^{\frac{\Delta E}{kT}} \qquad \text{Equation 2.1}$$

There has been a debate of the acid strength dependence on Si/Al ratios. Some chemists believe the Brønsted acid sites are more acidic in high Si/Al ratio zeolites than those in low Si/Al ratios. If this is true, Si/Al = 40 zeolites, as a better proton donator, would yield more $Z^-\cdots H_3O^+$ (13 ppm) than Si/Al = 15 zeolites, resulting in a more downfield chemical shift of the average exchange water peak. Admittedly, this is a plausible explanation for 8 ppm versus 7 ppm chemical shift for water peak in Si/Al = 40 and 17 at above 0.5 eqv water loadings. While, an alternative explanation can be proposed from the coverage sphere model. At higher Si/Al ratio conditions, each acid site is farther away separated, leading to less occupied acid sites of each water molecule, under the same reactive sphere. As a result, more bonded water complex, $Z^-H^+\cdots H_2O$ (4.8 ppm) and $Z^-\cdots H_3O^+$ (13 ppm), lead to the more downfield average exchange chemical shift. To identify the second hypothesis, ^{1}H NMR at different Larmor frequency should be sufficient. At higher Larmor frequency, the apparent coverage sphere should be smaller, leading to an upfield shift of the water peak.

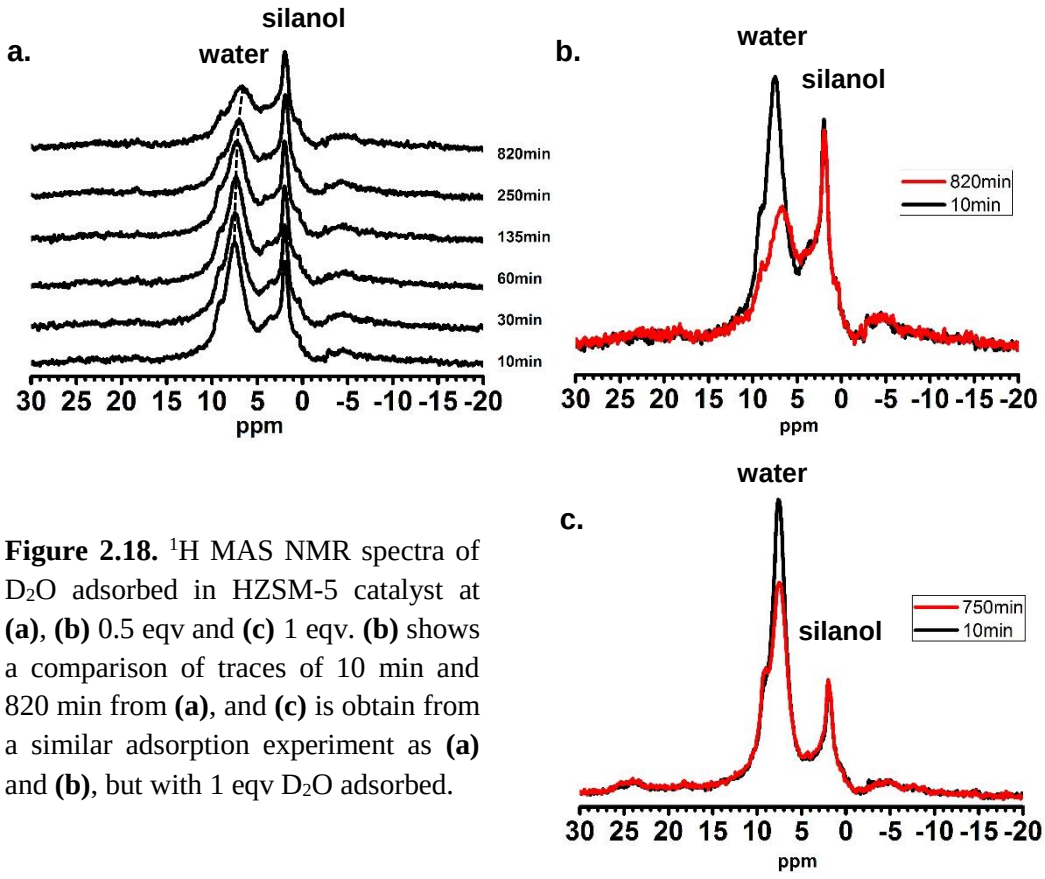

Figure 2.18. ^{1}H MAS NMR spectra of D_2O adsorbed in HZSM-5 catalyst at **(a)**, **(b)** 0.5 eqv and **(c)** 1 eqv. **(b)** shows a comparison of traces of 10 min and 820 min from **(a)**, and **(c)** is obtain from a similar adsorption experiment as **(a)** and **(b)**, but with 1 eqv D_2O adsorbed.

D_2O adsorption. Deuterated water, as an analogue of water, was also used to probe the catalyst acid site via ^{1}H MAS NMR. In contrast to H_2O, D_2O adsorption benefits from its special advantage in NMR analysis: no additional introduction of protons, other than the originals from acid sites. Because deuterium nuclei are silent in proton NMR, D_2O, behaving similarly with H_2O in zeolites, they have much less spectrum complicity. Figure 2.18 illustrates ^{1}H MAS NMR results of vapor-phase adsorptions of D_2O in HZSM-5 (15) at 0.5 eqv (Figure 2.18a and 2.17b) and 1 eqv (Figure 2.18c), respectively. Once 0.5 eqv D_2O was adsorbed into zeolite through vacuum-line, it was immediately inspected by ^{1}H NMR, shown as the bottom spectrum slice in Figure 2.18a. Then subsequent spectra were taken in course of elapse time to ensure a complete

intracrystalline diffusion of D_2O molecules. Surprisingly, the water peak kept losing its intensity for at least four hours, observed from 10 min to 250 min. Then the sample was sealed overnight (850 min) to obtain the final spectrum with completed diffusion. The 850-min spectrum was plotted together with the initial spectrum, shown in Figure 2.18b, for comparison.

It is surprising to observe that the water peak intensity does not hold constant after adsorption is finished, consequently, the spectrum intensity does not quantitatively indicate the amount of adsorbed water. Compared to 1 eqv adsorbed water in Figure 2.18b, the spectrum at 0.5 eqv (Figure 2.18a) shows larger intensity loss. A recommended reason can be accounted to the Rothwell-Waugh effect[41-42], which states that the molecular motion in coherence with the Magic Angle Spinning rate can broaden the relative peak beyond detection. This coherent motion must come from the acid-water interactions, which could be molecular reorientation of water (cluster) on the acid site; or the "Exchange II" process, that could be on the time scale of a couple of hundred microseconds, comparable to 250 μs (the time scale of MAS). In the cases of Figure 2.18, at early times after adsorption, water is concentrated on the acid sites that are close to the pore entrance (an extreme example shown in Figure 2.19), so not all of the acid sites are involved in the interactions. As water diffuses, the portion of water-acid interactions increase, causing more intensity loss.

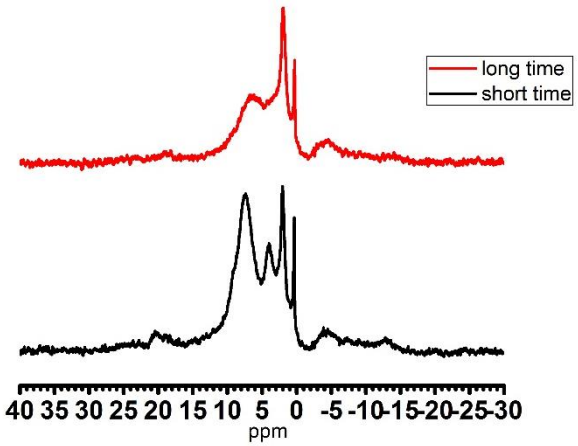

Figure 2.19. ^{1}H MAS NMR spectra of 0.2 eqv water adsorbed on HZSM-5 (15) very shortly after adsorption **(black)**, showing water is locally concentrated on the acid sites close to the pore openings, and after diffusion equilibrium **(red)**.

Another noticeable observation is the long elapse time required for the D_2O peak decrease. Surprisingly, Figure 2.18a indicates that more than 4 hours (similar for water, not shown) are needed to have D_2O achieve complete intracrystalline diffusion. It is plausible to suggest that the overall diffusion is inhomogeneous, meaning that, water adsorbed at acid sites diffuses slower than free water off the acid sites. At Stage I, the on-site water is in a dominating population. Therefore, even gaseous free water diffuses significantly faster, their low population make them a bottleneck that reduces the overall diffusion performances. It is reported that the diffusion coefficient in Silicalite-1, which has the MFI framework but contains no acid site, is higher than in ZSM-5.[43] This model explains why isobutane molecules diffuse much faster than water in zeolites, indicated by the entire acid peak shift from 4.2 ppm to 4.8 ppm in the ^{1}H NMR spectrum within 5 min after adsorption, see Figure 3.4. The lesser attraction from acid sites results in a larger amount of free isobutane molecules and, consequently, enhances the overall diffusion rate. In the case of benzene, one could expect that benzene has a comparable adsorption enthalpy with

water, thus it should have a similar slow adsorption rate as water. However, it also takes less than 5 min to have 1 eqv isobutane or benzene to finish a complete adsorption. Presumably, it is because benzene is less likely to form cluster on acid sites, leading to an enhanced overall diffusion rate. Note HZSM-5 at Si/Al = 15 adsorbs water much faster than Si/Al = 40, because the longer distances among acid sites in Si/Al =40 results in less chances of successful inter-acid site hopping. This model explains the reason that diffusivities of water are hard to be acquired by pulsed gradient NMR technique at small loadings, because the majority of water are localized at the acid sites.

2.3.2.1. Pulsed-field gradient (PFG) ^{1}H NMR for diffusion analysis

Interestingly, the pulsed-field gradient ^{1}H NMR method has shown supportive results to the two-type inhomogeneous diffusion analysis, shown in Figure 2.20. At room temperature, HZSM-5 (15) catalysts with variable amounts of water adsorbed was analyzed by PFG ^{1}H NMR method to obtain the diffusivities of internal water. The diffusivities of water loaded at 5, 10, 20 and 33 molecules/u.c., corresponding to ca. 1, 2, 3 and 5 eqv, were reported in Figure 2.14a. 1.5×10^{-10} m^2/s and 2.9×10^{-10} m^2/s were respectively detected for 1 and 2 eqv condition. However, two individual diffusivities appear at 3 eqv, and went back to one value at 5 eqv/u.c. The larger diffusivity observed at 3 eqv/u.c. could be highly responsible for inter-site diffusion, and the lower value for intra-site diffusion. At 1 and 2 eqv, the quantity of free water is so little and may not be detectable, on the contrary, at 5 eqv, on-site species are in large quantity that covers the inter-site free water signal, even though there is considerable free water at 5 eqv. With this said, we can claim that in Figure 2.20a, the increasing diffusion coefficients, 1.5×10^{-10} m^2/s, 2.9×10^{-10} m^2/s, and 2.6×10^{-9} m^2/s measured at 1, 2, and 3 eqv are originated from intra-site diffusion. The values, 2.6×10^{-9} m^2/s, and 2.5×10^{-9} m^2/s, which are one order of magnitude higher, correspond to the inter-site, or free water diffusion. At 3 eq, free water is in a comparable amount of bonded water, where they are both measurable by the diffusion NMR. We can call 3 eq the

transition loading from the bonded-water dominating scenario to the free water dominating scenario. The diffusion coefficients between HZSM-5 with Si/Al = 15 and 40 are compared in Figure 2.20b, indicating the catalyst at Si/Al = 40 has an earlier transition loading, 15 molecule/u.c. compared to 20 molecule/u.c. This makes sense because the acid sites in Si/Al = 40 catalysts are separated farther away, resulting in less formation of inter-site free water. This model still need to be verified. If true, less or no transition region should be observed for methanol, isobutane or benzene, because they form less or no clusters at acid sites.

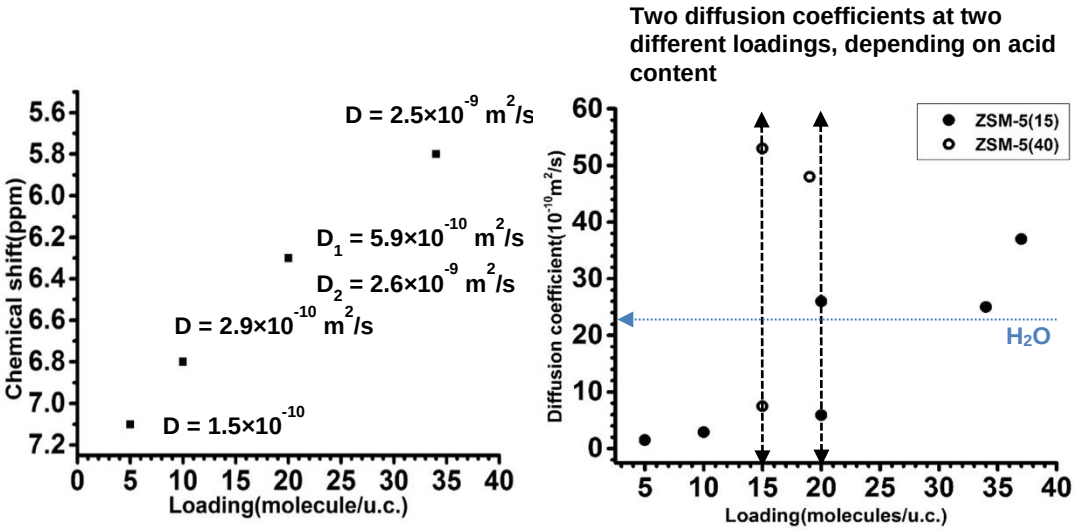

Figure 2.20. Diffusion coefficients for water in HZSM-5 measured via PFG stimulated ^{1}H NMR experiments, in which the diffusion coefficients are plotted versus **(a)** loading-dependent exchange-weighted average chemical shift of the intracrystalline water peak in Si/Al = 15 catalyst, and **(b)** water loading for two different Si/Al ratios. Note that two diffusion coefficients are observed for Si/Al = 15 at 20 water molecules/u.c. in **(a)** and **(b)**. The horizontal arrow in **(b)** indicates the known self-diffusion coefficient for water molecules in bulk liquid water.

Low temperature ^{1}H MAS NMR for 0.5 eqv adsorption. By reducing the temperature enough, the population-weighted average chemical exchange could be slowed down and resolved by NMR. In order to resolve the exchanging species, spectra of 0.5 eqv D_2O in HZSM-5 was

examined by proton NMR in a temperature span from 190 K – 340 K, illustrated in Figure 2.21. 0.5 eqv D_2O was adsorbed into dry HZSM-5 (15) at room temperature, followed by a quick proton NMR examination 15 min and 19 hrs after adsorption, shown in Figure 2.21b and 2.21a, respectively, to ensure the completion of the D_2O diffusion. The sample corresponding to Figure 2.21a was used for in-situ variable temperature NMR experiment. By flowing cold nitrogen gas into the NMR probe, the catalyst was quickly brought down to 190 K and heated up to 340 K gradually, shown as a stack plot in Figure 2.21c. First, the temperature-dependent change of the water peak intensity is clearly observed. From 190 K-270 K, water peak intensities are apparently lower than those above 300 K. Note the intensity of water peak at 300 K is comparable to that at room temperature, depicted in Figure 2.21a, indicating no extra water was adsorbed into the system. Moreover, in this VT experiment, the catalyst was constantly sealed in a 4-mm MAS NMR rotor, under a dry N_2 gas flow, leading to low chances of external water contaminations. The exact mechanism is not clear, however, it is reasonable that while lowering the temperature, water molecules tend to 'condense' on the acid sites, causing the broadness of the water peak. Second, the acid peak is resolved again at 190 K. It is less likely that $Z^-\cdots H_3O^+$, $Z^-H^+\cdots H_2O$ and Brønsted H^+ become resolved at this temperature, because $Z^-\cdots H_3O^+$ and $Z^-H^+\cdots H_2O$ are reported to coexist at 10 K.[23] In addition, from Figure 2.11, we know as long as water diffuses between acid sites, the energy is always enough for the transition between $Z^-\cdots H_3O^+$ and $Z^-H^+\cdots H_2O$. It is reported that water still diffuses in zeolite at least at 183 K.[44] Therefore, the most plausible explanation is the coverage sphere proposed in Figure 2.14 shrunk, as a consequence, the number of acid sites a water molecule can occupy becomes less, resulting in more pristine acid sites.

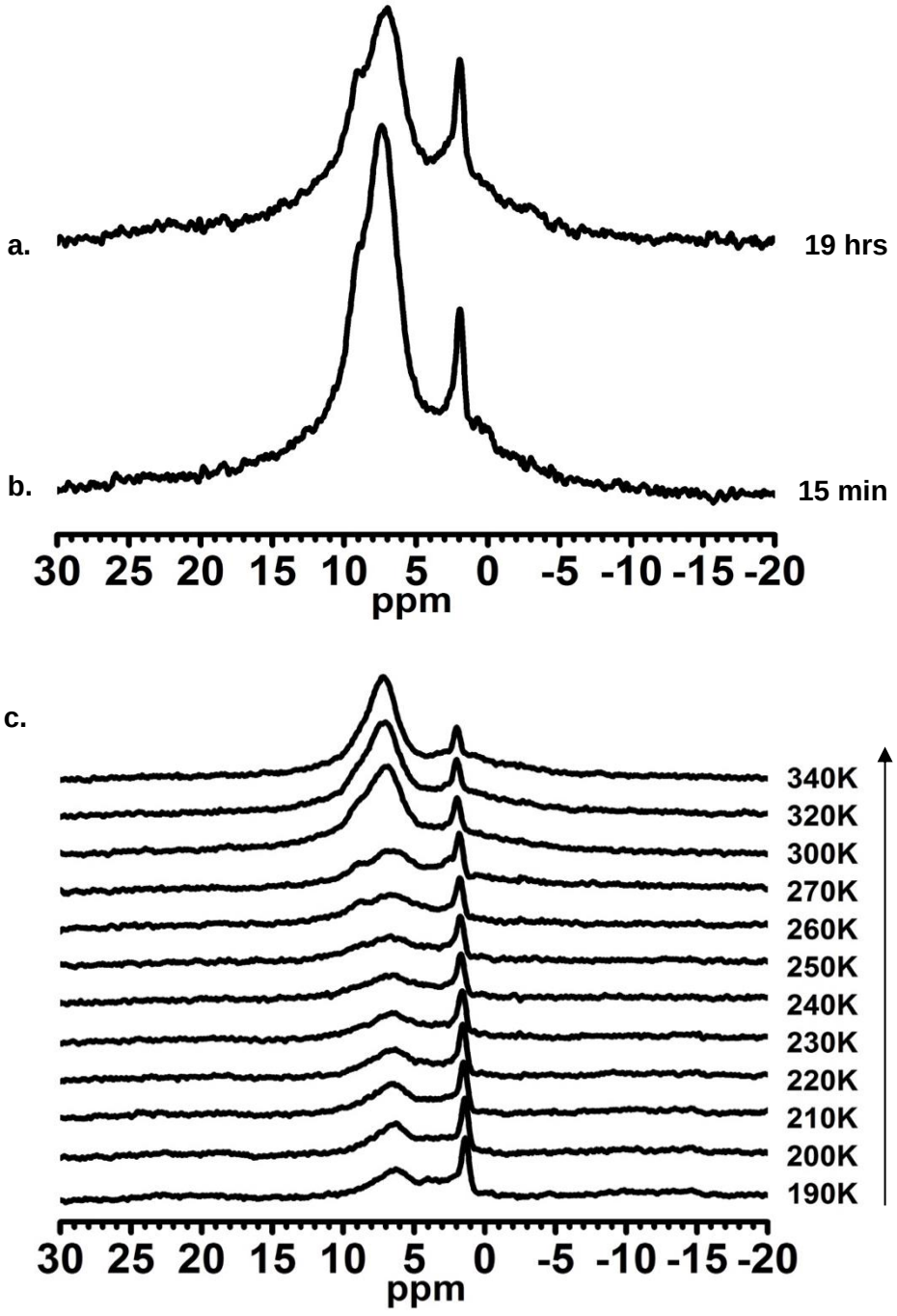

Figure 2.21. Variable temperature ^{1}H MAS NMR spectra of 0.5 eqv D_2O adsorbed via vac-line method. (a) and (b) show ^{1}H NMR spectra taken 19 hrs and 15 min after D_2O adsorption at room temperature. (c) shows the spectra of variable temperature experiment: the catalyst, the same as catalyst in (a), was cooled down to 190 K quickly and then heated up to 340 K gradually.

2.3.2.2. Stage II: 0.5 ~ 3 eqv H_2O. The building period of water clusters at acid sites.

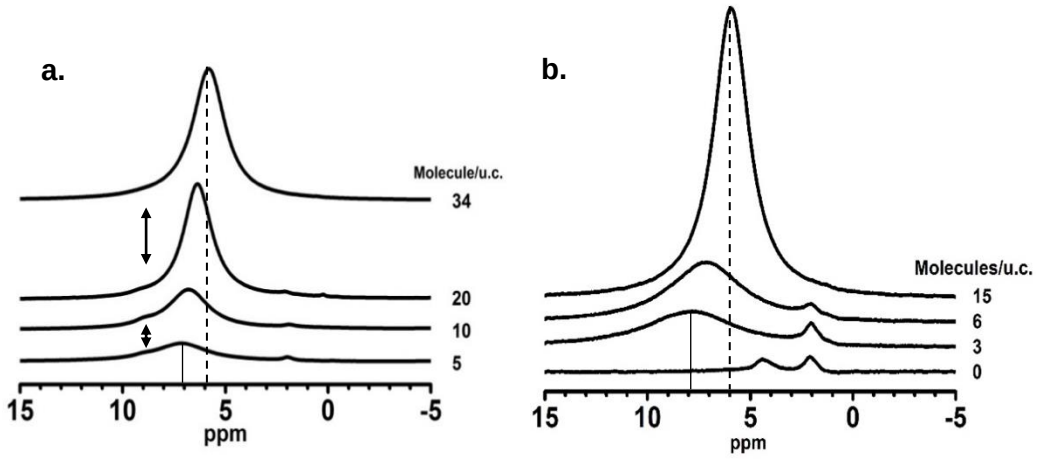

Figure 2.22. ^{1}H MAS NMR spectra of HZSM-5 catalysts exposed to ambient gas-phase moisture, similar to Figure 2.9, but as a function of quantitatively determined water loadings for **(a)** Si/Al = 15, and **(b)** Si/Al = 40. The water loadings here are significantly larger than those represented by the data in Figure 2.9. Note that the loading-dependent shift of the water peak to a common 5.8-5.9 ppm value (indicated by the dashed line) requires two times as much water per unit cell in **(a)** compared to **(b)**, indicating that interaction with acid sites is the dominant contribution to chemical shift. Also, the water peak chemical shift at the lowest loadings (solid line) shown is different by ca. 1 ppm, as seen previously in Figure 2.9.

Qualitative adsorptions using the rotor-exposure method were shown in Figure 2.22 as quick observation experiments. To obtain quantitative results, the experiments were repeated and weighed at each point prior to the spectroscopic experiment in order to calculate the number of water molecules per unit cell present. Each proton NMR spectrum in Figure 2.22 was obtained by individual adsorption procedures, using a microbalance to measure the weight increase of adsorbed water, as described in Section 2.2.3. Figure 2.22 depicts higher water loadings than those previously shown in Figure 2.9 and 2.10, evidenced by the lack of acid peaks, and reveals a loading-dependent water chemical shift that moves upfield as the water content increases. The loading-dependent change of the water peak to a common 5.8-5.9 ppm value (indicated by the

dashed line in Figure 2.22) requires two times as much water per unit cell in Figure 2.22a, compared to Figure 2.22b, indicating that interaction with acid sites is the dominant contribution to chemical shift. The initial chemical shift of the first formed water/acid site cluster is more downfield in the Si/Al = 40 (8 ppm) than the Si/Al = 15 case (7 ppm). In addition, the water peak linewidth during Stage II decreases upon adsorption, indication formation of more mobile water clusters.

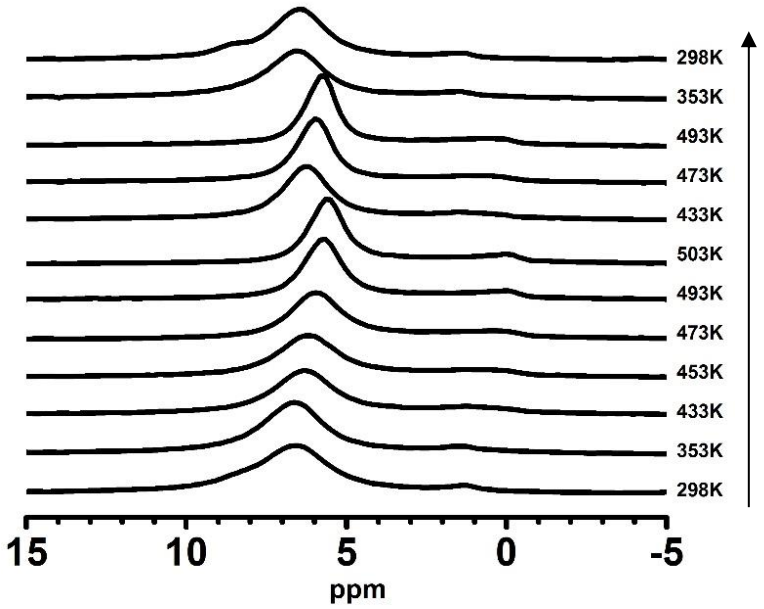

Figure 2.23. Variable temperature ^{1}H MAS NMR spectra for 2 eqv water in HZSM-5 (15). From bottom to top, the catalyst was heated from room temperature to 503 K, then brought back to 433 K, heated back to 493 K again, and cooled to room temperature step wise.

The in-situ high temperature ^{1}H MAS NMR method was applied HZSM-5 zeolites injected with 2 eqv water, illustrated in Figure 2.23. By heating the catalyst from room temperature to 503 K, the water peak was narrowed and moved upfield to 5.6 ppm. Interestingly, 5.6 ppm is the saturation chemical shift of water in zeolite by vapor adsorptions, see Figure 2.22

and 2.27. This observation suggests that at the condition of 2 eqv and elevated temperature, the water species shift from clusters to free channel water. In other words, the water cluster size an acid site can hold is much smaller at high temperatures. This information is significant for understanding water's role at usual catalytic temperatures. For instance, in methanol to hydrocarbon conversion conditions, even though water is produced in stoichiometric amounts, the amount of actual water in proximate to acid sites could be much less than that and heavily dependent on the temperature. Thus, even though water assist the hydrophobic carbon pool chemistry at room temperature, its impact at high temperatures need to be reevaluated.

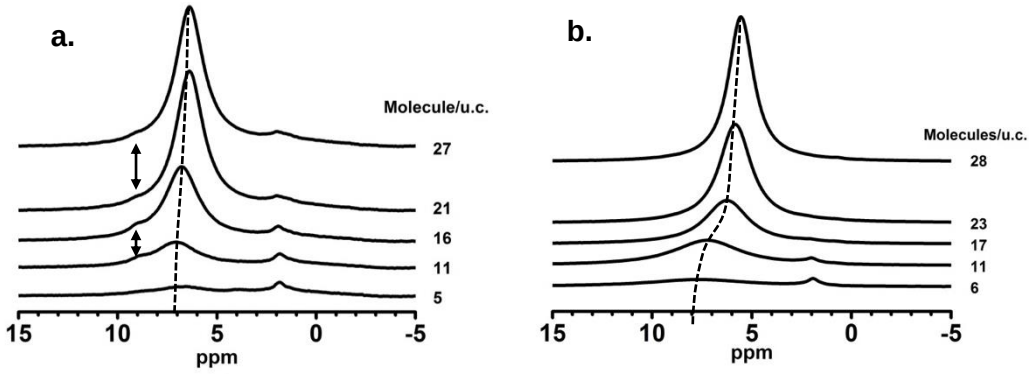

Figure 2.24. ^{1}H MAS NMR spectra of HZSM-5 catalysts exposed to liquid water using a microsyringe for quantitative adsorption: **(a)** Si/Al = 15 and **(b)** Si/Al = 40. Note the dramatic and abrupt upfield shift for the water peak with increasing water loading for the Si/Al = 40 catalyst, as was similarly observed for the Si/Al = 140 sample (not shown). The dashed line is shown only as a guide to the eye.

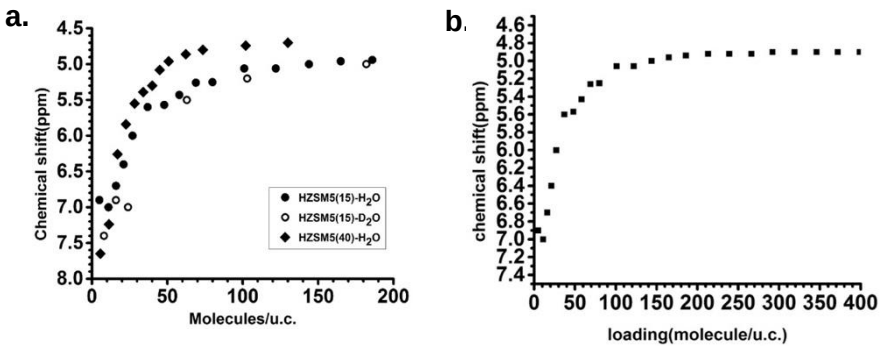

Figure 2.25. Loading-dependent exchanged-averaged water peak chemical shifts from ^{1}H MAS NMR spectra of HZSM-5 catalysts exposed to ambient gas-phase moisture, for **(a)** Si/Al = 15 versus Si/Al = 40, and **(b)** the complete titration curve for water loaded in Si/Al = 15 HZSM-5 up to 400 water molecules per unit cell, from liquid phase.

2.3.2.3. Stage III: 3 eqv ~ +∞ H_2O. Water peak shift from 7 ppm to 4.8 ppm.

Adsorptions via water vapor from ambient environment are not capable of obtaining water loadings above 5-6 eqv. For higher loading adsorptions, the liquid water injection approach was need. As described in the Section 2.2.3, using a 10-μL GC syringe, water can be injected from as low as 5 molecules per unit cell, which is at Stage II adsorption, to totally saturated amounts, i.e. > 300 molecules per unit cell. Figure 2.25 summarizes water loading-dependent proton NMR spectra as the water vapor adsorptions shown, but for catalysts exposed to liquid water by microsyringe. The liquid water injection results clearly illustrate the chemical shift trend of Stage III adsorption. Again, subsets of the exchanged-averaged loading-dependent water spectra are shown for the Si/Al = 15 and Si/Al = 40 systems, compared to similar loadings. Essentially identical conclusions are drawn from these data from the vapor-phase experiments. Initial chemical shifts of water (ca. 5 molecules/u.c., Stage II) are more downfield in the lower acid

density catalysts, i.e. 7, 7.5 and 8 ppm for Si/Al= 15, 25, and 40, recall Figure 2.9. Whereas, the chemical shift change more quickly per unit water added to the limiting value of 4.8 ppm observed for pure water. At this high-loading stage, free channel water gradually takes over the role of on-site water clusters. From ca. 3 eqv to 5 eqv, the exchange-averaged water peak of Si/Al = 15 ZSM-5 shifts from 7 ppm to 5.6 ppm, due to the increasing amount of free water. Note that the free water at this range is vapor like, knowing the upper limit of ambient adsorption is 5-6 eqv. The 5.6 ppm water peak is also observed in spectra of 2 eqv water in HZSM-5 (15) at high temperatures (Figure 2.23) and in liquid injection to ETS-modified zeolites (Figure 2.28), highly suggesting that 5.6 ppm is the chemical shift of free water in HZSM-5 channels.

At water loadings over 5 or 6 eqv, the water peak keeps moving upfield, eventually stopping at 4.8 ppm, the resonance of bulk liquid water. This is the range that liquid water forms in channel. The average-exchanged water chemical shift data over the range of water loadings are shown in Figure 2.25a, including the D_2O results. The data in Figure 2.25a are in agreement with Figure 2.24, in which it appears that the lower acid density Si/Al = 40 system reaches the equilibrium water chemical shift value of 4.8 ppm at significantly lower water loadings than that of the Si/Al = 15 catalyst. The loading-dependent results for H_2O and D_2O are identical within experimental uncertainty, except D_2O peak appears at 7.5 ppm at Stage II adsorption, instead of 7 ppm for H_2O.

2.3.2.4. The role of silanol groups

The role silanol groups play during adsorption is minor, however, evidence has shown that slow proton exchanges still occur between silanol groups and acid sites at Stage I.[32] Even at early Stage II, the water interaction of silanol groups can be observed in ^1H MAS NMR spectra. For example, the 0.4 eqv spectrum in Figure 2.10 shows clear distortion of the silanol peak by water. In Figure 2.26, The top ^1H MAS NMR spectrum describes excess liquid D_2O injected to dry HZSM-5

(middle spectrum). Then, the wet catalyst was evacuated under < 10^{-5} torr pressure for a few hours, shown in the bottom spectrum. Apparently, the disappearance of the acid and silanol peak suggests that all of the protons from acid sites and silanol groups were exchanged into the liquid D_2O phase, and then removed under vacuum.

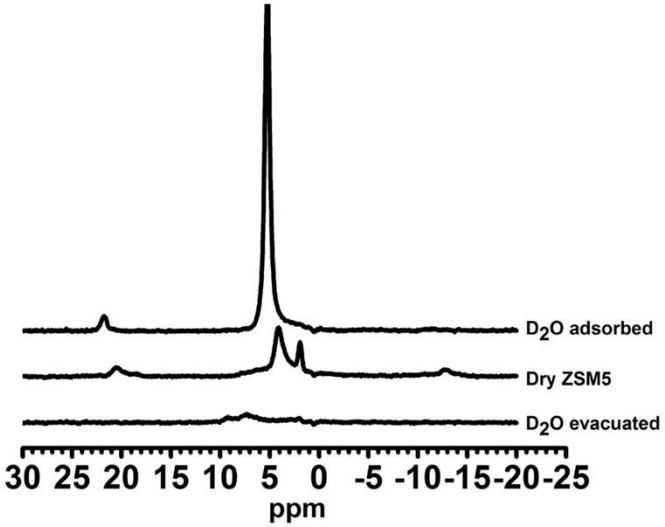

Figure 2.26. The top spectrum describes the ^1H MAS NMR spectrum of excess liquid D_2O injected to dry HZSM-5 (middle spectrum). The bottom spectrum depicts the result of the catalyst with excess D_2O evacuated under < 10^{-5} torr pressure for a few hours, showing a complete exchange between D_2O and silanol protons.

2.3.3. Adsorption using hydrophobic zeolites

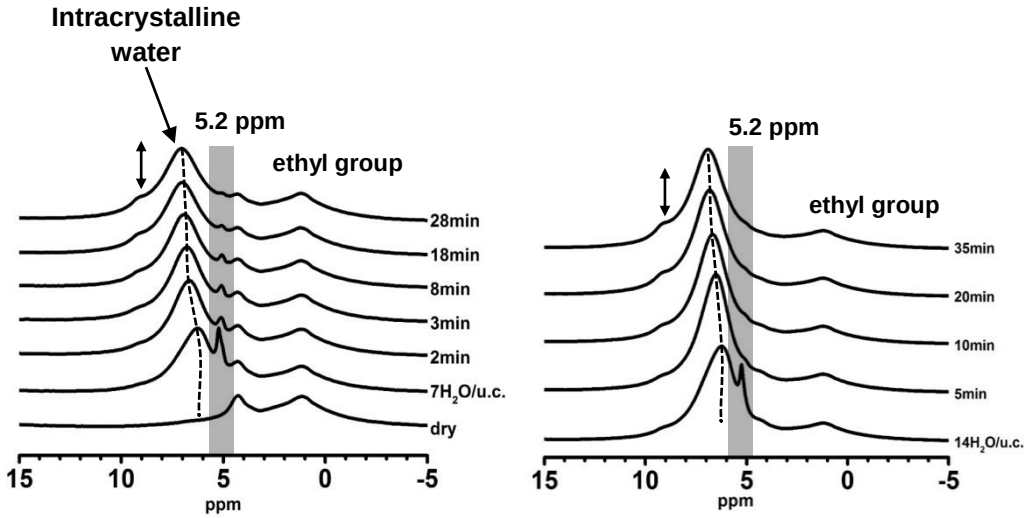

Figure 2.27. ^{1}H MAS NMR spectra of ETS-HZSM-5 (Si/Al = 15) catalyst exposed to liquid water using a microsyringe for quantitative adsorption. In **(a)**, the dry catalyst is shown in the first trace for reference, followed by exposure to 7 H_2O/u.c. in the second trace. Subsequent traces are acquired as a function of time for the single liquid water exposure step. The catalyst in **(b)** is the same as in **(a)**, but with the addition of one more 7 H_2O/u.c. exposure step for a total of 14 H_2O/u.c. The shaded box shows a previously unobserved extracrystalline liquid water peak, which disappears with time. The 9-ppm peak is again noted with the double-headed arrow. The dashed lines are shown only as guides to the eye.

About 1 eqv liquid water was injected directly to hydrophobically modified HZSM-5, with the ^{1}H MAS NMR spectra shown in Figure 2.27. Remarkably, organosilane (i.e. ETS) groups on the surface of zeolite crystallites are capable to keep the liquid water from entering into the internal pores of the catalyst. The shaded grey box in Figure 2.27 shows a sharp peak that appears with the first water adsorption step, and each subsequent steps, which comes from water in the liquid phase and presumably residing in any extracrystalline space. An intracrystalline water peak rises at 6 ppm, but shifts downfield as a function of time, coincident with the disappearance of the extracrystalline water peak. What Figure 2.27 suggests is that unlike the neat HZSM-5, liquid

water does not penetrate the intracrystalline zeolite ETS-HZSM-5 volume, but must first undergo phase transition to the vapor state.

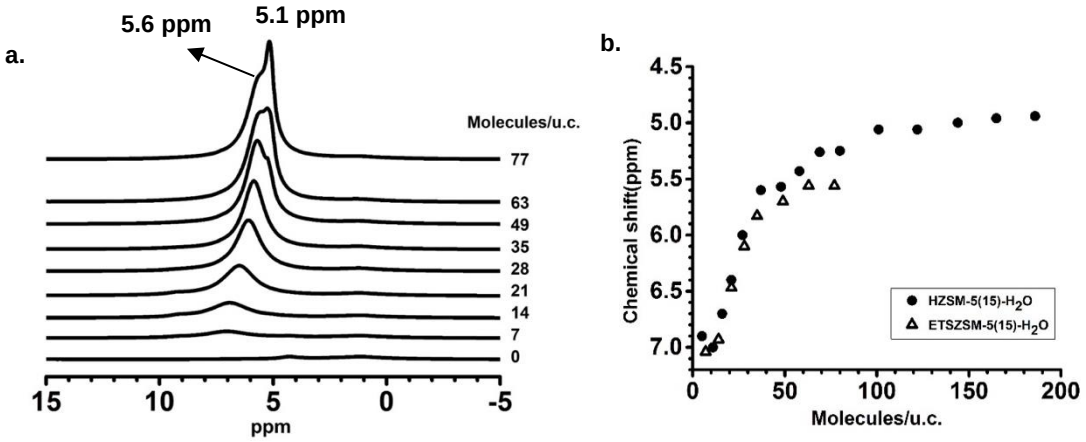

Figure 2.28. a) ^{1}H MAS NMR spectra of ETS-HZSM-5 (Si/Al = 15) catalyst exposed to liquid water using a microsyringe for quantitative adsorption, as in Figure 2.22, but where several hours elapsed between water exposure and spectral acquisition. b) The comparison of water chemical shift dependence with water loadings of hydrophobic ETS-HZSM-5 and normal HZSM-5 catalysts.

Figure 2.28 shows results similar to Figure 2.27, in which ETS-HZSM-5 is exposed to quantitative amounts of liquid water but where several hours passed between water addition and spectral acquisition, and where much higher water loadings were accessed. Unlike Figure 2.27, no extracrystalline bulk water peak is observed in Figure 2.28, and the intracrystalline water peak shifts upfield with increasing water loading, as expected from the vapor-phase water data. However, the exchange-averaged water chemical shift stops at 5.3−5.6 ppm for the ETS-HZSM-5 between 50 and 80 waters per unit cell, and it does not change with increased water loadings. The time delay between acquiring the data for the last two points in Figure 2.28 was more than 24 h. After ~35 water molecules per unit cell, a sharp peak is observed near 5.1−5.3 ppm, similar to

that seen above in Figure 2.27, which only increases with increased liquid water exposure, even when up to 17 h of equilibration time exists between adsorption and spectral acquisition. This is confirmed with the D_2O control experiment shown in Figure 2.29; a sharp extracrystalline water peak is observed at loadings greater than ~35 molecules per unit cell. Interestingly, 35 water molecules per unit cell is consistent with the maximum water loading measured in Figure 2.5, and in the same range as expected from the curve inflections shown in Figure 2.28b. Thus, the clear picture that emerges from the data in Figures 2.24, 2.26, and 2.27, as well as that in Figure 2.29, is that zeolite surface hydrophobization prohibits liquid water interaction with both the exterior and interior surface volumes of the catalyst, and thus framework acid sites are effectively protected from potential liquid water solvation. Water must first vaporize from the liquid phase before it can diffuse into the intracrystalline channels of ETS-HZSM-5.

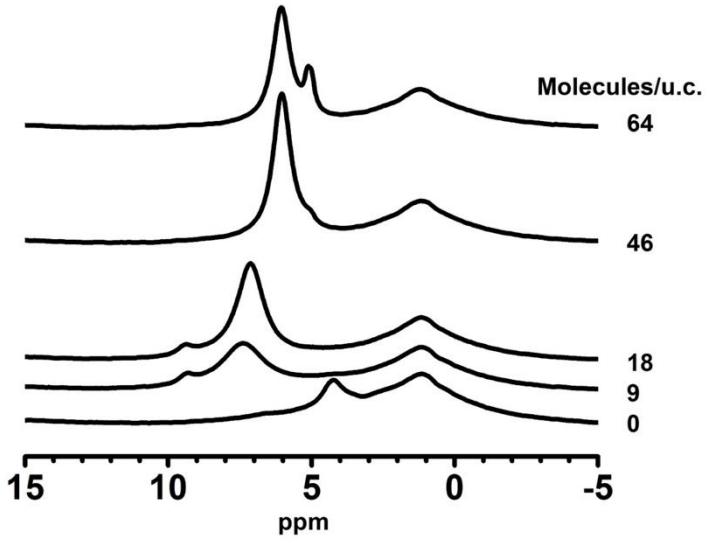

Figure 2.29. ^1H MAS NMR spectra for D_2O in ETS-HZSM-5 as a function of its loading per zeolitic unit cell.

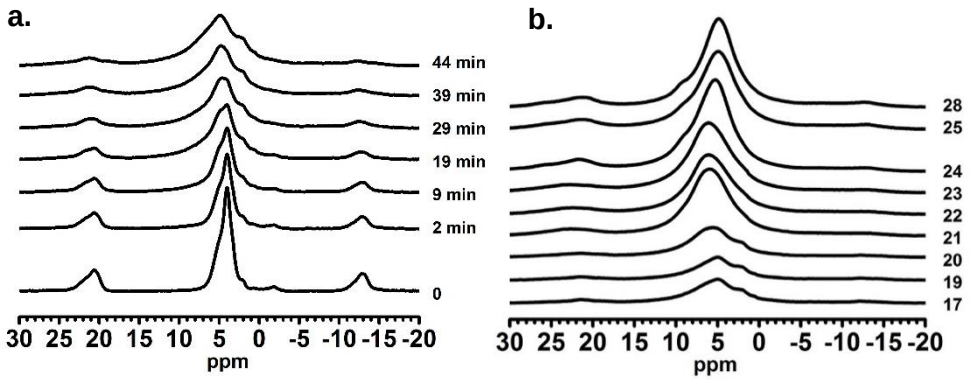

Figure 2.30. ^{1}H MAS NMR spectra for HY Si/Al = 2.6 zeolite with water loaded via ambient exposure method. Spectra in both **(a)** and **(b)** are plotted as a function of exposure time. Spectra in **(b)** do not have accurate exposure time measured, but are plotted in the increasing trend labeled by exposure numbers. The 17-spectrum in **(b)** is a continuation of the 44-minspectrum in **(a)**.

2.3.4 Water adsorption on HY zeolite

Figure 2.30 illustrates the loading-dependent ^{1}H NMR spectra of HY at Si/Al = 2.6. The bottom trace in Figure 2.30a shows the spectrum of a dry catalyst. It is well known that the signal at 2 ppm is due to nonacidic silanol groups, while the sharp 3.9-ppm signal due to acid sites pointing into the large cages (supercages in Y zeolite). The 4.9-ppm signal, appearing as a left shoulder of the 3.9-ppm peak, is due to acid sites pointing into small cages (sodalite cages in Y zeolite). The water in Figure 2.30 was qualitatively loaded by the ambient exposure approach, as described in Figure 2.4, i.e. more exposure time indicating more water was adsorbed into the catalyst. With water loading increased, the sharp 3.9 ppm peak decreases first (from 2 min to 19 min spectra), indicating that only the acid sites at supercages, which is more accessible by water molecules, are titrated. However, it is unclear if the sodalite acid peak is interacted by water just from the ^{1}H NMR inspection. In contrast to HZSM-5, HY zeolites are not a good model catalyst for fundamental study because of their complicated pore structures, which is the reason that ZSM-5

zeolites are chosen in this contribution. What different from HZSM-5 ambient exposure results is, the water peak finally moved to 4.8 ppm but not 5.6 ppm, shown in the spectrum labeled as "28" in Figure 2.30b. The spectra in Figure 2.30b are in the ascending order of exposure time, but without quantified adsorption information. Spectrum "28" was obtained from the catalyst exposed for more than 2 days, thus must has reached the saturation condition. Why does the water vapor cause the HY zeolite's water peak shift to 4.8 ppm at saturation, whereas, 5.6 ppm for ZSM-5 zeolite? One of the possible reason is that the Si/Al ratio of HY zeolite used is 2.6, resulting in very short acid site distances that could favor the formation of continuous phased water. Unlike HZSM-5, the sidebands of "wet" HY 2.6 are significantly stronger. The spectrum "28" in Figure 2.30b is shown in Figure 2.31 with a broader frequency range, where, the fifth fold of the water sidebands are still observable. It could be due to the stronger dipolar coupling caused by the higher acid density.

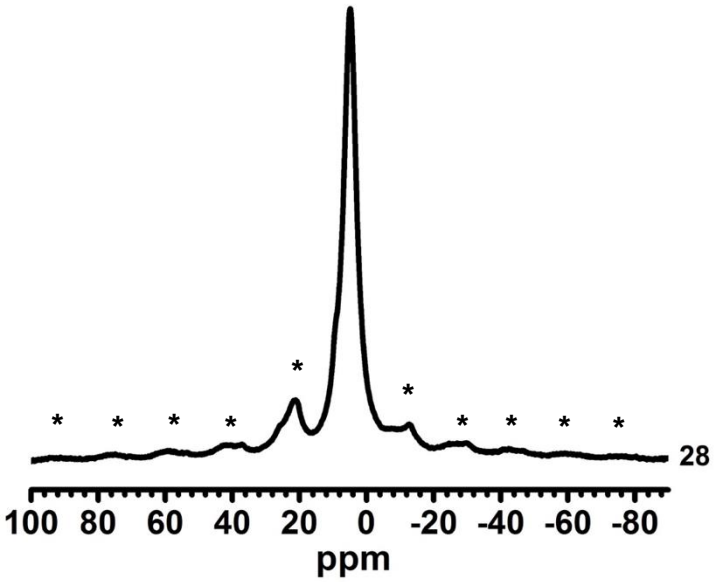

Figure 2.31. ^{1}H MAS NMR spectrum of water in HY zeolite previously mentioned in Figure 2.30b, labeled as spectrum 28, now shown in a larger chemical shift range.

2.4. Conclusion

In this chapter, a comprehensive investigation of water and zeolite interactions was approached by ^{1}H MAS NMR method coupled with different types of adsorption methods. The water interactions in acidic zeolite has been understood to a new level, shown in Table 2.1.

	Water/eqv.	$Z^{-}H^{+}\cdots H_2O$	$Z^{-}\cdots H_3O^{+}$	H^{+}	H_2O
Stage I	0 ~ 0.05	**Low**	**Low**	**High**	**Negligible**
	0.05 ~ 0.5	**High**	**High**	**High**	**Negligible**
Stage II	0.5 ~ 3	**High**	**High**	**Low**	**Low**
Stage IIII	3 ~ ∞	**Low**	**Low**	**Negligible**	**High**

Table 2.1. A summary of suggested amounts proton species at different stages of water adsorption.

The NMR data indicate acid sites play dominating roles at all stages, especially at Stage I and II. However, the numerical numbers of loading amounts in the first column are estimated numbers, based on observations on the Si/Al = 15 HZSM-5 catalyst. Si/Al = 25 and 40 zeolites show similar trends upon adsorption but have not been investigated thoroughly yet. At 0 ~ 0.05 eqv, the acid site decreases dramatically, and at 0.05 ~ 0.5 eqv, a downfield shifting water peak was observed. At Stage I, water is able to diffuse between different acid sites, and according to our observation, the amount of pristine acid sites is considerable. Whether a water molecule diffuses via hopping or reconfiguration mechanism is not experimentally investigated, but the former is preferred. The reconfiguration mechanism might be possible in HY 2.6 zeolites, where the acid sites are close enough, since water peak stops at 4.8 ppm (the resonance of bulk liquid water) by excess adsorption of water vapor, while the value is 5.6 ppm for HZSM-5 (15). Importantly, the Stage I results suggest that a single water molecule is capable to deprotonate the Brønsted acid

sites in HZSM-5. At stage II, with water amounts further increased, the acid sites are titrated up, evidenced by the disappearance of the acid peak and the chemical-shift unchanged water peak, i.e. 7 ppm for ZSM-5 (15) and 8 ppm for ZSM-5 (40). When water is loaded up to this level, the water clusters are gradually formed at acid sites. The water peak, e.g. 7 ppm for ZSM-5 (15), intensity increases while the line-width decreases with water loading increased, indicating formation of water clustered ions, e.g. $H_5O_2^+$ and $H_7O_3^+$. The silanol groups do interact with water, however, in a slow exchange regime. It is not until two or three eqv that free water molecules is observable by pulsed-field gradient ^{1}H NMR. At stage III, the water adsorbed on acid sites are close to saturation, resulting in abrupt increasing amount of free water. The amount of free water keeps increasing with increasing amount of external water additions, and gradually overwhelms the on-site water species.

2.5. References

1. Corma, A., Inorganic Solid Acids and Their Use in Acid-Catalyzed Hydrocarbon Reactions. *Chemical Reviews* **1995,** *95* (3), 559-614.
2. Nikolla, E.; Román-Leshkov, Y.; Moliner, M.; Davis, M. E., "One-Pot" Synthesis of 5-(Hydroxymethyl)furfural from Carbohydrates using Tin-Beta Zeolite. *ACS Catalysis* **2011,** *1* (4), 408-410.
3. Kabalan, I.; Lebeau, B.; Nouali, H.; Toufaily, J.; Hamieh, T.; Koubaissy, B.; Bellat, J.-P.; Daou, T. J., New Generation of Zeolite Materials for Environmental Applications. *The Journal of Physical Chemistry C* **2016,** *120* (5), 2688-2697.
4. Wang, H.; Pinnavaia, T. J., MFI Zeolite with Small and Uniform Intracrystal Mesopores. *Angewandte Chemie International Edition* **2006,** *45* (45), 7603-7606.
5. Choi, M.; Cho, H. S.; Srivastava, R.; Venkatesan, C.; Choi, D.-H.; Ryoo, R., Amphiphilic Organosilane-Directed Synthesis of Crystalline Zeolite with Tunable Mesoporosity. *Nat Mater* **2006,** *5* (9), 718-723.

6. Corma, A.; Diaz-Cabanas, M. J.; Jorda, J. L.; Martinez, C.; Moliner, M., High-throughput Synthesis and Catalytic Properties of a Aolecular Sieve with 18- and 10-Member Rings. *Nature* **2006,** *443* (7113), 842-845.

7. Gounder, R.; Davis, M. E., Beyond Shape Selective Catalysis with Zeolites: Hydrophobic Void Spaces in Zeolites Enable Catalysis in Liquid Water. *AIChE Journal* **2013,** *59* (9), 3349-3358.

8. Ennaert, T.; Van Aelst, J.; Dijkmans, J.; De Clercq, R.; Schutyser, W.; Dusselier, M.; Verboekend, D.; Sels, B. F., Potential and Challenges of Zeolite Chemistry in the Catalytic Conversion of Biomass. *Chemical Society Reviews* **2016,** *45* (3), 584-611.

9. Zapata, P. A.; Faria, J.; Ruiz, M. P.; Jentoft, R. E.; Resasco, D. E., Hydrophobic Zeolites for Biofuel Upgrading Reactions at the Liquid-Liquid Interface in Water/Oil Emulsions. *Journal of the American Chemical Society* **2012,** *134* (20), 8570-8578.

10. Vjunov, A.; Hu, M. Y.; Feng, J.; Camaioni, D. M.; Mei, D.; Hu, J. Z.; Zhao, C.; Lercher, J. A., Following Solid-Acid-Catalyzed Reactions by MAS NMR Spectroscopy in Liquid Phase-Zeolite-Catalyzed Conversion of Cyclohexanol in Water. *Angewandte Chemie International Edition* **2014,** *53* (2), 479-482.

11. Tian, P.; Wei, Y.; Ye, M.; Liu, Z., Methanol to Olefins (MTO): From Fundamentals to Commercialization. *ACS Catalysis* **2015,** *5* (3), 1922-1938.

12. Ilias, S.; Bhan, A., Mechanism of the Catalytic Conversion of Methanol to Hydrocarbons. *ACS Catalysis* **2013,** *3* (1), 18-31.

13. Haw, J. F.; Song, W.; Marcus, D. M.; Nicholas, J. B., The Mechanism of Methanol to Hydrocarbon Catalysis. *Accounts of Chemical Research* **2003,** *36* (5), 317-326.

14. T. Xu, J. L. White, U. S. Patent 6,743,747 (2004), priority filing and PCT published February 24, **2000**

15. T. Xu, J. L. White, U. S. Patent 6,734,330 (2004)**,** priority filing and PCT published July 13, **2000**.

16. White, J. L., Methanol-to-hydrocarbon Chemistry: The Carbon Pool (R)Evolution. *Catalysis Science & Technology* **2011,** *1* (9), 1630-1635.

17. Huo, H.; Peng, L.; Grey, C. P., Low Temperature ^{1}H MAS NMR Spectroscopy Studies of Proton Motion in Zeolite HZSM-5. *The Journal of Physical Chemistry C* **2009,** *113* (19), 8211-8219.

18. Kanellopoulos, J.; Gottert, C.; Schneider, D.; Knorr, B.; Prager, D.; Ernst, H.; Freude, D., NMR Investigation of Proton Mobility in Zeolites. *Journal of Catalysis* **2008,** *255* (1), 68-78.

19. Olson, D. H.; Haag, W. O.; Borghard, W. S., Use of Water as a Probe of Zeolitic Properties: Interaction of Water with HZSM-5. *Microporous and Mesoporous Materials* **2000,** *35–36* (0), 435-446.

20. Zhang, L.; Chen, K.; Chen, B.; White, J. L.; Resasco, D. E., Factors that Determine Zeolite Stability in Hot Liquid Water. *Journal of the American Chemical Society* **2015,** *137* (36), 11810-11819.

21. Zhao, Z.; Xu, S.; Hu, M. Y.; Bao, X.; Peden, C. H. F.; Hu, J., Investigation of Aluminum Site Changes of Dehydrated Zeolite H-Beta during a Rehydration Process by High-Field Solid-State NMR. *The Journal of Physical Chemistry C* **2015,** *119* (3), 1410-1417.

22. Hunger, M., Multinuclear Solid-state NMR Studies of Acidic and Non-Acidic Hydroxyl Protons in Zeolites. *Solid State Nuclear Magnetic Resonance* **1996,** *6* (1), 1-29.

23. Smith, L.; Cheetham, A. K.; Morris, R. E.; Marchese, L.; Thomas, J. M.; Wright, P. A.; Chen, J., On the Nature of Water Bound to a Solid Acid Catalyst. *Science* **1996,** *271* (5250), 799-802.

24. Bordiga, S.; Regli, L.; Lamberti, C.; Zecchina, A.; Bjørgen, M.; Lillerud, K. P., FTIR Adsorption Studies of H_2O and CH_3OH in the Isostructural H-SSZ-13 and H-SAPO-34: Formation of H-Bonded Adducts and Protonated Clusters. *The Journal of Physical Chemistry B* **2005,** *109* (16), 7724-7732.

25. Sauer, J., Probing Catalysts with Water. *Science* **1996,** *271* (5250), 774-775.

26. Marchese, L.; Chen, J.; Wright, P. A.; Thomas, J. M., Formation of Hydronium at the Broensted Site in SAPO-34 Catalysts. *The Journal of Physical Chemistry* **1993,** *97* (31), 8109-8112.

27. Kletnieks, P. W.; Ehresmann, J. O.; Nicholas, J. B.; Haw, J. F., Adsorbate Clustering and Proton Transfer in Zeolites: NMR Spectroscopy and Theory. *ChemPhysChem* **2006,** *7* (1), 114-116.

28. Li, H.; Mahanti, S. D.; Pinnavaia, T. J., Water Mediated Proton Transfer in a Mesostructured Aluminosilicate Framework: An ab Initio Molecular Dynamics Study. *The Journal of Physical Chemistry B* **2005,** *109* (46), 21908-21914.

29. Benco, L.; Demuth, T.; Hafner, J.; Hutschka, F., Spontaneous Proton Transfer in Na Zeolites. *Chemical Physics Letters* **2000,** *330* (3–4), 457-462.

30. Alberti, A.; Martucci, A., Proton Transfer Mediated by Water: Experimental Evidence by Neutron Diffraction. *The Journal of Physical Chemistry C* **2010,** *114* (17), 7767-7773.

31. Termath, V.; Haase, F.; Sauer, J.; Hutter, J.; Parrinello, M., Understanding the Nature of Water Bound to Solid Acid Surfaces. Ab Initio Simulation on HSAPO-34. *Journal of the American Chemical Society* **1998,** *120* (33), 8512-8516.

32. Beck, L. W.; White, J. L.; Haw, J. F., 1H{27Al} Double-Resonance Experiments in Solids: An Unexpected Observation in the 1H MAS Spectrum of Zeolite HZSM-5. *Journal of the American Chemical Society* **1994,** *116* (21), 9657-9661.

33. Janda, A.; Bell, A. T., Effects of Si/Al Ratio on the Distribution of Framework Al and on the Rates of Alkane Monomolecular Cracking and Dehydrogenation in H-MFI. *Journal of the American Chemical Society* **2013,** *135* (51), 19193-19207.

34. Dec, S. F.; Bronnimann, C. E.; Wind, R. A.; Maciel, G. E., Comparison of the ^{1}H NMR Analysis of Solids by the CRAMPS and MAS-Only Techniques. *Journal of Magnetic Resonance (1969)* **1989,** *82* (3), 454-466.

35. Tanner, J. E., Use of the Stimulated Echo in NMR Diffusion Studies. *The Journal of Chemical Physics* **1970,** *52* (5), 2523-2526.

36. Hunger, M.; Freude, D.; Pfeifer, H., Magic-Angle Spinning Nuclear Magnetic Resonance Studies of Water Molecules Adsorbed on Brønsted- and Lewis-acid Sites in Zeolites and Amorphous Silica-Aluminas. *Journal of the Chemical Society, Faraday Transactions* **1991,** *87* (4), 657-662.

37. Brunner, E.; Beck, K.; Koch, M.; Heeribout, L.; Karge, H. G., Verification and Quantitative Determination of a New Type of Brønsted Acid Sites in H-ZSM-5 by ^{1}H Magic-Angle Spinning Nuclear Magnetic Resonance Spectroscopy. *Microporous Materials* **1995,** *3* (4–5), 395-399.

38. Freude, D., Enhanced Resolution in the ^{1}H NMR Spectra of Zeolite H-ZSM-5 by Heteronuclear Dipolar-Dephasing Spin-Echo MAS. *Chemical Physics Letters* **1995,** *235* (1–2), 69-75.

39. Bronnimann, C. E.; Zeigler, R. C.; Maciel, G. E., Proton NMR Study of Dehydration of the Silica Gel Surface. *Journal of the American Chemical Society* **1988,** *110* (7), 2023-2026.

40. Hunger, M., Brønsted Acid Sites in Zeolites Characterized by Multinuclear Solid-State NMR Spectroscopy. *Catalysis Reviews* **1997,** *39* (4), 345-393.

41. Rothwell, W. P.; Waugh, J. S., Transverse Relaxation of Dipolar Coupled Spin Systems Under RF Irradiation: Detecting Motions in Solids. *The Journal of Chemical Physics* **1981,** *74* (5), 2721-2732.

42. White, J. L.; Brant, P., Direct Detection of Miscibility in Saturated Polymer Blends. *Macromolecules* **1998,** *31* (16), 5424-5429.

43. Arı, M. U.; Ahunbay, M. G.; Yurtsever, M.; Erdem-Şenatalar, A., Molecular Dynamics Simulation of Water Diffusion in MFI-Type Zeolites. *The Journal of Physical Chemistry B* **2009,** *113* (23), 8073-8079.

44. Harris, K. D. M.; Xu, M. C.; Thomas, J. M., Probing the Evolution of Water Clusters During Hydration of the Solid Acid Catalyst H-ZSM-5. *Philos. Mag.* **2009,** *89* (33), 3001-3012.

CHAPTER III

DISCOVERY OF WATER'S POSITIVE EFFECT ON C-H BOND ACTIVATIONS

3.1 Introduction

Most of the zeolite-catalyzed reactions, such as catalytic cracking, methanol to hydrocarbon conversion (MTH), etc., occur in hydrophobic environments. One may argue that methanol molecules are hydrophilic. However, the hydrocarbon pool molecules, the key intermediates of the conversions, are aromatic molecules and are totally hydrophobic. Almost all of the traditional zeolite based reactions are executed at high temperatures exceeding 250 °C.[1] In MTH conversion, questions such as "What species has the first C-C bond?", "How does the bond form?", are the key questions of understanding the mechanisms. However, the early stages of the conversion are still not clearly revealed, because the secondary and tertiary stages form at the same time scale with the primary stage, and thus the primary products are usually consumed or covered by secondary and tertiary products.[2] In 2006, the C-H bond activation in zeolite was demonstrated by Truitt et al. for the first time,[3] shown in Figure 3.1. Truitt et al. showed that H/D exchanges take places when isobutane-d_{10} is adsorbed on zeolite HZSM-5 at extremely mild conditions: room temperatures, one equivalent and less than one atmosphere pressure. At such mild conditions, the

time scale of zeolite-catalyzed reactions can be reduced to a new level, possibly making the catalytic steps distinguishable. The low temperature analogous reactions can be a new approach to reveal early stage mechanisms of typical zeolite based catalysis.

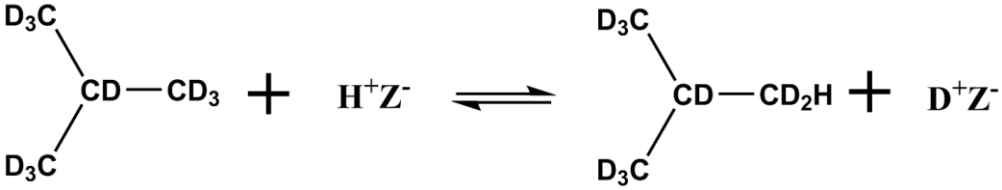

Figure 3.1. H/D exchanges between isobutane-d_{10} and acidic ZSM-5 take places at room temperature.

Our recent research suggest that water plays an unexpected, positive role for this room temperature isobutane proton exchange reaction. The discovery of water's new positive role is revealed by in-situ MAS NMR method. Historically, water has always been considered to reduce the catalyst activity. First, water is a competitive base that strongly adsorbs at the acid site, thereby inhibiting proton availability for hydrocarbon reagents.[4-6] Second, at high-temperatures, the presence of water may lead to lattice dealumination and loss of acidity. Finally, in the case of zeolites, the presence of condensed water causes severe losses in crystallinity and catalytic activity.[7] In this research, we show that water can both enhance and suppress the activity of alkane reactivity in zeolites. When a small amount, << 1 eqv, of water is co-adsorbed, the rate of isobutane C-H reactivity in zeolite can be enhanced by one order of magnitude. The reactivity is suppressed when water appears at large loadings.

3.2 Experimental

3.2.1. Isobutane adsorption method. Zeolites used were activated as described in Section 2.2.1. Similar as the vacuum-line method for water adsorption, a vacuum-line equipped with a

CAVERN type apparatus was used for quantitative adsorption. A fixed quantity of catalyst was placed in a 7 mm zirconia MAS NMR rotor in the CAVERN apparatus, evacuated and sealed, and the adsorbate vapor was introduced in the vacuum line to an initial pressure, illustrated schematically in Figure 3.2. A desired pressure drop was used to control the adsorption quantity after exposure to the catalyst. The initial pressure and pressure drop vary with the vacuum line/CAVERN body volumes, the adsorbate molecules, the catalyst quantities and their Si/Al ratios. For example, to adsorb isobutane-d10 (C/D/N Isotopes Inc.) onto HZSM-5 catalyst, 40 mg catalyst was loosely packed into the rotor. Subsequently, 20 torr of initial pressure and 3.2 torr of pressure drop were used to determine when 1 eqv of isobutane-d_{10} was adsorbed. In all stack plots shown, spectral traces in a single stack plot are from the same sample unless otherwise noted.

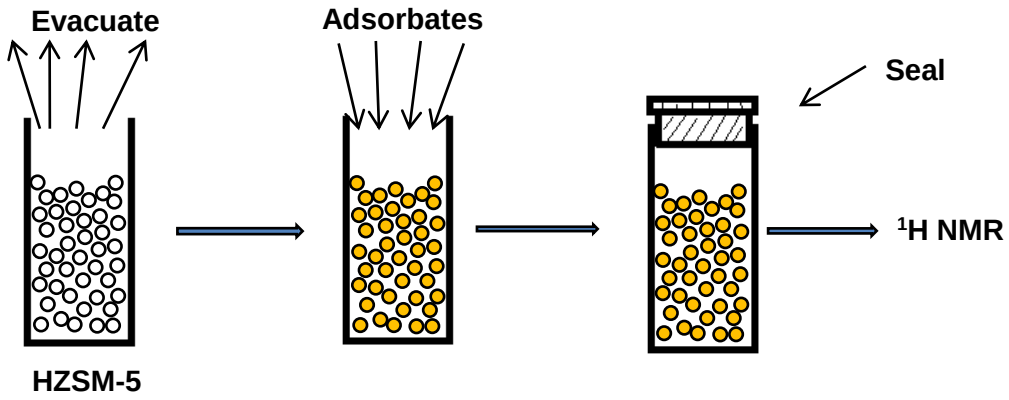

Figure 3.2. Scheme of an adsorption experiment

3.2.2. H/D exchange experiments. In-situ solid state ^{1}H MAS NMR methods were used to inspect the reactions. For dry-catalyst experiments, 1 eqv of isobutane was adsorbed into both ZSM-5 (15) as described above and then tested by ^{1}H NMR. The H/D exchanges took place immediately after adsorptions, while the adsorption processes usually took 2-4 minutes for completion. The initial H/D exchange spectra were typically acquired 10-15 minutes following the initial exposure. The following spectra were then taken as a function of time to follow the reaction, as shown in Figure 3.4. For experiments involving water, catalysts were qualitatively

exposed to ambient exposure in a 7 mm rotor to adsorb water moisture. After ambient exposure, the wet catalyst was characterized by ^{1}H MAS NMR to confirm the water loadings as shown in Figure 3.3. After NMR characterization, they were opened inside the glove box to avoid ambient exposure, immediately inserted to the CAVERN body, sealed, and transferred to the vacuum line for subsequent isobutane-d_{10} co-adsorption.

3.2.3. NMR measurements. ^{1}H MAS (magic-angle spinning) NMR data were collected on a Bruker DSX-300 MHz spectrometer, with spinning rate of 5 kHz, using a single 3.8 μs $\pi/2$ excitation pulse. Recycle delays were 10 seconds for dry zeolites, as relaxation measurements yielded T_{1H} value of 1.9-2.0 seconds. For catalysts exposed to any reagent or water, a 1-second recycle delay was sufficient for acquisition of quantitative spectra, since T_1's were reduced to 0.1-0.2 s following adsorption. However, to be consistent, 10-second recycle delays were used for both dry and "wet" experiments. Typically, 64 scans were acquired per spectrum.

3.3 Results and discussion

Using the rotor-ambient-exposure method described in Chapter II, HZSM-5 catalysts with and without trace amount of water were prepared, and characterized by ^{1}H MAS NMR, as displayed in Figure 3.3. Recall from Chapter II that the Brønsted acid site peak decreases abruptly with trace amount of water adsorbed, i.e. < 0.1 eqv. From the water adsorption results (Figure 2.10), we know that less than 0.05-eqv water was adsorbed in catalyst (b). Both catalyst (a) and (b) were then loaded with 1 eqv isobutane-d_{10}, and subsequently inspected by in-situ ^{1}H NMR.

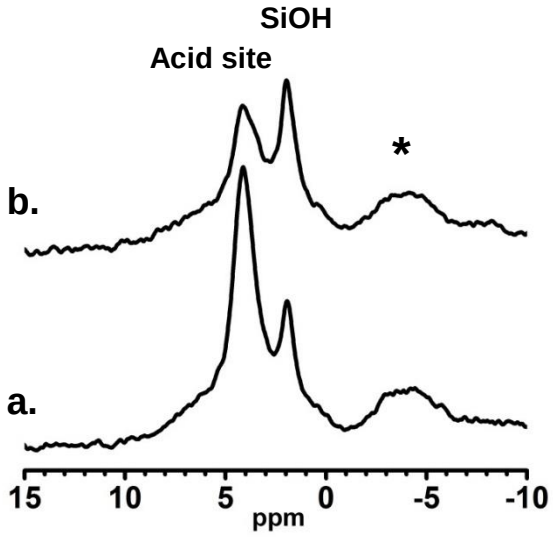

Figure 3.3. ^{1}H MAS NMR spectra of identically-prepared Si/Al = 15 HZSM-5 catalysts, in which an apparent loss of Brønsted acid site intensity at 4.2 ppm is observed in (b) versus (a). The broad signal denoted by * is a constant-area background signal from the probe. The spectra were obtained at 5 kHz MAS speeds.

Figure 3.4 shows the time series spectra obtained following adsorption of isobutane-d_{10} on catalyst (a) and (b) in Figure 3.3. The starting catalyst, i.e. prior to isobutane adsorption, corresponds to that shown in Figure 3.3a, and similarly, Figure 3.4b corresponds to that shown in Figure 3.3b. In each case, 1 eqv isobutane-d_{10} was adsorbed using the CAVERN-adsorption method. Note that the isobutane pressure started at 20 torr and ended at 16 torr, with respect to the pressure before and after adsorption. Therefore, the actual partial pressure of isobutane inside the closed rotor must be less than 16 torr, since the adsorption into the catalyst did stop even after the rotor was sealed. Therefore, the absolute pressure inside the sealed rotor is not measurable, but it must be less than 16 torr. After adsorption, ^{1}H MAS NMR spectra were obtained as a function of time, plotted in Figure 3.4. Two key features are apparent in these data: 1) The Brønsted acid peak originally at 4.2 ppm shifts to 4.9-5.1 ppm with subsequent intensity decrease as H/D

exchange occurs with isobutane-d_{10}, and 2) a protonated peak arises at 1.1 ppm, corresponding to newly formed C-H species in isobutane. The silanol peak at 1.9 ppm is unaffected throughout the reaction.

Once isobutane molecules are adsorbed, protons on acid sites and deuteriums on isobutane molecules undergo reversible exchange immediately, see Figure 3.4. However, the excess amount of deuterium over proton, i.e. D:H = 10:1 at 1 eqv loading, leads to almost complete transfer of protons from acid sites to the methyl groups. Because deuterium nucleus is silent in ^{1}H NMR, the exchange extension can be greatly followed by observing the reduction of the acid peak and the increment of the methyl peak, which are labled in Figure 3.4 for clarity. The H/D exchange between isobutane-d_{10} and HZSM-5 is not new, but the suprising observation in Figure 3.4 is. That is, the exchange rate is <u>much higher</u> with the presence of water than without water, considering that water typically inhibits solid acid activities. The difference is clearly seen by comparisons of individual time points in Figure 3.4a to the relative points in Figure 3.4b, e.g. 165 min versus 174 or 45 versus 44 min, where the former methyl peak intensities are much higher than the latter ones.

While not shown here, the exchange reactions shown in Figure 3.4a were also measured after twelve days of reaction to ensure isotopic equilibration. The integrated area ratio of the isobutane CH_3 peak to the acid site signal ranged from 8.5-10:1, which is near the expected 9:1 ratio for the targeted 1 equivalent isobutane loading. This control experiment demonstrates that our MAS rotor system is sealed and no loss of isobutane or ingress of water occurs, and that within reasonable error, we can control the intended isobutane adsorption amount. The results depicted in Figure 3.4 are representative of results observed in multiple experiments. Comparisons of the spectral differences in Figure 3.3, the first spectra in each of the time series shown in Figure 3.4, and the water interactions observed in Chapter II, i.e. Figure 2.9 and 2.10, lead us to propose that the key difference between these two catalysts is the co-adsorbed water at

Stage I level. For the sake of discussion, we will call the catalyst in 3.3a/3.4a the "dry" catalyst, and the one in 3.3b/3.4b the "wet" catalyst.

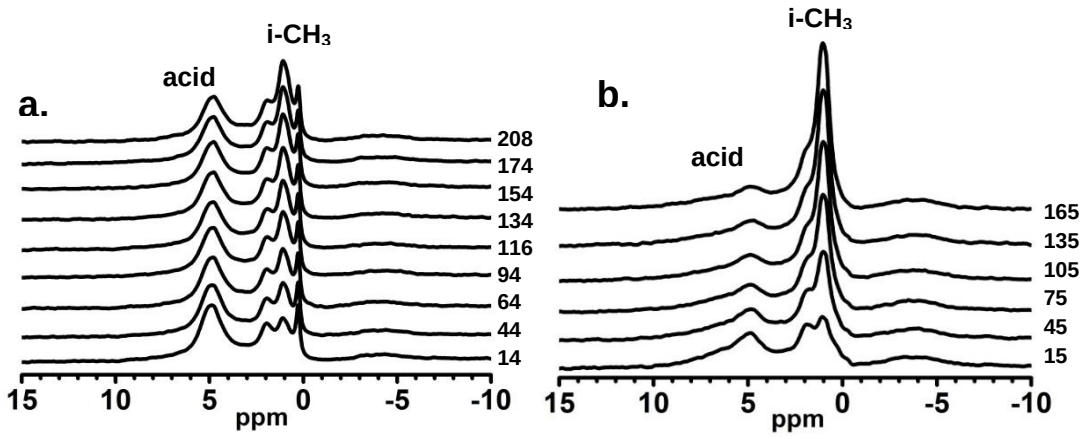

Figure 3.4. ^{1}H MAS NMR exchange stack plots at 296 K of **(a)** a catalyst corresponding to that shown in Figure 3.3a and **(b)** a catalyst corresponding to that in spectrum 3.3b, in which 0.94 and 1.0 equivalent of isobutane-d_{10} are adsorbed, respectively. The total elapsed time following isobutane adsorption, in minutes, is indicated. The very sharp peak at 0.2 ppm in **(a)** is from an inert polydimethylsiloxane (solid) chemical shift and intensity standard, which verifies the ca. 1-ppm change in chemical shift for the acid site following adsorption, and the constant silanol signal intensity.

Kinetic analysis The time dependent spectra in Figure 3.4 provide abundant information for kinetic analysis. Peak deconvolutions were approached by using OriginLab software, via a combined Gaussian-Lorentzian simulation method, see Equation 3.1, where y_0 = baseline, x_c = peak center, A = amplitude, w = width (full width at half maximum), s = shape.

$$y = y_0 + \frac{A}{1 + e^{0.5(1-s)\left(\frac{x-x_c}{w}\right)^2 s\left(\frac{x-x_c}{w}\right)^2}} \qquad \text{Equation 3.1}$$

Using this method, the acid (4.8 ppm), silanol (3 ppm) and methyl (1 ppm) peaks can be well resolved. A deconvolution example, adapted from the 134-min spectrum in Figure 3.4a, is shown in Figure 3.5. Note there are always strong sidebands of the acid peak, marked with stars in Figure 3.5, because acid sites rarely undergo exchanges between each other, leading to strong

anisotropic dipolar interactions.[8] To ensure quantitative analysis, the sidebands must be counted and added up to their relative main peak intensity. Note the small acid peak in this dry condition compared to a regularly calcined catalyst in Figure 2.1b.

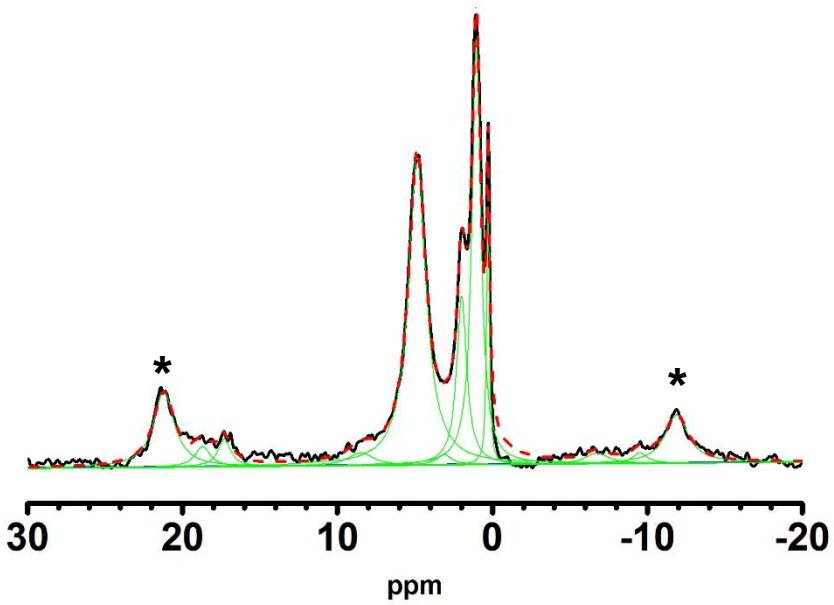

Figure 3.5. An example showing peak deconvolution result using the combined Gaussian-Lorentzian method. Note: solid black line = original spectra, dashed red line = convoluted spectra, green lines = resolved peaks.

Since the NMR signal is quantitative, the intensity of each resolved peak can be used as 'concentration' for kinetic analysis. Using "CD" as a short term for isobutane-d_{10}, the exchange reaction can be simplified as

$$CD + H^+ \underset{k_{-1}}{\overset{k_1}{\rightleftharpoons}} CH + D^+$$

Using 'm, n, o, p' to represent the partial reaction order of each specie, the overall reaction rate can be obtained,

$$Rate = k_1[CD]^m[H^+]^n - k_{-1}[CH]^o[D^+]^p = -\frac{d[H^+]}{dt} = \frac{d[CH]}{dt}$$

Because deuterium is in excess, especially at initial conditions, the reverse reaction can be ignored, thus the term $k_{-1}[CH]^o[D^+]^p \approx 0$. Also, simplify $k_1[CD]^m$ to k', got

$$Rate = k_1[CD]^m[H^+]^n = k'[H^+]^n = -\frac{d[H^+]}{dt} = \frac{d[CH]}{dt}$$

Normally, only one acid site is believed to be involved in each exchange, so n = 1. Then the consumption rate of the acid proton can be derived as

$$k'[H^+] = -\frac{d[H^+]}{dt}$$

$$ln\left(\frac{[H^+]}{[H^+]_0}\right) = -k't \qquad \text{Equation 3.2}$$

Using $[H^+]_0$ and $[CH]_\infty$ as notations for the moles of initial acid site and final

$$[H^+] = [H^+]_0 - [CH] = [CH]_\infty - [CH]$$

Where $[H^+]_0 = [CH]_\infty$. Thus, the rate of the formation of [CH] can be expressed as

$$ln\left(\frac{\left[[H^+]_0 - [CH]\right]}{[CH]_\infty}\right) = -k't$$

$$ln\left(\frac{\left[[CH]_\infty - [CH]\right]}{[CH]_\infty}\right) = -k't$$

$$ln\left(1 - \frac{[CH]}{[CH]_{\infty}}\right) = -k't \qquad \text{Equation 3.3}$$

Equation 3.2 and 3.3 were used as the basic functions to convert ^{1}H NMR spectra to kinetic plots. k' is the rate reported rate constant, in unit s^{-1}.

The quantitative treatment, via Equation 3.2 and 3.3, of the data shown in Figure 3.4, is summarized in Figure 3.6. Integrated peak areas for the isobutane CH_3 (1.1 ppm) and the acid site (4.2 ppm) signals are plugged into Equation 3.2 and 3.3 separately, then plotted versus the reaction time for the initial rate region of the exchange. The positive slope corresponds to the growth of CH_3 signal from H/D exchange, while the negative slope is from the decreasing acid site signal. The "dry" versus "wet" results, corresponding to the experiments in 3.4a versus 3.4b, are denoted by open and closed symbols, respectively. Usually, the acid peak of a "wet" catalyst is broadened because of the water-acid site, thus, the deconvolution is less accurate than for a "dry" spectrum. However, the CH_3 peak is generally sharp and well resolved, and thus more dependable for analysis. There are two important conclusions from this data. First, the reaction with the dry catalyst exhibits equal rate constants for the loss of the acid site signal and the gain of the isobutane CH_3 signal, as expected for a two-site H/D exchange process between the catalyst and the reactant. Second, the exchange rate constant for the growth of the CH_3 proton signal in the "wet" catalyst is an order of magnitude larger than in the dry system, and it is larger than its corresponding acid site signal change (solid points). The observation that the growth of the "wet" CH_3 signal is faster than the loss of the Brønsted acid site signal is consistent with our proposal that this catalyst has some residual water. The residual water can exchange with the acid site, serving as a secondary proton source to replenish the acid signal following a deuterium exchange event with the isobutane-d_{10} through a three-site exchange process.

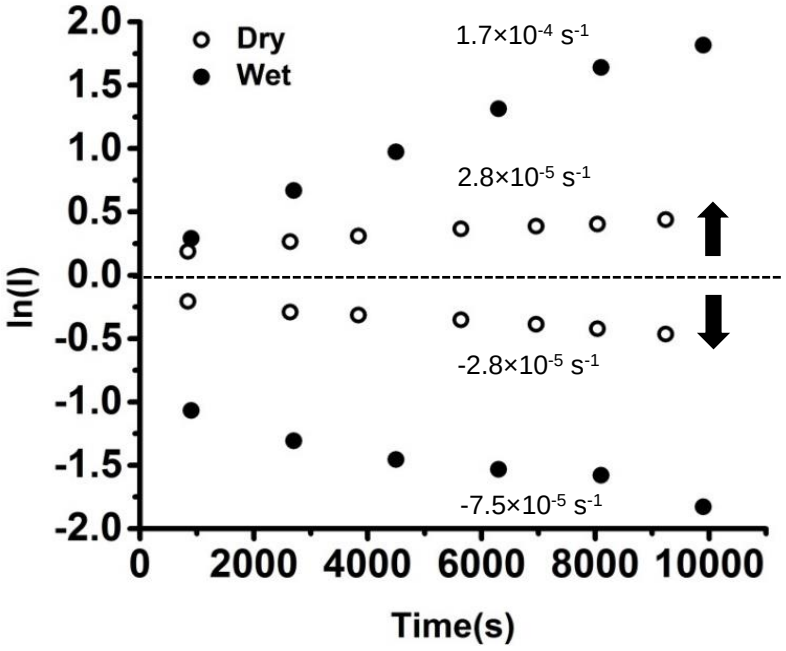

Figure 3.6. Semilogarithmic plot for the room-temperature exchange data shown in Figure 3.4, with areas taken from the 1.1 ppm isobutane CH_3 (positive points) and 5.0 ppm acid site (negative points) peaks. Note that the rate constants provided in the figure indicate identical exchange rates for the reaction in the dry catalyst, but inequivalent methyl and acid proton signal intensity changes for the less dry, or "wet", catalyst.

Control experiments of which water at different amounts were adsorbed onto dry HZSM-5 via ambient exposure, followed by 1 eqv isobutane adsorption. A graphical summary of the relationship between the reaction rate for isobutane C-H activation reaction and catalyst water content is shown in Figure 3.6, with reduced exchange rates occurring once the water content increases above the ca. 0.3 eqv level.

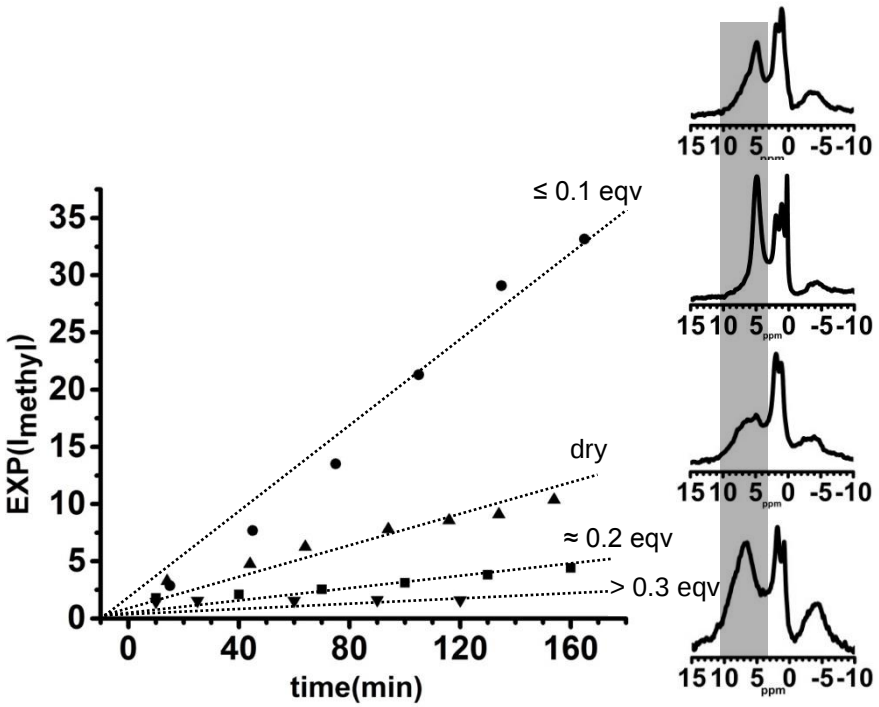

Figure 3.6. Linearized single-exponential growth plots of the isobutane CH_3 peak area in the ^1H MAS exchange spectra as a function of reaction time, for four different water loadings in equivalents. The dashed lines are simply drawn as guides to the eye through the raw data points. The corresponding spectra for the first time point in the exchange series are shown near their trend line, ordered from top to bottom. Note that the ca. ≤ 0.1 eqv loading corresponds to a spectrum with clear acid site peak but no obvious water peak (shaded box inset). The water loading of the bottom two catalysts were not quantified, while, one has neither a well-defined water nor acid peak, and the other has a well-defined water peak but no acid site peak. Rough loadings can be obtained by comparing Figure 2.10.

3.4. Conclusion

Zeolite-catalyzed alkane C-H bond activation reactions carried out at room temperature, low pressure, and low reagent loadings demonstrate that water can act either to increase or to suppress the observed reaction rates. Isobutane reaction rate constants are *increased by a factor of 10* at water loadings in the range of ca. ≤ 0.1 water molecule per catalyst active site relative to the dry catalyst. Conversely, too much water, i.e. > 0.2 eqv, retards isobutane reaction, which can be

understood based on the much higher proton affinity of water clusters compared to single water or isobutane molecules. These results indicate that water can be an active participant in reactions involving hydrophobic molecules in solid acid catalysts. Such conditions exist in well-known catalytic reactions, e.g., methanol-to-hydrocarbon and biomass-generated ethanol-to-hydrocarbon chemistries, since stoichiometric water is a first-formed byproduct. Further experiments with better control of water loadings using aromatic reagents will be presented in Chapter III.

3.5. References

1. Martínez, C.; Corma, A., Inorganic Molecular Sieves: Preparation, Modification and Industrial Application in Catalytic Processes. *Coordination Chemistry Reviews* **2011,** *255* (13–14), 1558-1580.
2. Haw, J. F.; Song, W.; Marcus, D. M.; Nicholas, J. B., The Mechanism of Methanol to Hydrocarbon Catalysis. *Accounts of Chemical Research* **2003,** *36* (5), 317-326.
3. Truitt, M. J.; Toporek, S. S.; Rovira-Truitt, R.; White, J. L., Alkane C−H Bond Activation in Zeolites: Evidence for Direct Protium Exchange. *Journal of the American Chemical Society* **2006,** *128* (6), 1847-1852.
4. Corma, A.; Marie, O.; Ortega, F. J., Interaction of Water with the Surface of a Zeolite Catalyst during Catalytic Cracking: A Spectroscopy and Kinetic Study. *Journal of Catalysis* **2004,** *222* (2), 338-347.
5. Zhao, Y. X.; Wojciechowski, B. W., The Consequences of Steam Dilution in Catalytic Cracking. *Journal of Catalysis* **1996,** *163* (2), 365-373.
6. Kletnieks, P. W.; Ehresmann, J. O.; Nicholas, J. B.; Haw, J. F., Adsorbate Clustering and Proton Transfer in Zeolites: NMR Spectroscopy and Theory. *ChemPhysChem* **2006,** *7* (1), 114-116.

7. Zhang, L.; Chen, K.; Chen, B.; White, J. L.; Resasco, D. E., Factors that Determine Zeolite Stability in Hot Liquid Water. *Journal of the American Chemical Society* **2015,** *137* (36), 11810-11819.

8. Baba, T.; Komatsu, N.; Ono, Y.; Sugisawa, H., Mobility of the Acidic Protons in H−ZSM-5 As Studied by Variable Temperature ^{1}H MAS NMR. *The Journal of Physical Chemistry B* **1998,** *102* (5), 804-808.

CHAPTER IV

WATER'S IMPACT ON THE REACTIONS OF AROMATIC MOLECULES IN ZEOLITES

4.1. Introduction

The results of isobutane experiments have taught us a remarkably unexpected role that water plays in zeolite catalysis. However, isobutane, containing only C-H and C-C bonds, poses the consequent questions: Is the water's positive effect on zeolite catalyzed reactions more general than isobutane? Aromatic molecules, known as the star molecules in carbon pool mechanism, are chosen to be test molecules for water's effect.

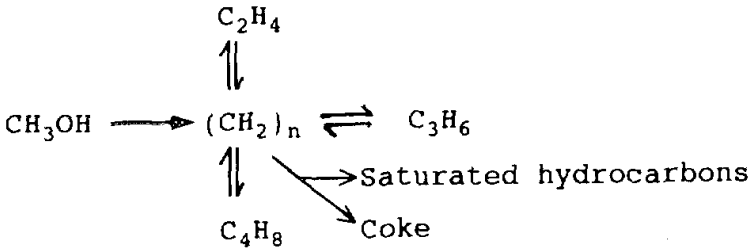

SCHEME 1. Carbon pool mechanism.

Figure 4.1. Carbon pool mechanism in zeolite based Methanol to Hydrocarbon (MTH) conversion, adapted from reference 7.

Methanol to Hydrocarbon conversion and carbon pool mechanism

The methanol to Hydrocarbon (MTH) process over acidic zeolites, first discovered by Exxon Mobil in 1976,[1] has regained interest in recent years as the global energy demand increases and the conventional energy resources decrease. In addition, methanol is renewable from feedstocks such as natural gas[2], coal[3-4], and biomass[5-6]. Dahl (1994) pointed out that certain types of chemicals, now known as carbon pool species, have to form first to initiate the MTH conversion, illustrated in Figure 4.1.[7] However, it was not until 2000 that Xu and White uncovered the aromatic nature of the carbon pool species.[8-9] To date both the carbon pool identifications and mechanisms are well developed, shown in Figure 4.2.[10] Despite the type of zeolite catalyst used, or the type of product targeted (Figure 4.2a), the carbon-pool molecules have to be built up for further conversion. Figure 4.2b shows the two well-known catalytic cycles of the carbon pool mechanism. In the aromatic cycle, side chain alkylation and dealkylation reactions are the most common chemistry occuring. Usually, the formation of carbon pool is the rate-limiting step in MTH conversions.

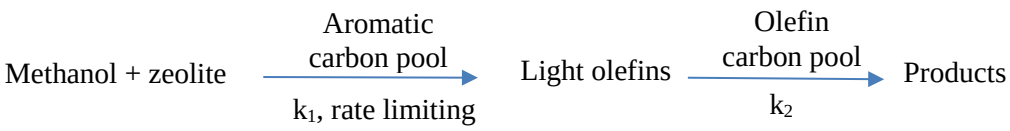

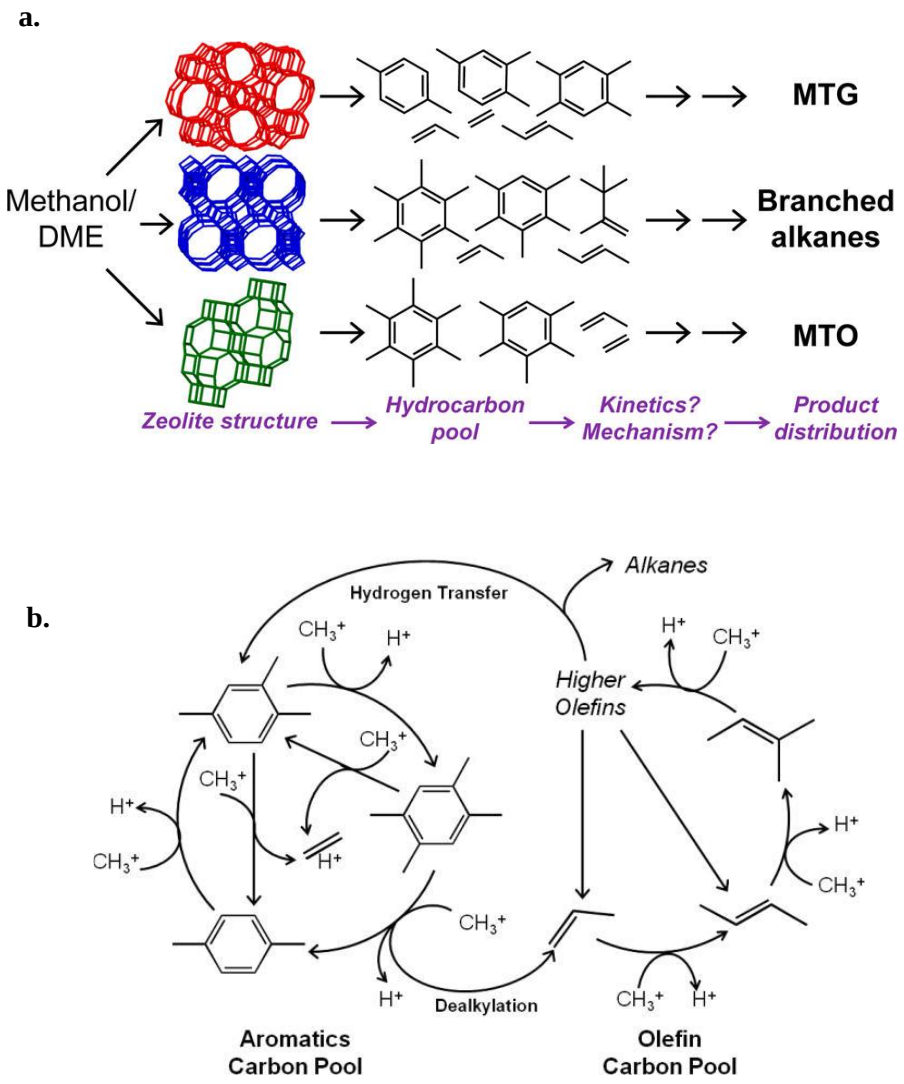

Figure 4.2. Modern insights into carbon pool mechanism (adapted from reference 10). **(a)** An overview of Methanol to Hydrocarbon conversion via zeolites showing the carbon pool species are mostly aromatic molecules. **(b)** Scheme showing side chain alkylation and dealkylation reactions are the basic chemistry occurring in the carbon pool mechanism.

Even though water has been historically considered as deleterious reagent, there are a few instances in which water has been found to exhibit a positive effect on selectivity by virtue of its ability to prevent secondary reactions from occuring by strongly adsorbing at Brønsted acid sites and reducing product readsorption events. For example, selectivity enhancements for methanol-

to-hydrocarbon conversions through water co-addition have been reported for many years,[11-12] and even very recently the origin of this effect has been attributed to water's competitive adsorption properties.[13] Interestingly, for an alcohol reagent like methanol, which generates water in the condensation step to dimethyl ether, the addition of even more water leads to increased selectivity to primary products like small olefins.

However, none of the cases mentioned above have shown if water can improve the catalyst's intrinsic activity. More interesting, and only recently recognized, are cases in which the catalytic activity is actually promoted by the presence of water. For example, in a gas-phase Fischer-Tropsch study involving Ru catalysts, Hibbitts et al.[14] showed that CO activation is increased through water-mediated hydrogen transfer. Similarly, Yoon et al.[15] demonstrated that activity in Rh-catalyzed biphasic conversions of lignin-derived molecules increased in the presence of co-fed water by enhancing a key hydrodeoxygenation step on the bifunctional catalyst. Water's role in each of these cases proceeded *only* through interaction with the metal, not a solid acid function. A few reports in the literature suggest that introduction of small amounts of water can increase reactions rates in pure solid-acid catalysts. For example, Zhao et al.[16] reported an enhancement in rates over zeolite catalysts, showing increased methylpentane isomerization rates upon introduction of small amounts of water over HY zeolites. More recently, Motokura et al. demonstrated that addition of water in the range of 1-5 wt% relative to the mass of the proton-exchanged montmorillonite catalyst increased reaction rates between bulky alkenes by over an order of magnitude.[17] Finally, computational studies suggest that water might enhance ring alkylation/dealkylation steps in the critical carbon-pool mechanism in MTH chemistry through stabilizing the transition state.[18]

In this chapter, benzene activation in acidic HZSM-5 catalysts was investigated in the presence of controlled water addition. Benzene was chosen due to the fact that single-ring aromatics are germane to so many hydrocarbon processes in zeolites, for its critical role in the

carbon pool mechanism in MTH chemistry, and perhaps most significantly its role as a precursor to large polycyclic aromatics that ultimately lead to zeolite deactivation at high temperature. Reactions between benzene and the zeolite HZSM-5, carried out at low pressure, room temperature, and equimolar benzene-to-acid site stoichiometry, revealed that controlled addition of sub-stoichiometric amounts of water, i.e., less than one equivalent, increases the rate of isotopic $^{1}H/^{2}H$ exchange between benzene-d_6 and the surface acid site by almost an order of magnitude relative to the control case in which dry zeolite is used. This result is unexpected, given that water is typically viewed as lowering zeolite activity and is utilized in that manner to help improve selectivity to primary reaction products. *Importantly, water's activity promotion effect was only observed with high acid density catalysts, i.e., at Si/Al = 15, but was not observed for catalysts with Si/Al = 40.* The fact that sub-stoichiometric water addition significantly increased reaction rates for aromatic hydrocarbons in acidic zeolites is not anticipated from the literature, and potential mechanisms to explain these surprising results as well as their dependence on the acid site density are discussed.

4.2. Experimental

Benzene-d_6 H/D exchange experiments. Catalysts HZSM-5 at Si/Al = 15 and Si/Al = 40 were activated as demonstrated in Section 2.2.1. The calcined zeolite catalysts were always inspected by ^{1}H MAS NMR to confirm the calcination quality before further use. Benzene-d_6 was quantitatively adsorbed via the vacuum-line-CAVERN method, similar as quantitative water and isobutane-d_{10} adsorption. The initial pressure of the vacuum line adsorption is 10 torr for benzene-d_6, noticing 20 torr was used for isobutane adsorption. For water coadsorbed experiments, catalysts with water loadings ranging from 0.05 to 1.0 eqv were prepared via exposure to controlled amounts of water vapor on a vacuum line. Each catalyst with water loading was sealed overnight to allow water diffusion and equilibration within the catalysts, and then characterized by ^{1}H MAS NMR to confirm the water loadings. After NMR characterization, they were opened

inside the glove box to avoid exposure to any additional water, immediately inserted to the CAVERN body, sealed, and transferred to the vacuum line for subsequent Benzene-d_6 adsorption.

Figure 4.3. A 125 mL Parr reactor.

Aromatic alkylation and dealkylation experiments. High temperature ^{1}H MAS NMR and a specially designed batch reactor method, coupled with cumene cracking and ethylbenzene dealkylations have been used to examine the water's impact to the catalyst activity. The high temperature NMR setup is shown in Figure 1.14. The batch reactor design is shown in Figure 4.18, using a 125 mL Parr acid digestion bomb. Note the valid volume of the reactor is determined by the Teflon insert, which is 100 ml. The designed upper temperature limit for this reactor is 250 °C.

NMR measurements. For benzene-d_6 experiments, ^{1}H MAS NMR data were collected on a Bruker DSX-300 MHz spectrometer, with spinning rate of 5 kHz, using a single 3.8 μs $\pi/2$ excitation pulse. Recycle delays were 10 seconds for dry zeolites, as relaxation measurements yielded T_{1H} value of 1.9-2.0 seconds. For catalysts exposed to any reagent or water, a 5-second

recycle delay was sufficient for acquisition of quantitative spectra, since T_1's were reduced to 0.1-0.2 s following adsorption. Typically, 16 scans were acquired per spectrum, resulting in a 90 s acquisition period. Unless otherwise noted, all spectra were acquired at room temperature.

For high temperature in-situ experiments, ^{1}H MAS NMR data were collected on a Chemmagnetic 300 MHz spectrometer, with spinning rate of 5 kHz, using a single 4 μs π/2 excitation pulse.

4.3. Results and discussion

4.3.1. In situ ^{1}H MAS NMR investigation of water's effect on the H/D exchange between Benzene-d_6 and HZSM-5.

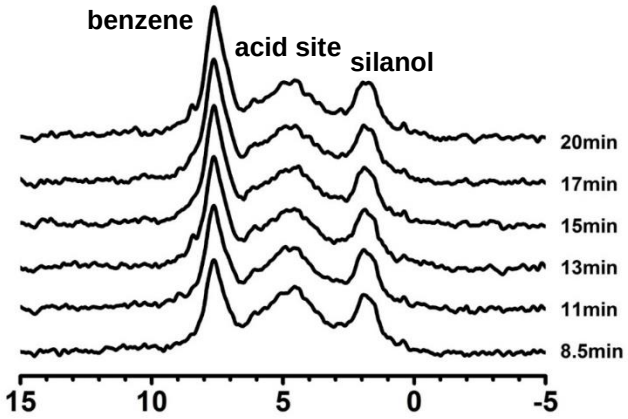

Figure 4.4. Representative in-situ ^{1}H MAS NMR spectra as a function of time following adsorption of 1 eqv benzene-d_6 on dry HZSM-5 (Si/Al = 15).

The in situ ^{1}H MAS NMR spectra of 1-eqv benzene adsorbed on dry HZSM-5 (15) in course of reaction time is shown in Figure 4.4. The Brønsted acid site peak is centered at 4.8 ppm, and broadened because of H-π bonding between acid protons and benzene rings. From Figure 4.4, one observes that the total area of the benzene peak at 7.5 ppm increases as

proton/deuterium exchange occurs, with a concomitant decrease in the overall area of the acid site resonance.

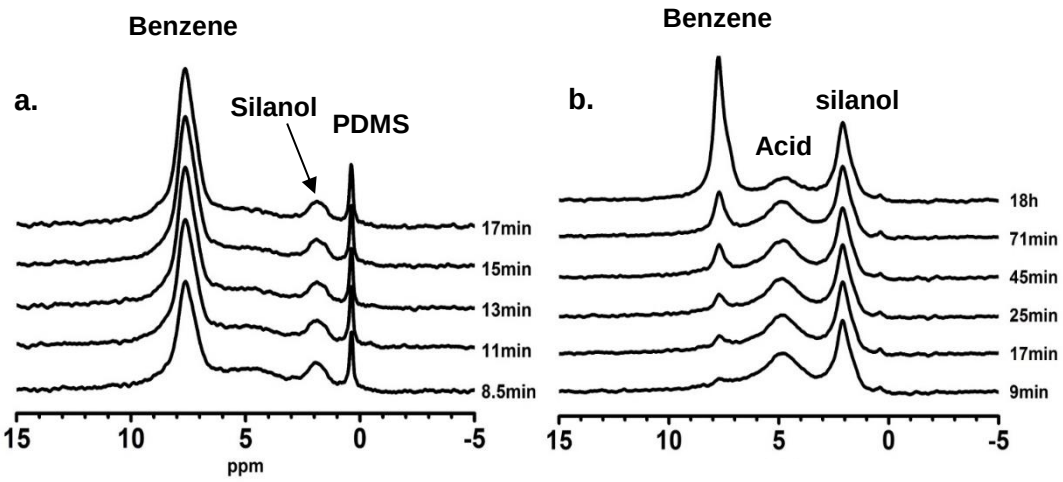

Figure 4.5. Representative in-situ ^{1}H magic-angle spinning (MAS) NMR spectra as a function of time following adsorption of 1 eqv benzene-d_6 on **(a)** HZSM-5 at Si/Al = 15 with 0.1 eqv water, and **(b)** HZSM-5 at Si/Al = 40 with 0.06 eqv water. Note the much longer timescales in **(b)**. The narrow peak near 0.2 ppm in each case is an inert chemical shift standard added to the experiment (polydimethylsiloxane/PDMS).

Figure 4.5 shows comparable experimental results, but in the presence of co-adsorbed water. Two different acid site density catalysts were investigated; Si/Al = 15 shown in 4.5a, and Si/Al = 40 in 4.5b. From Figure 4.5, it is evident that the relative area of the benzene peak (7.5 ppm) compared to the non-reactive silanol peak (2.0 ppm) is much larger in 4.5a than in 4.5b, as might be expected for first-order kinetics in relation to the number of acid sites. In addition, it is also evident that a resolved acid site still exists after 18 h for the Si/Al = 40 case, while it is essentially consumed after 17 minutes in the Si/Al = 15 reaction.

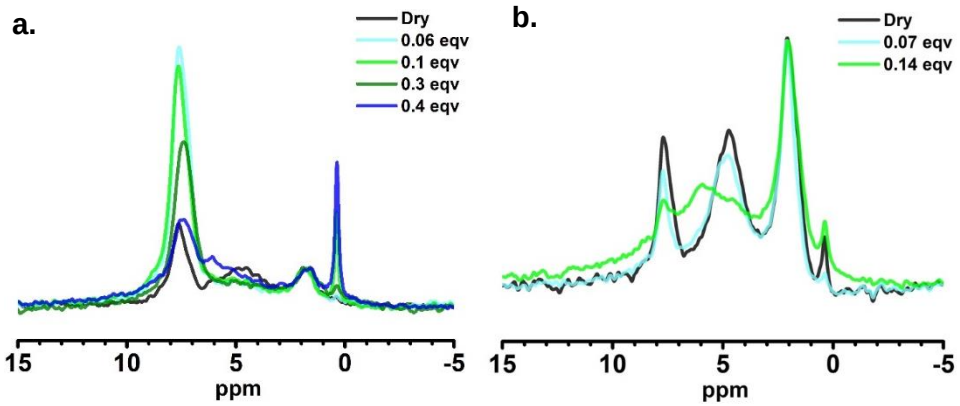

Figure 4.6. In-situ ^{1}H MAS NMR spectra acquired at a fixed reaction time after adsorption of 1-eqv benzene-d_6 on HZSM-5 catalysts, with the indicated water loadings by color, on **(a)** Si/Al = 15 at 17 minutes after adsorption, and **(b)** Si/Al = 40 at 45 minutes after adsorption. Note the significant increase in reaction rate in **(a)** with water addition compared to the dry catalyst, particularly at 0.05-0.1 eqv water, but reaction rate reduction in **(b)** with water addition.

From the raw data acquired over multiple experimental runs, differences in reactivity with varying Si/Al in the absence and presence of different water loadings are apparent, and are summarized in Figure 4.6. Results for Si/Al = 15 are shown in 4.6a, and Si/Al = 40 in 4.6b, with the selected spectra shown taken after a fixed reaction time following adsorption of 1 eqv of benzene-d_6 on the catalysts. All spectra in 4.6a were acquired 17 min after adsorption, while those in 4.6b at 45 minutes after adsorption. As a reminder, the sharp peak at 0.2 ppm is the inert solid chemical shift standard PDMS, used as a reference to help interpret adsorbate or reaction-induced chemical shift changes.

Two conclusions are apparent from the data in Figure 4.6. First, Figure 4.6a shows that the rate of hydrogen/deuterium exchange between benzene and the Brønsted acid site is significantly larger in all cases where water is adsorbed relative to the dry Si/Al = 15 catalyst, with the exception of the 0.4 eqv experiment. While the 0.4 eqv results appears comparable to the

dry catalyst result after 17 minutes of reaction, increasing the water loading above 0.4 eqv resulted in decreased reaction rates relative to the dry HZSM-5. The exchange reaction is much faster when ca. 0.1 eqv of water is co-adsorbed on the catalyst versus the completely dry catalyst, with little acid site signal in the 4 to 6 ppm region remaining after 17 minutes. Secondly, Figure 4.6b indicates that reaction in the presence of water always reduced the reaction rate compared to the dry Si/Al = 40 catalyst, even for water loadings in excess of 0.14 eqv (not shown).

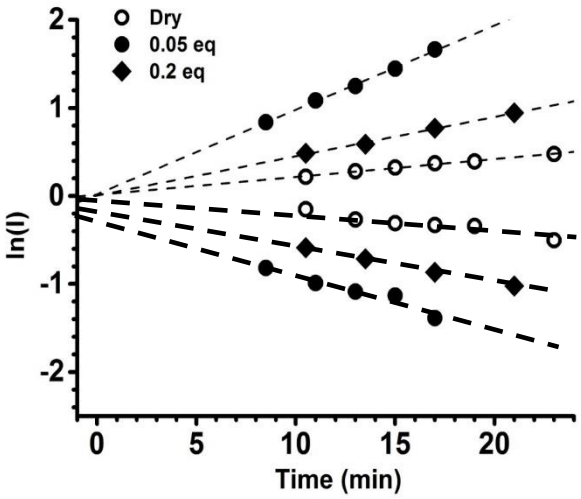

Figure 4.7. Representative rate plots for the total integrated areas of the benzene (positive slope) and zeolite acid site (negative slope) peaks in the in-situ NMR experiments, as a function of reaction time and water loading, in the Si/Al=15 catalyst. Linear regression fits are plotted through the positive benzene points, while the lines through the negative acid site points are drawn only as guides to the eye.

Raw data from which the reaction rates were calculated are shown in Figure 4.7 for three of the high acid density experiments, with a complete summary of rate constants as a function of water loading shown in Figure 4.7. Note from Figure 4.7 that the rate of benzene signal growth exactly equals the rate of Brønsted acid site signal decay for the dry HZSM-5. However, once

water is added, the Brønsted signal is no longer clearly resolved due to its interaction/exchange with water protons, as shown in Figure 2.10. Therefore, reaction rate constants in the presence of water were extracted via regression analysis of only the benzene signal growth, as it is well resolved. Figures 4.7 and 4.8 indicate that the addition of about 0.1 eqv of water increases the benzene H/D exchange reaction by almost an order of magnitude relative to the dry catalyst.

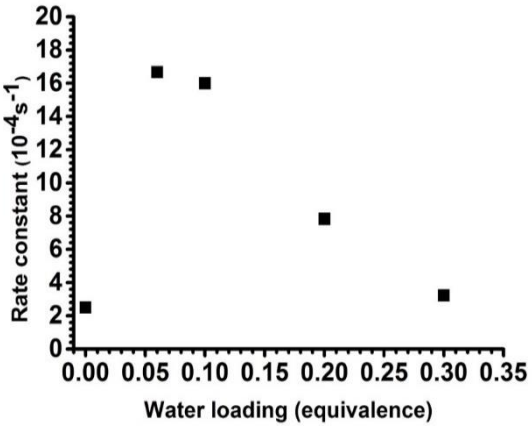

Figure 4.8. Rate constant versus water loading for the reaction obtained from the full kinetic rate plots on each sample. Individual points were calculated by time-dependent analysis of peak integrals of rising benzene ^{1}H signal following isotopic exchange with the acid site.

Figure 4.8 indicates that maximum reaction rates were obtained when 0.05-0.1 eqv of water was present on the catalyst when benzene-d_6 was adsorbed, in excess of 8 times that measured in the dry catalyst experiments. Figure 4.8 suggests that at room temperature and low pressures (ca. 0.01 atm), water should be present in sub-stoichiometric amounts, specifically Stage I adsorption, for maximum hydrocarbon reactivity in a static reaction. However, this conclusion is only appropriate at the room temperature and low-pressure conditions used for those experiments, and may not apply for zeolite/hydrocarbon reactions at high temperatures, or under flow reactor conditions.

4.3.2. Mechanism discussion. What is the reason for the reactivity enhancement? Why does it only require such small amounts of water?

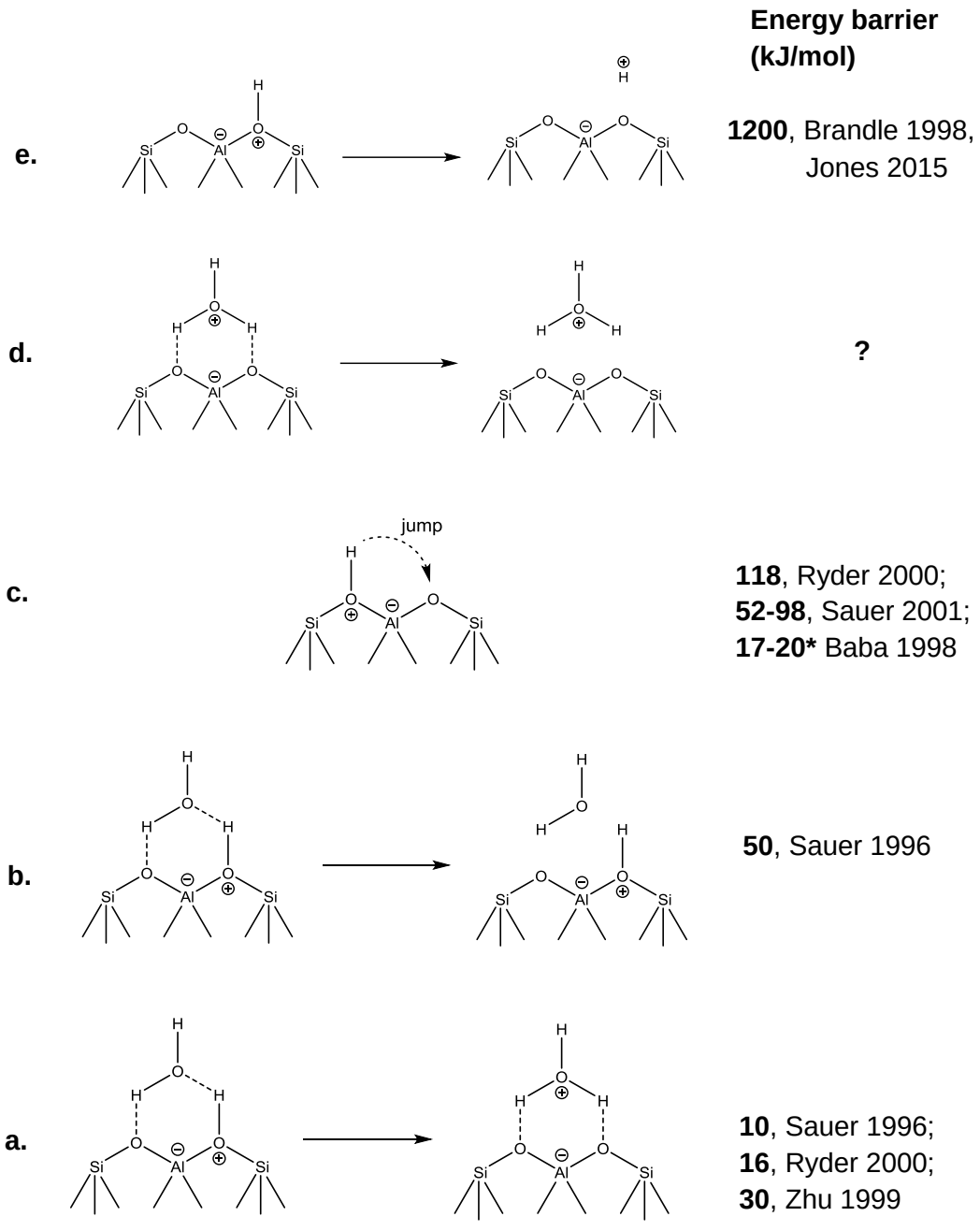

Figure 4.9. Five possible types of protonic specie conversions at Stage I adsorption. The bolded numbers on the right of each conversion is the relative energy barrier reported in the literature.

The first reason is that water is capable to significantly mediate the on-site proton transfer at very small loadings. Figure 4.9 summarizes the energy barriers of the most possible protonic specie conversions, excluding silanol interactions, in zeolites at Stage I_a level of water adsorption. Even though uncertainties are present due to the computational limitations, the values are accurate enough to be ranked in an increasing sequence from (a) to (e). The energy of the dehydroniumation of bonded water (Figure 4.9d) has not been seen in literature, but it should be higher than the on-site proton jumps (Figure 4.9c), because the separation of charges is required. By comparison, it is quite possible that the dry acid site is not the most reactive site because of its strong H-O bond. Either deprotonation (Figure 4.9e, 1200 kJ/mol)[19-20] or on-site jump (Figure 4.9c, ca. 100 kJ/mol)[19, 21] has high energy barrier to overcome. However, water molecules can significantly mediate the on-site proton transfer (Figure 4.9a), by reducing the energy barrier to ca. 10 kJ/mol, which is even lower (1 kJ/mol) from our NMR measurements. Note that Baba et al. reported low energy barriers, i.e. 17-20 kJ/mol, for proton on-site jumps, however, by looking at their ^{1}H NMR spectra, it is obvious that their catalysts contain residual water, presented as downfield shoulders by acid peaks. Thus, their values actually respond to the energy barrier in Figure 4.9a. Interestingly, Ryder's DFT calculation suggests *"even as little as 1 ppm of water per acidic proton, an amount indistinguishable by most experimental means, will reduce the apparent activation energy from 118 kJ/mol for completely dry H-ZSM-5 to ~17 kJ/mol".*[21] Their calculation also showed that the on-site jumping frequency of a proton is mediated from 10^{-8} s^{-1} to 10^9 s^{-1}, by introductions of water. Alberti et al. also proposed that *"undetectable amounts"* of water is important in the zeolitic catalyst in catalytic processes, concluded from their neutron diffraction results.[22]

The most efficient loadings of water for enhancing the benzene H/D exchange are observed at very small amounts, such as 0.05 eqv and 0.1 eqv. Apparently, water loadings above

stage II, i.e. the loadings that water clusters start forming, are not synergistic conditions for the catalyst's performance. Because, a) the water clusters strongly stabilize the proton due to their high proton affinities, and b) the clusters block the catalyst pores. However, at small loadings, for example, Stage I_a, since the acid sites are in excess, each water molecule resides on the acid site undergoing on-site jumps and occasionally hops to neighbor acid sites. The free water in the channels is rare, therefore, does not influence the accessibility of the channels. We do not have the computational data of the residence time (or weighted population fraction) for either water bonded on acid sites or free channel water, however, it is believed that the former is much longer than the latter. Estimated values of the fraction of acid site-bonded water, illustrated in Table 4.1, as guidance, can be obtained by calculation via the adsorption energy, e.g. 50 kJ by Sauer and 4-10 kJ/mol (very rough) from our NMR results. The NMR data in Chapter II suggest $Z^-\cdots H_3O^+$ and $Z^-H^+\cdots H_2O$ exist simultaneously before water clusters are formed. The calculation of chemical exchange theory coupled with the partition function shows the fraction of hydronium-formed water is 27 % at 123 K, 40 % and 298 K, tabulated in Table 4.1. Note the $Z^-\cdots H_3O^+$ fraction shows strong temperature dependence using Sauer's results (10 kJ/mol), but not with our NMR based results (1 kJ/mol).

Again, the deprotonation energy of the Brønsted acid site is 1200 kJ/mol, see Figure 4.9e. However, the deprotonation energy of a hydronium ion is only ca. 700 kJ/mol. Theoretically, the latter should be more acidic and thus more reactive. The question is how much energy is needed to deprotonate "a single water molecule bonded on an acid site". As mentioned before, it is well accepted that water can deprotonate the zeolite acid proton at large loadings. However, our group is the first showing the best evidence of one-water-molecule deprotonation. It is possible that the hydronium ions play important roles in enhancing the activity of the catalyst, by enhancing the acidity of the acid site, however, only at very small loadings.

	Sauer's ab initio data ΔE_1 = 10 kJ/mol, ΔE_2 = 50 kJ/mol		**Our data ΔE_1 = 1 kJ/mol, ΔE_2* = 4-10 kJ/mol**	
Temp/K	Fraction of $Z^-\cdots H_3O^+$	Fraction of free H_2O	Fraction of $Z^-\cdots H_3O^+$	*Fraction of free H_2O
120	4.4E-05	3.9E-18	2.7E-01	2.3E+04
198	2.3E-03	2.8E-11	3.5E-01	4.3E+02
298	1.7E-02	9.8E-08	4.0E-01	5.7E+01
398	4.6E-02	5.6E-06	4.3E-01	2.1E+01
498	8.2E-02	6.4E-05	4.4E-01	1.1E+01
598	1.2E-01	3.2E-04	4.5E-01	7.5E+00

Table 4.1. Boltzmann distribution based on Sauer's computational results and our experimental results. ΔE_1 is the energy barrier between $Z^-H^+\cdots H_2O$ and $Z^-\cdots H_3O^+$, and ΔE_2 is the energy barrier between $Z^-H^+\cdots H_2O$ and free water. The fraction of each specie is calculated based on chemical exchange equation and the partition function, shown as Equation 2.1. Note the starred values are not as accountable as the rest values.

The discussion above explains the water has positive impact to the catalyst activity only at small loadings. However, it does not explain why water has no synergistic impact on the Si/Al =40 catalyst. If the water's positive effect is due to the enhancement of the intrinsic acidity on the Brønsted acid site, the synergistic effect should be observed on Si/Al = 40 ZSM-5 as well. The Si/Al ratio influence on the water impact is not only seen in this room temperature in-situ condition, it is as well observed in a flow reactor condition above 200 ˚C, from an unpublished work of a collaborator, Dr. Crossley group (Oklahoma University). The Si/Al = 40 experiments

need to be repeated to attain solid confirmation of the effect, because it could provide key information of understanding the main mechanism. Therefore, what properties in low-density zeolites that could eliminate the water's synergistic impact? Si/Al ratio pose attentions to the Al site distance, and the location of the acid site, i.e. acid sites at straight channels vs. channel intersections.[23-27] It is also believed that the confinement environment has impact on the activity, due to the entropy benefits.[28-31] Usually, channel-protons are more reactive than intersection-protons. Jones et al showed the evidence that Si/Al =40 ZSM-5 does not contain channel acid sites.[25] Is the channel confinement required for the water enhancement? Control experiments using one dimensional 10-member ring zeolites, such as ZSM-22, could be interesting. The proposed hydronium ion mechanism, though not conflict with, does not support the Si/Al effect directly.

4.3.3. High temperature in situ ^{1}H MAS NMR investigation of water's effect on dealkylation of ethylbenzene and cumene

It is clear that water facilitates the C-H bond activations for isobutane and benzene, i.e. aliphatic and aromatic molecules, despite their molecular differences. Water could facilitate other zeolite-catalyzed reactions more generally. How does water perform on a real hydrocarbon reaction at high temperatures? As mentioned in the introduction, the side chain alkylation and dealkylation of aromatic molecules are the most important types of reactions in zeolitic chemistries. Ethylbenzene dealkylation and cumene cracking are well-known as test reactions for probing catalyst efficiency.[32-34] Ethylbenzene, cumene and butylbenzene reactivity increases with the increase of the side chain size, i.e. butylbenzene > cumene > ethylbenzene.[35] Butylbenzene and those aromatic derivatives containing side chains larger than butyl group are not considered as test molecules, because they are not only too reactive, but also too big to fit in ZSM-5 zeolite pores. A simple comparison between the dealkylation reaction of either ethylbenzene or cumene at conditions with and without water could reveal the water's effect.

4.3.3.1. Ethylbenzene dealkylation.

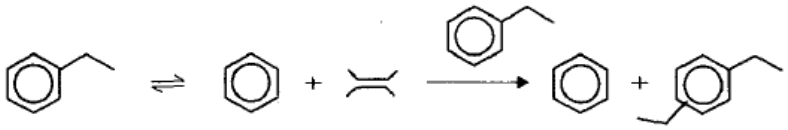

Scheme 1 Mechanism of transalkylation via dealkylation/alkylation

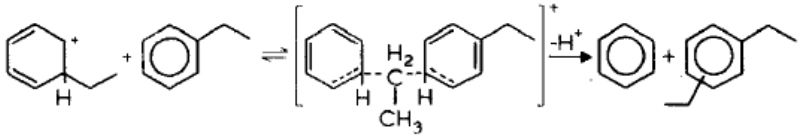

Scheme 2 Mechanism of transalkylation after McCaulay and Lien[30] and Brown and Smoot[31]

Figure 4.10. Probable reactions occur for ethylbenzene catalyzed by acidic zeolites. Adapted from reference 28.

Alkylation and dealkylation both happen when ethylbenzene is present in zeolite at reaction temperature, usually above 150 °C.[32, 36] Most of the ethylbenzene reactions in zeolites were conducted by flow reactors coupled with the GC-MS detection. However, reports of in-situ NMR results are rare. At high temperature, neither flow reactor nor in-situ NMR method can stop the reaction at the dealkylation step. Note that scheme 1 in Figure 4.10 is the most probable pathway in ZSM-5 catalysts[37], because of shape selectivity. However, ^{1}H NMR is not able to elucidate the aliphatic protons among ethylbenzene, diethylbenzene or multi-ethylbenzene. A representative result of high temperature in-situ ^{1}H NMR spectra of ethylbenzene adsorbed on HZSM-5 (15) is illustrated in Figure 4.11. 1 eqv liquid ethylbenzene was injected into dry HZSM-5 (15) catalyst, sealed in a Chemagnetics 7 mm MAS rotor, elevated to 230 °C stepwise. However, no obvious dealkylation was observed, due to the low resolution in the aliphatic region. A flow reactor coupled with GC-MS is recommended to replace the ethylbenzene test.

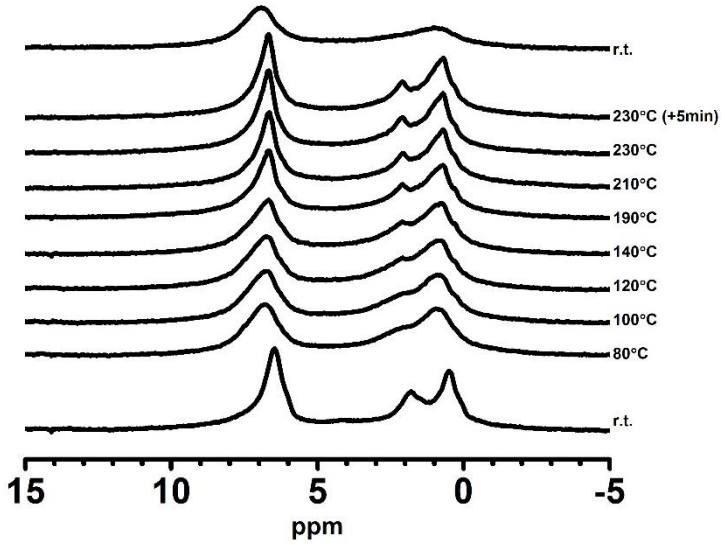

Figure 4.11. High temperature in-situ ^{1}H MAS NMR spectra of 1 eqv ethylbenzene in HZSM-5 (15).

4.3.3.2. Cumene cracking. In addition to ethylbenzene dealkylation, cumene cracking was also investigated by the in-situ high temperature NMR method. At desired temperatures, cumene first cracks into benzene and propylene, demonstrated in Figure 4.12. Propylene is much more reactive than ethylene. Thus, propylene, once formed, is immediately adsorbed on acid sites, undergoing oligomerization reactions. However, ethylene does not oligomerize in zeolites at room temperature. The high reactivity of propylene can prevent alkylation from taking place; thus, providing obvious dealkylations for ^{1}H NMR detection.

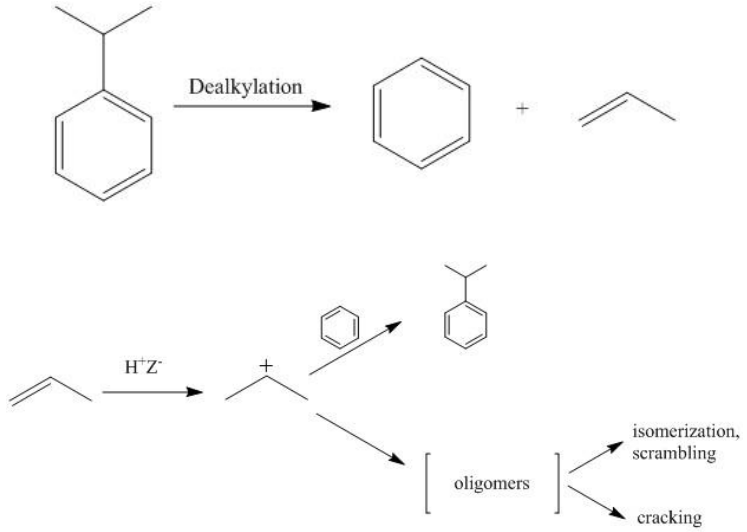

Figure 4.12. Cumene cracking in zeolites

PDMS was used as an inert internal reference for convenient peak calibrations, especially for high temperature spectra. However, the PDMS intensity decreases with increasing the temperature, by a comparison between Figure 4.13a and 4.13d, where the ^{1}H NMR spectra were acquired on a same sample at 200 ˚C and room temperature. By changing the delay time d_1, it is observed that 20 seconds was required for a complete T_1 relaxation. In short, PDMS is not appropriate for quantitative analysis for cumene cracking experiments in the absence of long T_1-relaxation delays, since PDMS is on high-temperature side of its minimum; however, it is still sufficient and necessary for peak calibration.

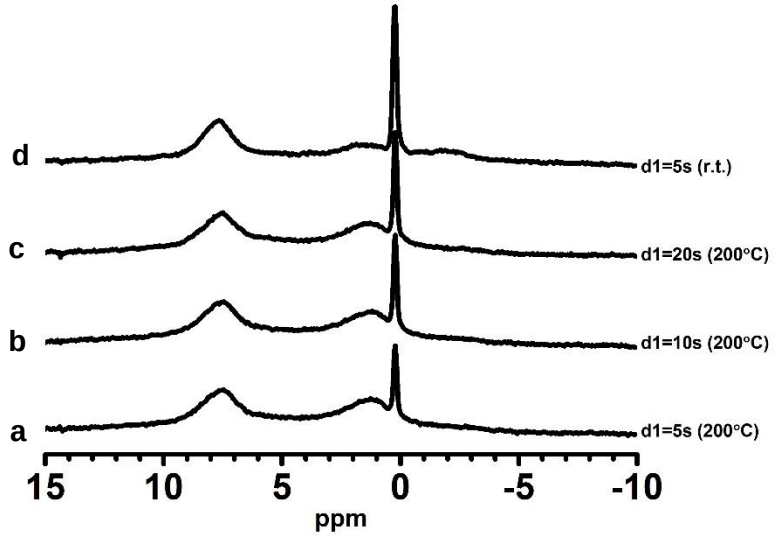

Figure 4.13. **(a)** and **(d)** shows the intensity of PDMS decreases with the increase of temperature. **(a)**, **(b)** and **(c)** the intensity increases with the increase of delay time, d_1, indicating at least 20 seconds needed for a quantitative analysis of PDMS.

Once liquid cumene is injected into zeolites, it is necessary to wait for the cumene molecules to diffuse into the catalyst pores. The ^{1}H NMR spectra in Figure 4.14 shows the difference before and after diffusion, as well as the influence of co-adsorbed water upon cumene adsorption. Figure 4.14a and 4.14c were acquired immediately after the injection of cumene, showing sharp liquid-like cumene peaks, in which the aromatic peak centered at 7.2 ppm, the methine (CH) at 2.7 ppm, and the methyl (CH_3) at 1.1 ppm. Again, the sharp peak at 0.2 ppm is from the inert internal reference PDMS. In Figure 4.14, (a) and (b) were in the dry condition, (c) and (d) were exposed to 1-eqv water before cumene. Although Figure 4.14a and 4.14c are the same, Figure 4.14b and Figure 4.14d show obvious differences after letting the systems reach diffusion equilibrium. An up-field shift of the entire cumene peak occurred after diffusion without the presence of water. However, a down-field shift observed in the presence of 1-eqv water. The difference of chemical shift change suggests that water and cumene must coexist in proximity of acid sites, leading to a change of the electronic environment around cumene.

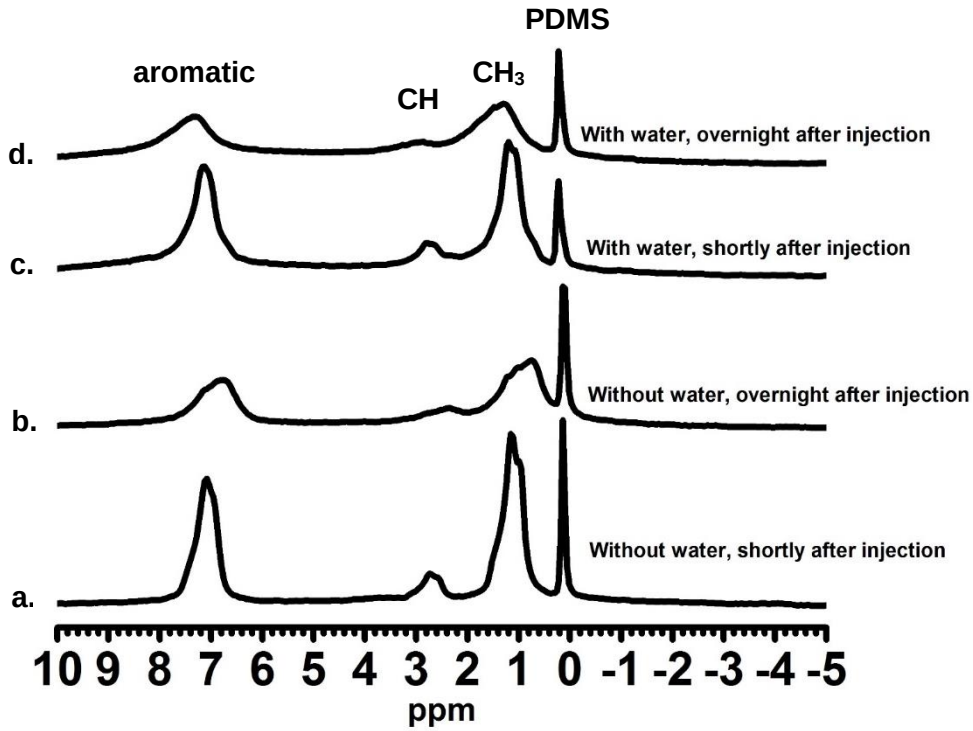

Figure 4.14. ^{1}H MAS NMR spectra of 1 eqv cumene adsorbed in HZSM-5 (15) at room temperature. The condition of each catalyst is labeled in the figure.

A representative ^{1}H MAS NMR spectra of an in-situ high temperature experiment for cumene cracking is demonstrated in Figure 4.15. Clearly, the dealkylation occurred after the 13-min-heating at 200 °C. The spectra from 13-min to 60-min show aliphatic peaks that are clearly changed. However, both the catalyst and the organic reagent are sealed in the closed rotor, which is a closed reaction system. Again, like the ethylbenzene system, the ^{1}H NMR spectrum is not sufficient to distinguish the isopropyl group of cumene and the scrambled aliphatic products formed after cracking. Once the rotor was cooled back to temperature after the reaction, the cap was taken off for a few minutes, and then placed back for another spectrum, shown as the top spectrum in Figure 4.14. The aliphatic peak, which was prominent in of the other spectra, almost disappeared, because the aliphatic products diffuse out while the cap was taken off.

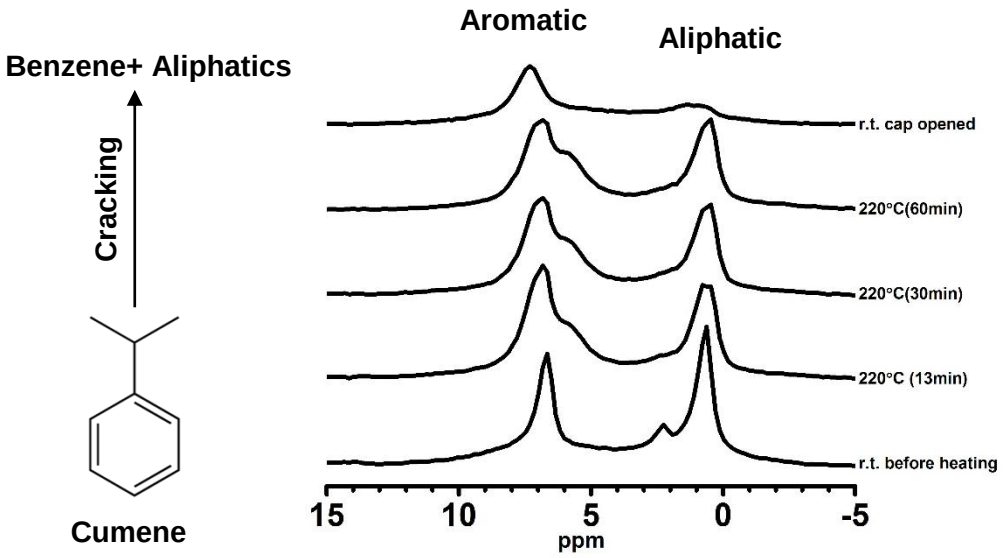

Figure 4.15. In-situ ^{1}H MAS NMR spectra of cumene, with 1 eqv water co-adsorbed, in HZSM-5, heated to 220 °C.

With the problem caused by the closed system, reactions were also tested in a newly designed open system by replacing the traditional rotor cap with a bored cap (a grooved Teflon cap but bored through the center). Figure 4.16a shows spectra of a HZSM-5 (15) catalyst loaded with 1 eqv cumene at elevated temperatures in an open system. Even though the cumene escapes from the system as well, it is obvious that the cracking reactions took places at 120 °C, which is lower than in a closed system. The bottom spectra labeled as "Closed system" in Figure 4.16b show the comparable experiment in a closed system, where the catalyst loaded with 1 eqv cumene was heated up to 120 °C, however, with no obvious changes observed. Interestingly, by replacing the bored cap (open system) with a traditional cap (closed system), and then reheating it stepwise to 120 °C, the reaction occurred, shown in the spectra labeled as "Open system", evidenced by the down-field shift of the aromatic peak and the decreased aliphatic/aromatic ratio.

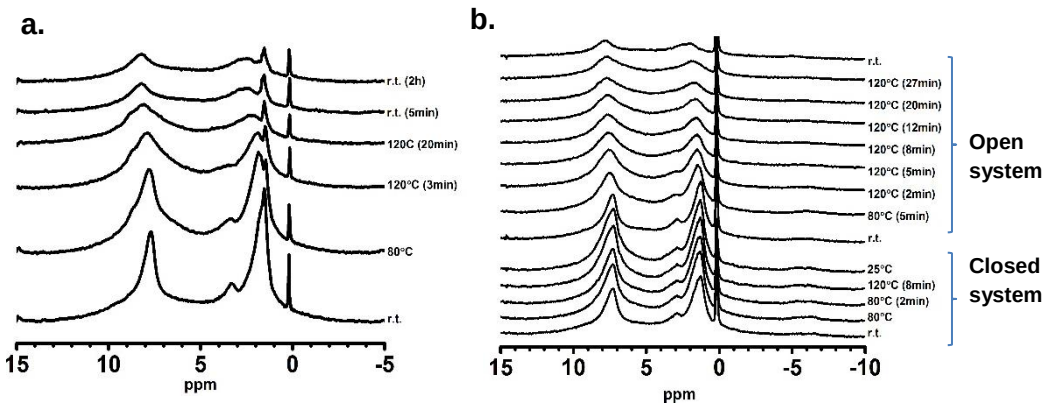

Figure 4.16. ^{1}H NMR spectra of cumene cracking at variable temperatures in **(a)** an open system, using a bored-through Teflon cap, and **(b)** a closed system for one heating-cooling cycle and an open system for a subsequentialheating cycle.

Conclusion high temperature in-situ NMR experiments. The water effect is not clearly observed by the high temperature in-situ NMR experiments yet. More modifications of the method are required for further study. However, useful information is attained. First, water and cumene can coexist in proximities of acid sites. Second, the cracking and aliphatic product scrambling are the major reactions for in-situ cumene cracking. Thus, it is a potential test reaction for evaluating the water effect. Third, the reaction occurs at 120 °C in an open system, but at higher temperature in a closed system, presumably due to Le Chatelier's principle.

4.3.4 Batch reactor test on cumene cracking and toluene disproportionation

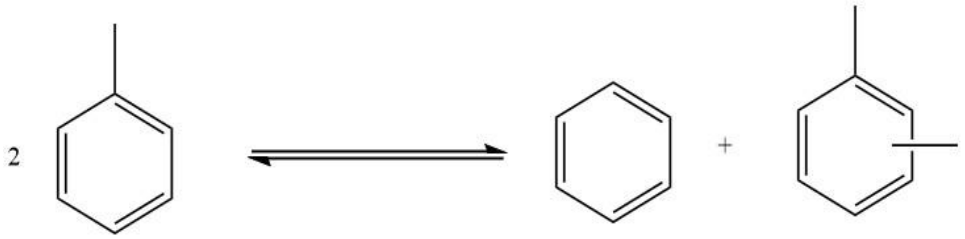

Figure 4.17. Scheme of toluene disproportionation catalyzed by acidic zeolites.

4.3.4.1. Toluene disproportionation. Zeolites have been extensively used for toluene disproportionation (Figure 4.14) and transalkylation processes to obtain more useful benzene, which is a key raw material of many petrochemical intermediates, and xylene, an important starting material for synthesizing fibers, plasticizers and resin.[38-40] The toluene disproportionation can be used to test the water effect on aromatic dealkylation reactions. As reported, the disproportionation temperature for a fixed-bed reactor is usually carried out in the temperature range 300 °C - 400 °C.[38] In addition, the desired products, benzene and xylene, are distinct in GC-MS detections. A special batch reactor setup was designed for this reaction, depicted in Figure 4.18.

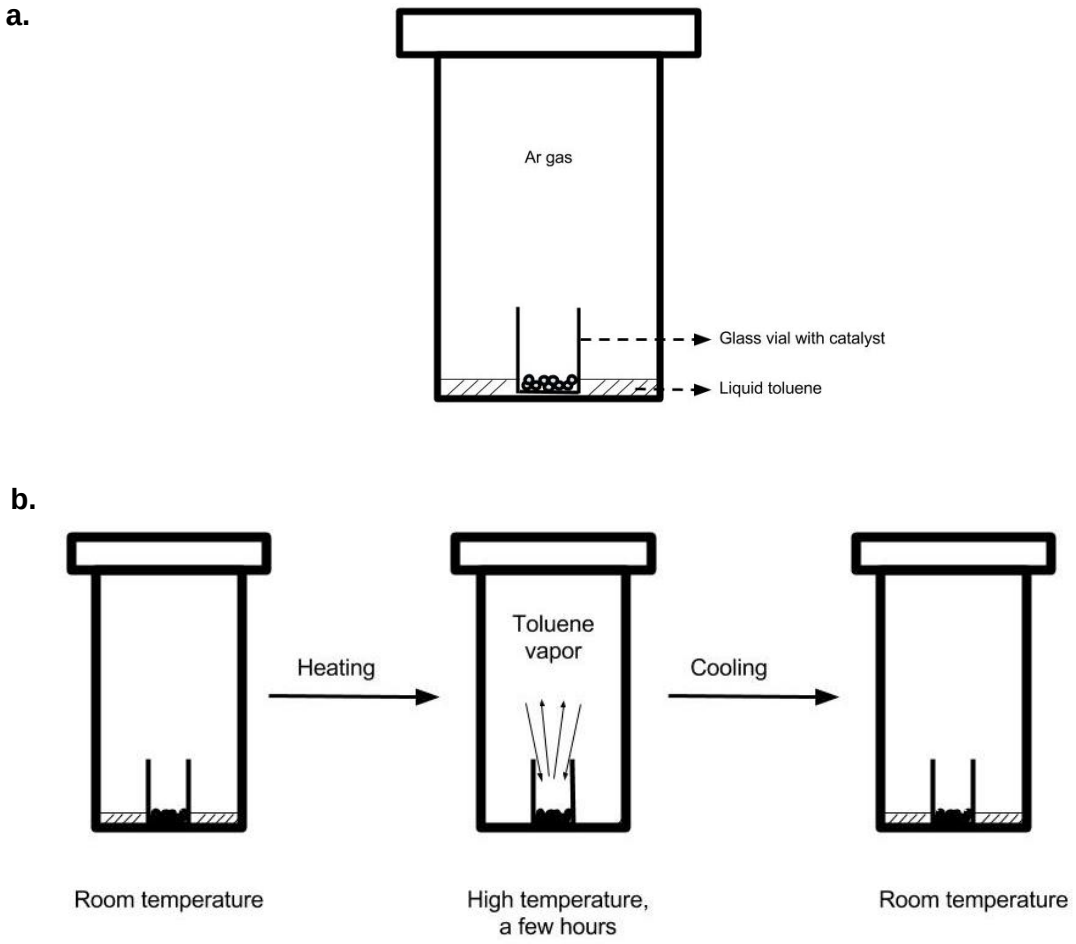

Figure 4.18. The batch reactor designed for toluene disproportionation tests.

4.3.4.2. The batch reactor design. In this design, the catalyst is placed in a glass vial separated from the liquid reagent toluene, illustrated in Figure 4.18a. Consequently, the system is sealed and protected by argon gas throughout the reaction. Oxygen is very reactive, therefore must be completely removed before heating to reaction conditions, otherwise, unnecessary oxidation reactions will take place. Figure 4.19 shows a GC result of a reaction containing 2 ml Toluene and 100 mg HZSM-5 (15) catalyst, heated at 200 °C for 4 hours, however, without argon protection. The 100-ml Teflon cup, which is in direct contact with the reactants, must be cleaned

completely to avoid the effects from the residual contaminants. According to experiences, 70 ml nitric acid solution sealed in the reactor and heated at 150 °C for a few hours will decompose most of the organic contaminants. A following procedure using deionized water to replace nitric acid, at 170 °C for another few hours should be sufficient to remove all of the residual contaminants.

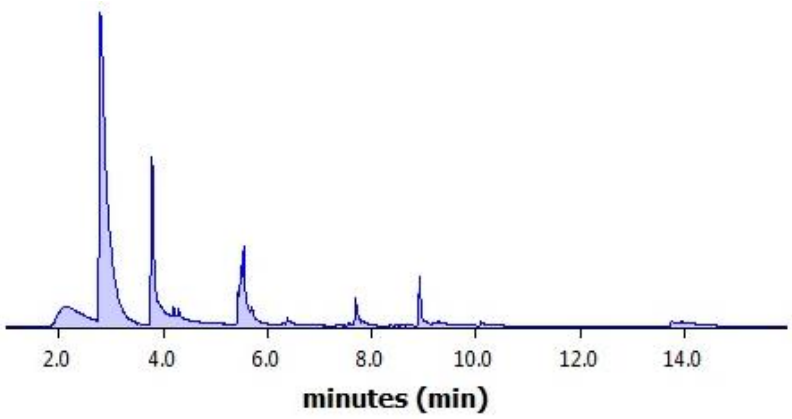

Figure 4.19. 2 ml toluene and 100 mg HZSM-5 (15) in Parr reactor at 200 °C for 4 hrs with air.

For toluene, the vapor pressure at varying temperature[41] from 110 °C to 257 °C, as well as the critical volume for the 100-ml Parr reactor is tabulated in Table 4.2. The critical volume, obtained via idea-gas-law calculation, is the minimum amount of toluene required to form liquid phase at correlated temperature in a 100-ml Parr reactor. A similar table for cumene is presented in Table 4.3, in which the Vapor-liquid equilibrium (VLE) data are calculated by the Antoine eqution.[42] The critical volume provides a good rule of thumb of the amount of reagent to be loaded at selected temperatures. For example, the best situation is that at desired temperatures all reagents are vaporized, to reach a dynamic solid-gas heterogeneous condition. Once the reaction

is finished, the whole reactor is quenched by room-temperature water. While quenching, the vapor gas will condense on the cold interior wall of the reactor, leaving the catalyst dry in the glass vial. As a result, the liquid organic reagent and the solid catalyst are isolated after the reaction, allowing convenient GC-MS detections.

4.3.4.3. Tabulated Vapor-liquid equilibrium (VLE) data of toluene and cumene.

T/°C	P/torr	Critical volume/ml
110.7	760.0	0.34
129.5	1276.8	0.54
149.5	2128.0	0.86
161	2926.0	1.15
175.5	3936.8	1.49
186.5	4651.2	1.72
194	5304.8	1.93
203.5	6277.6	2.24
214.4	7516.4	2.62
226	9028.8	3.07
234.5	10070.0	3.37
246	12160.0	3.98
250	12958.0	4.21
253.5	13269.6	4.28
257.2	13444.4	4.31

Table 4.2. The vapor pressure (adapted from reference 41) of toluene at varying temperatures and their correlated critical volume for the Parr reactor.

T/° C	P/torr	Critical volume/ml
130	409.8	0.23
132	434.8	0.24
134	460.9	0.25
136	488.3	0.27
138	517.0	0.28
140	547.1	0.30
142	578.5	0.31
144	611.4	0.33
146	645.7	0.34
148	681.5	0.36
150	719.0	0.38
152	758.0	0.40
154	798.7	0.42
156	841.2	0.44
158	885.4	0.46
160	931.4	0.48
162	979.3	0.50
164	1029.2	0.53
166	1081.0	0.55
168	1134.8	0.57
170	1190.7	0.60
172	1248.8	0.63
174	1309.1	0.65
176	1371.6	0.68
178	1436.4	0.71

Table 4.3. The vapor pressure of toluene at varying temperatures and their correlated critical volume for the Parr reactor.

4.3.4.4. Representative GC-MS spectra of toluene disproportionation and cumene cracking.

Toluene disproportionation

Using the experimental setup shown in Figure 4.18, 0.5 ml toluene and 100 mg HZSM-5 (15) catalyst were sealed in a Parr reactor, heated and held at 210 °C for 2 hrs. According to Table 4.2, 0.5 ml toluene will be completely vaporized in the 100-ml reactor at 210 °C. A representative Gas Chromatography spectrum is shown in Figure 4.20. Surprisingly, ethylmethylbenzene instead of xylene was obtained as the major product. However, co-loadings of 1, 2 or 3 eqv H_2O did not show obvious change to ethylmenthylbenzene intensity.

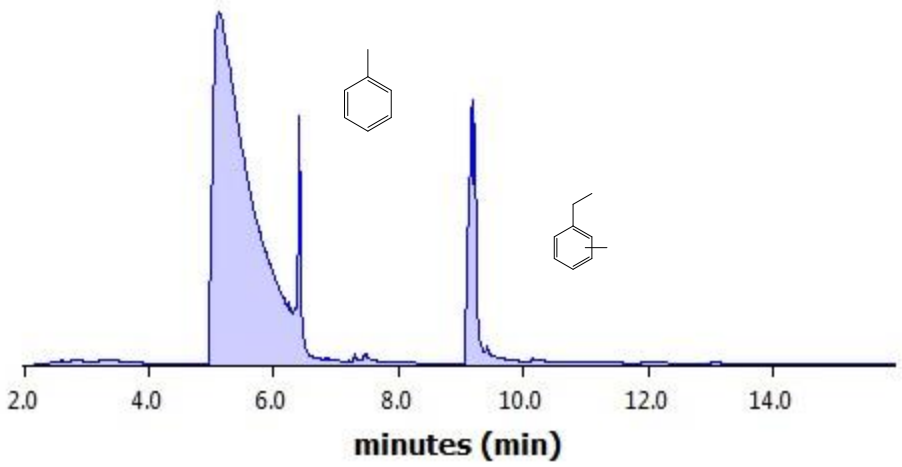

Figure 4.20. 0.5 ml toluene and 100 mg HZSM-5 (15) in Parr reactor at 210 °C with Ar protected. The peak assignment is approached from Mass Spectroscopy analysis.

Cumene cracking. Since cumene is more reactive, it is used to in the Parr reactor test. By experience, the experimental condition is optimized to 0.5 ml cumene, 50 mg HZSM-5 (15) at 170 °C. Figure 4.21a, 4.21b and 4.21c show the GC spectra of the reactions held at the desired condition for 1, 1.5 and 2 h without extra water. Figure 4.21d, 4.21e and 4.21f show the spectra of analogous reactions as the in (a), (b) and (c), but with 4 eqv H_2O loaded in the system. The time dependence of the spectra is apparent, i.e., the longer the reaction time, the more products are formed. Peak assignments, representatively shown in Figure 4.21c, are approached by Mass Spectroscopy analysis. Obviously, not only side chain crackings, but also transalkylations happened. It is interesting that the very first product formed is not benzene, but toluene. In addition to 4 eqv, the water loading has been controlled to 0.2 eqv, 1 eqv, 2 eqv and 3 eqv, however no significant impact, as in the room temperature benzene reaction was seen.

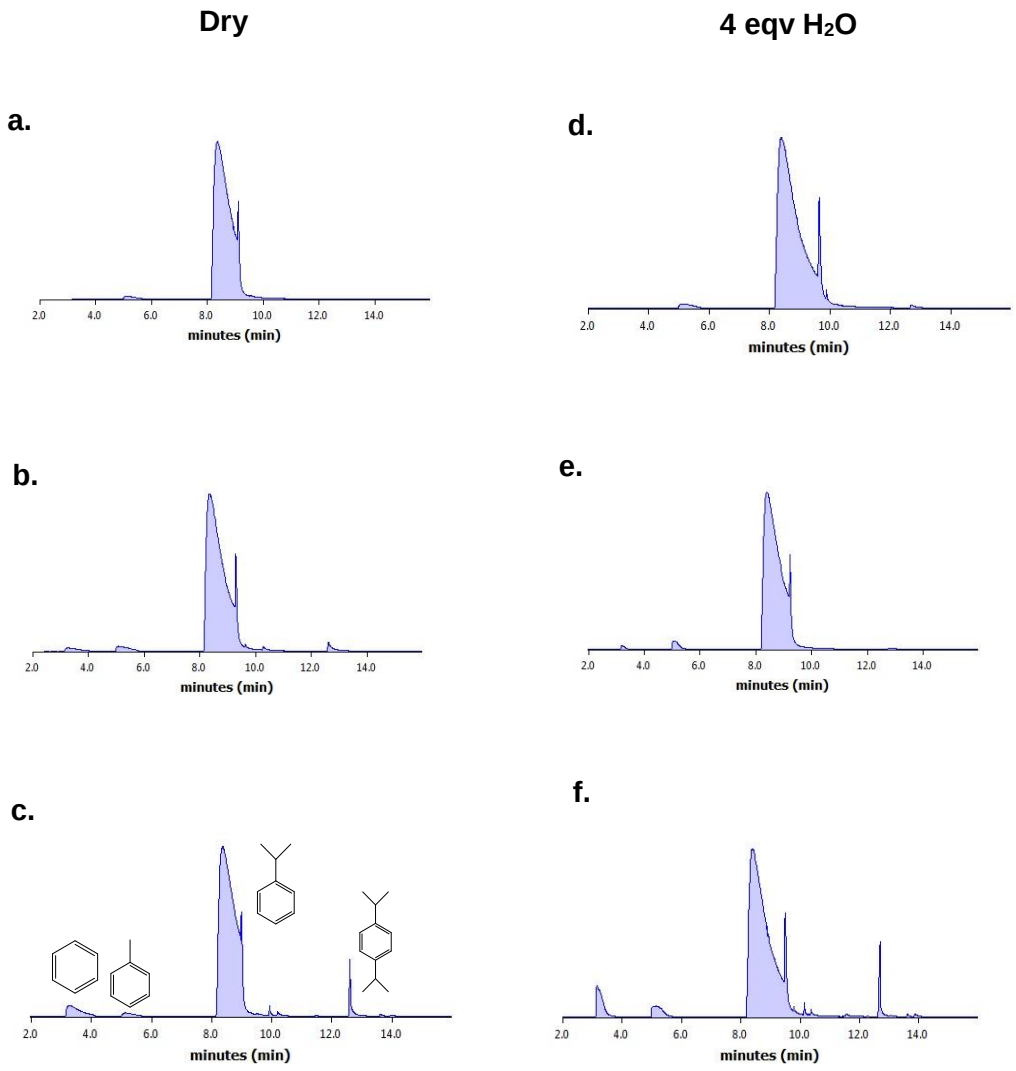

Figure 4.21. From **(a)** to **(f)**, each experiment was conducted with 0.5 ml cumene and 50 mg HZSM-5 (15), heated to 170 °C. **(a)**, **(b)** and **(c)** were reacted without water for 1, 1.5 and 2 hours, respectively. **(d)**, **(e)** and **(f)** were reacted with 4 eqv water for 1, 1.5 and 2 hours, respectively. The peak assignment is approached from Mass Spectroscopy analysis, labeled in **(c)**.

Overall, the Parr reactor method shows more promising results than the high temperature in-situ NMR method. In addition, the GC spectra of both toluene and cumene both show greatly

resolved product peaks which are convenient for quantitative analysis. As learned from chapter II or Table 4.1, at high temperature, the fraction of effective water, the water bonded on acid sites, is low due to the low desorption energy, i.e. 10 kJ/mol calculated by Sauer. Thus, at same loadings of water, the impact is higher at low temperature. The high temperature spectra of 2 eqv water in ZSM-5, shown in Figure 2.23, clearly indicate that the fraction of water species in zeolite shift toward the free water, causing a upfield shift of the water peak, i.e., from 7 ppm at room temperature to 5.6 ppm at 220 ˚C.

4.4. Conclusion

In-situ MAS NMR experiments indicate that appropriate amounts of water can actually increase hydrocarbon reactivity in solid acid catalysts like zeolites. The unexpected activity enhancement afforded by water only occurs at low water loadings, and more specifically at sub-stoichiometric amounts relative to the hydrocarbon reagent and acid site concentration. In addition, reaction rates are only enhanced by water for the high acid density catalyst with Si/Al = 15, and not observed for the catalyst with Si/Al = 40. These unexpected results suggest that water can actively participate in hydrocarbon reactions inside zeolites, even for completely non-polar hydrocarbons like simple aromatics. Probable mechanisms for this enhancement are proposed, which is the hydronium ion formed on the acid site, but not the clusters. At loadings higher than ca. 0.4 eqv., the formation of water clusters definitely will kill the acid site activity. Water's impact on aromatic alkylation/dealkylation reactions at high catalytic temperatures, for example, toluene disproportionation, cumene cracking, etc., are still under investigation. In addition, these unexpected results suggest that existing applications involving solid acid catalysis could potentially realize benefits in catalyst reactivity, catalyst lifetimes, and less severe operating conditions by investigating water as an active component of the reaction.

4.5. References

1. Chang, C. D.; Silvestri, A. J., The Conversion of Methanol and other O-Compounds to Hydrocarbons over Zeolite Catalysts. *Journal of Catalysis* **1977,** *47* (2), 249-259.
2. Hickman, D. A.; Schmidt, L. D., Production of Syngas by Direct Catalytic Oxidation of Methane. *Science* **1993,** *259* (5093), 343-346.
3. Laurendeau, N. M., Heterogeneous Kinetics of Coal Char Gasification and Combustion. *Progress in Energy and Combustion Science* **1978,** *4* (4), 221-270.
4. Wen, W.-Y., Mechanisms of Alkali Metal Catalysis in the Gasification of Coal, Char, or Graphite. *Catalysis Reviews* **1980,** *22* (1), 1-28.
5. Asadullah, M.; Ito, S.-i.; Kunimori, K.; Yamada, M.; Tomishige, K., Biomass Gasification to Hydrogen and Syngas at Low Temperature: Novel Catalytic System Using Fluidized-Bed Reactor. *Journal of Catalysis* **2002,** *208* (2), 255-259.
6. Sutton, D.; Kelleher, B.; Ross, J. R. H., Review of Literature on Catalysts for Biomass Gasification. *Fuel Processing Technology* **2001,** *73* (3), 155-173.
7. Dahl, I. M.; Kolboe, S., On the Reaction Mechanism for Propene Formation in the MTO Reaction over SAPO-34. *Catalysis Letters* **1993,** *20* (3), 329-336.
8. T. Xu, J. L. White, U. S. Patent 6,743,747 (2004), priority filing and PCT published February 24, **2000**
9. T. Xu, J. L. White, U. S. Patent 6,734,330 (2004**),** priority filing and PCT published July 13, **2000**.
10. Ilias, S.; Bhan, A., Mechanism of the Catalytic Conversion of Methanol to Hydrocarbons. *ACS Catalysis* **2013,** *3* (1), 18-31.
11. Marchi, A. J.; Froment, G. F., Catalytic Conversion of Methanol to Light Alkenes on SAPO Molecular Sieves. *Applied Catalysis* **1991,** *71* (1), 139-152.

12. Wu, X.; Anthony, R. G., Effect of Feed Composition on Methanol Conversion to Light Olefins over SAPO-34. *Applied Catalysis A: General* **2001,** *218* (1–2), 241-250.

13. De Wispelaere, K.; Wondergem, C. S.; Ensing, B.; Hemelsoet, K.; Meijer, E. J.; Weckhuysen, B. M.; Van Speybroeck, V.; Ruiz-Martínez, J., Insight into the Effect of Water on the Methanol-to-Olefins Conversion in H-SAPO-34 from Molecular Simulations and in Situ Microspectroscopy. *ACS Catalysis* **2016,** *6* (3), 1991-2002.

14. Hibbitts, D. D.; Loveless, B. T.; Neurock, M.; Iglesia, E., Mechanistic Role of Water on the Rate and Selectivity of Fischer–Tropsch Synthesis on Ruthenium Catalysts. *Angewandte Chemie International Edition* **2013,** *52* (47), 12273-12278.

15. Yoon, K.; Kim, K.; Wang, X.; Fang, D.; Hsiao, B. S.; Chu, B., High Flux Ultrafiltration Membranes Based on Electrospun Nanofibrous Pan Scaffolds and Chitosan Coating. *Polymer* **2006,** *47* (7), 2434-2441.

16. Zhao, Y. X.; Wojciechowski, B. W., The Consequences of Steam Dilution in Catalytic Cracking. *Journal of Catalysis* **1996,** *163* (2), 365-373.

17. Motokura, K.; Matsunaga, S.; Noda, H.; Miyaji, A.; Baba, T., Water-Accelerated Allylsilylation of Alkenes Using a Proton-Exchanged Montmorillonite Catalyst. *ACS Catalysis* **2012,** *2* (9), 1942-1946.

18. De Wispelaere, K.; Hemelsoet, K.; Waroquier, M.; Van Speybroeck, V., Complete Low-barrier Side-chain Route for Olefin Formation during Methanol Conversion in H-SAPO-34. *Journal of Catalysis* **2013,** *305*, 76-80.

19. Brändle, M.; Sauer, J., Acidity Differences between Inorganic Solids Induced by Their Framework Structure. A Combined Quantum Mechanics/Molecular Mechanics ab Initio Study on Zeolites. *Journal of the American Chemical Society* **1998,** *120* (7), 1556-1570.

20. Jones, A. J.; Iglesia, E., The Strength of Brønsted Acid Sites in Microporous Aluminosilicates. *ACS Catalysis* **2015,** *5* (10), 5741-5755.

21. Ryder, J. A.; Chakraborty, A. K.; Bell, A. T., Density Functional Theory Study of Proton Mobility in Zeolites: Proton Migration and Hydrogen Exchange in ZSM-5. *The Journal of Physical Chemistry B* **2000,** *104* (30), 6998-7011.

22. Alberti, A.; Martucci, A., Proton Transfer Mediated by Water: Experimental Evidence by Neutron Diffraction. *The Journal of Physical Chemistry C* **2010,** *114* (17), 7767-7773.

23. Dědeček, J.; Sobalík, Z.; Wichterlová, B., Siting and Distribution of Framework Aluminium Atoms in Silicon-Rich Zeolites and Impact on Catalysis. *Catalysis Reviews* **2012,** *54* (2), 135-223.

24. Janda, A.; Bell, A. T., Effects of Si/Al Ratio on the Distribution of Framework Al and on the Rates of Alkane Monomolecular Cracking and Dehydrogenation in H-MFI. *Journal of the American Chemical Society* **2013,** *135* (51), 19193-19207.

25. Jones, A. J.; Carr, R. T.; Zones, S. I.; Iglesia, E., Acid Strength and Solvation in Catalysis by MFI Zeolites and Effects of the Identity, Concentration and Location of Framework Heteroatoms. *Journal of Catalysis* **2014,** *312* (0), 58-68.

26. Vjunov, A.; Fulton, J. L.; Huthwelker, T.; Pin, S.; Mei, D.; Schenter, G. K.; Govind, N.; Camaioni, D. M.; Hu, J. Z.; Lercher, J. A., Quantitatively Probing the Al Distribution in Zeolites. *Journal of the American Chemical Society* **2014,** *136* (23), 8296-8306.

27. Perea, D. E.; Arslan, I.; Liu, J.; Ristanovic, Z.; Kovarik, L.; Arey, B. W.; Lercher, J. A.; Bare, S. R.; Weckhuysen, B. M., Determining the Location and Nearest Neighbours of Aluminium in Zeolites With Atom Probe Tomography. *Nat Commun* **2015,** *6*.

28. Bhan, A.; Gounder, R.; Macht, J.; Iglesia, E., Entropy Considerations in Monomolecular Cracking of Alkanes on Acidic Zeolites. *Journal of Catalysis* **2008,** *253* (1), 221-224.

29. Gounder, R.; Iglesia, E., The Roles of Entropy and Enthalpy in Stabilizing Ion-Pairs at Transition States in Zeolite Acid Catalysis. *Accounts of Chemical Research* **2012,** *45* (2), 229-238.

30. Gounder, R.; Jones, A. J.; Carr, R. T.; Iglesia, E., Solvation and Acid Strength Effects on Catalysis by Faujasite Zeolites. *Journal of Catalysis* **2012,** *286*, 214-223.

31. Gounder, R.; Iglesia, E., The Catalytic Diversity of Zeolites: Confinement and Solvation Effects within Voids of Molecular Dimensions. *Chemical Communications* **2013,** *49* (34), 3491-3509.

32. Tsai, T.-C.; Liu, S.-B.; Wang, I., Disproportionation and Transalkylation of Alkylbenzenes over Zeolite Catalysts. *Applied Catalysis A: General* **1999,** *181* (2), 355-398.

33. Ivanova, I. I.; Nesterenko, N. S.; Fernandez, C., In Situ MAS NMR Studies of Alkylaromatics Transformations over Acidic Zeolites. *Catalysis Today* **2006,** *113* (1–2), 115-125.

34. Ivanova, I. I.; Brunel, D.; Nagy, J. B.; Derouane, E. G., An In Situ ^{13}C MAS NMR Study of Benzene Isopropylation over H-ZSM-11: Cumene Formation and Side-reactions. *Journal of Molecular Catalysis A: Chemical* **1995,** *95* (3), 243-258.

35. Song, W.; Haw, J. F.; Nicholas, J. B.; Heneghan, C. S., Methylbenzenes Are the Organic Reaction Centers for Methanol-to-Olefin Catalysis on HSAPO-34. *Journal of the American Chemical Society* **2000,** *122* (43), 10726-10727.

36. Huang, J.; Jiang, Y.; Marthala, V. R. R.; Hunger, M., Insight into the Mechanisms of the Ethylbenzene Disproportionation: Transition State Shape Selectivity on Zeolites. *Journal of the American Chemical Society* **2008,** *130* (38), 12642-12644.

37. Karge, H. G.; Ladebeck, J.; Sarbak, Z.; Hatada, K., Conversion of Alkylbenzenes over Zeolite Catalysts. I. Dealkylation and disproportionation of ethylbenzene over mordenites. *Zeolites* **1982,** *2* (2), 94-102.

38. Odedairo, T.; Balasamy, R. J.; Al-Khattaf, S., Toluene Disproportionation and Methylation over Zeolites TNU-9, SSZ-33, ZSM-5, and Mordenite Using Different Reactor Systems. *Industrial & Engineering Chemistry Research* **2011,** *50* (6), 3169-3183.

39. Das, J.; Bhat, Y. S.; Halgeri, A. B., Selective Toluene Disproportionation over Pore Size Controlled MFI Zeolite. *Industrial & Engineering Chemistry Research* **1994,** *33* (2), 246-250.

40. Wu, J.-C.; Leu, L.-J., Toluene Disproportionation and Transalkylation Reaction over Mordenite Zeolite Catalysts. *Applied Catalysis* **1983,** *7* (3), 283-294.

41. Krase, N. W.; Goodman, J. B., Vapor Pressure of Toluene up to the Critical Temperature. *Industrial & Engineering Chemistry* **1930,** *22* (1), 13-13.

42. Gregorowicz, J.; Kiciak, K.; Malanowski, S., Vapour Pressure Data for 1-Butanol, Cumene, n-Octane and n-Decane and Their Statistically Consistent Reduction with the Antoine Equation. *Fluid Phase Equilibria* **1987,** *38* (1), 97-107.

CHAPTER V

FUTURE WORK

5.1. Water interaction

Apparently, water adsorbed at substoichiometric level, i.e. Stage I, is more interesting, therefore, should be emphasized in the future. However, it is important to notice that categorization of the adsorption levels strongly depend upon the temperature. Questions like, can the acid site be deprotonated by a single water molecule? For future, a few suggestions and important questions that need to be explored are stated below.

1. The "coverage sphere" need to be verified by further experiments. For example, methods like varying temperature, and using other adsorbates, such as methanol, H_2S, isobutane, benzene, etc., can be helpful. The adsorption should be controlled at Stage I or, more specifically, Stage I_a level. For such adsorbates like isobutane and benzene, there should not be Stage II range, due to the lack of adsorbate-adsorbate interaction.
2. What are the time scales of "Exchange I", between $Z^-\cdots H_3O^+$ and $Z^-H^+\cdots H_2O$; and "Exchange II", between $Z^-H^+\cdots H_2O$ and $Z^-H^+ + H_2O$, at room temperature? 2D NMR techniques are highly recommended.

3. Following question 2, what are the energy barrier of water-acid adsorption and desorption, in other words, of "Exchange II"?
4. Variable temperature NMR inspections of Stage I adsorption.
5. As mentioned in P55, quick NMR inspections of water loaded at Stage II at different Larmor frequencies would be interesting. The water peak, for example 7 ppm for Si/Al = 15 ZSM-5, should shift downfield for larger Larmor frequency.
6. Computational chemistry should be applied to obtain accountable activation energies for mentioned in Figure 4.19.
7. Defect-free and Al-siting-controlled zeolites have not been investigated in this research yet. However, it would be interesting to conduct control experiments on these special zeolites. In addition, the synthetic methods for making these special catalysts are well developed, as seen in the literature cited in Section 1.2.5. At high Si/Al ratios, where the effect of silanol groups cannot be neglected anymore (Figure 2.9d), it is hard to address the water interactions with acid sites. Therefore, defect-free high Si/Al ratio catalysts can be very interesting and useful. The effect of pairing acid sites, which is the situation that two aluminum tetrahedrals are only separated by one silicon tetrahedral, has could be evaluated. For example, Cu^{II} can be used to titrate the pairing Al site, leaving the single Al site alone.

5.2 Hydrocarbon reactions

Finding out the mechanism of the water impact on zeolite activity is long time goal. Temperature, the Al siting, and the acid density should be the key factors.

1. The batch Parr reactor and the toluene disproportionation, cumene cracking systems are still useful. The challenging part is to exclude undesired contaminations.
2. Temperature at 200 °C or 300 °C seems too high for testing water effect in a batch reaction system. However, it is not a problem for flow reactor systems. Nevertheless, in a flow system,

which is an open system, the exact amounts of water or reagent adsorbed on acid site (or their residence time) is not possible to be measured. While the fundamental studies mentioned in section 5.2, such as the exchanging rate, the activation energy, can provide enough information of picturing the situation in flow reactor systems. High temperatures do not favor the batch reactor, however, slightly high temperature range, i.e. room temperature to 100 °C, could be interesting. The next step is to find out a test reaction that is slow enough for observation. Apparently, isobutane and benzene exchanges are too fast at these temperatures. What about benzene derivatives, such as chlorobenzene?

3. We have seen the water impact on zeolite activity. What about a weaker base, methanol? Changing analogous molecules with water could be another route for the long-term run.

5.3 Outlook

By exploring this research, numerous natural properties of zeolite are and will be further revealed. The water's positive impact, though does not have instant applications, is instructive for understanding the zeolite intrinsic activity from the molecular level. Once the mechanism is resolved, it may lead to a new pathway for catalyst design.

VITA

Kuizhi Chen

Candidate for the Degree of

Doctor of Philosophy

Thesis: WATER CAN INCREASE ZEOLITE CATALYST REACTIVITY

Major Field: Chemistry

Biographical:

Education:

Completed the requirements for the Doctor of Philosophy in Chemistry at Oklahoma State University, Stillwater, Oklahoma in May 2017.

Completed the requirements for the Bachelor of Science in Chemistry at Lanzhou University, Lanzhou, Gansu/China in May 2011.

Experience: None.

Professional Memberships: American Chemical Society